A THESIS

FOR THE DEGREE OF DOCTOR OF PHILOSOPHY

Propane dry reforming over crystalline catalyst: Enhancement of synthesis gas production and its catalytic properties

SUDHAKARAN MOOPRI SINGER PANDIYARAJAN

Major of Energy & Chemical Engineering

FACULTY OF APPLIED ENERGY SYSTEM

GRADUATE SCHOOL

JEJU NATIONAL UNIVERSITY

August -- 2018

Propane dry reforming over crystalline catalyst: Enhancement of synthesis gas production and its catalytic properties

Sudhakaran Moopri Singer Pandiyarajan

(Supervised by Professor Young Sun Mok)

A thesis submitted in partial fulfillment of the requirement for the degree of

Doctor of Philosophy

2018. 06

The thesis has been examined and approved.

Prof. **Young Jin Hyun** Thesis Director,		Department of Chemical and Biological Engineering, Jeju National University
Prof. **Sang Baek Lee** Thesis Committee Member		Department of Chemical and Biological Engineering, Jeju National University
Prof. **Heon Ju Lee** Thesis Committee Member		Department of Energy Engineering, Engineering, Jeju National University
Prof. **Sang Jae Kim** Thesis Committee Member		Department of Mechatronics Engineering, Jeju National University
Prof. **Young Sun Mok** Thesis Committee Member and Supervisor		Department of Chemical and Biological Engineering, Jeju National University

June 2018

Major of Energy & Chemical Engineering

Plasma Application Laboratory

Faculty of Applied Energy System

Graduate School

Jeju National University

My humble effort

I

Dedicate

To My Beloved Mother, Father,

Sister, Brother, Friends

&

My Beloved Wife

&

Respected

Teachers and Professors

Acknowledgments

I would like to express my sincere gratitude to the many individuals who contributed to the success of my work. First of all, I would like to thank my supervisor *Prof. Young Sun Mok*. Through his positive and open-minded attitude and his enthusiasm and optimism toward research on chemical engineering, he created the legacy of the free, vivid, intelligent, friendly and communicative research atmosphere in the lab. I feel fortunate to be able to work in such environment. His excellent guidance, constant support in all circumstances have been invaluable throughout my graduate career. Without him, this work would not have been possible.

I extend my sincere thanks to thesis evaluation director **Prof. Hyun Young Jin** and thesis committee members, **Prof. Sang Baek Lee**, **Prof. Lee Heon Ju** and **Prof. Sang Jae Kim** for their time, interest, excellent suggestions, and support to finish my thesis.

My immense sense of gratitude to beloved friend **Dr. Ganesh Kumar Veerasubramani** and his family for their constant support, advice, care, and encouragement in research as well as in life.

Special thanks to him invaluable help for the admission in this our department as well as for his support and guidance to me, especially at the beginning, the most challenging time of my course.

I would like to express my gratitude to **Dr. Mani Sanjeeva Gandhi,** who gave me such an opportunity to do Ph.D. at our university. I would like to convey my sincere thanks to **Dr. Jayakodi Karuppiah** for his support to start up the research work and constant support to teach all kind of works in my Ph.D. I feel happy to get such an excellent lab mate, who made the pleasant working environment in the lab. I sincerely thank **Dr. Antony Ananth, Dr. Trinh Quang Hung, Dr. Jin Oh Jo, Dr. Duc Ba Nguyen** for their valuable support. I also thank them for their continuous encouragement to my life even at the outside lab during my research carrier. I am very much grateful to my friends and

colleagues **Mr. Mokter Md. Hossain, Mrs. Sulthana Lamia, Mr. Tae Heon Ihm. Mr. Byeong Ju Lee, Mr. Ho-Chul Kang, Mr. Devkota** for their kind help, cooperation and creating a friendly atmosphere in the laboratory. I thank all of them for useful discussion of our work and lab presentations, and the fun we have together after work on the campus, especially at MT and lab dinner.

I am glad to have friends in Jeju who always given right environment on the campus. I would like to thank **Dr. Radhakrishnan** and **Dr. Karthikeyan Krishnamoorthy** for their fun-filled moment and constant support during initial days. I would like to thank **Dr. Dharaneedharan, Dr. Anilkumar, Dr. Kaliannan Thiyagarajan, Dr. Saravanakumar Balasubramaniam, Dr. Ananathakumar Ramadoss, Dr. Umasuthan, Dr. Ganesan, Dr. Sodhi, Dr. Raj Mogre, Dr. Nagamalleswara Rao Alluri, Dr. Arunkumar Chandrasekhar, Dr. Sophia Selvarajan, Mr. Suresh Rai, Mr. Parthiban Pazhamalai, Dr. Srikanth, Dr. Sakthivel, Ms. Yuvashree Purusothaman, Mrs. Saipriya, Mr. Vivek Venkateshwaran, Ms. Kausalya Ganesan, Mr. Surjit Sahoo, Mr. Vimal, Mr. Nirmal, Mr. Prem, Ms. Sinthuja, Mr. Sravan Kumar, Mr. Rajveer, Mr. Nilojan, Mr. Kugan, Ms. Saranya** for giving me so many beautiful memories to cherish during my stay in Jeju.

I would like to thank the following Jeju friends, who made homely environment during my stay in Jeju "**Mr. Adikari, Dr. Kamran, Dr. Siddique, Dr. Shahid, Dr. Farrukh, Dr. Waqar, Mr. Sachith, Mr. Susaara, Mr. Frenado, Mr. Gilsane, Dr. Bak, Mrs. Sirajana and Mr. Rahuman.**"

I must thank the university administration for providing me full tuition fee waiver. I also thank the university administration and **BK 21** plus fellowship for providing me sufficient funds for my living. I would like to thank the personnel of the Chemical and Biological Engineering department for their kindness and a great help in official issues. I am grateful to the staffs at the

center for research facilities (CRF) at this university for providing the instrument facilities to carry out my research.

I extend my sincere thanks to **Dr. Gunasekar**, **Dr. Pithchmuthu,** and **Dr. Vinoth Kumar** for his help, guidance, and encouragement to complete my thesis successfully. I would like to thank some of the friends in Korea, **Dr. Ramasundaram**, **Dr. Ranjit Bose**, **Dr. Yuvaraj**, **Dr. Senthilkumar**, **Dr. Selva**, **Dr. Vijaya Sankar**, **Mr. Vinoth Gansen**, **Mr. Vijayaraj**, **Dr. Selva Kumar**, **Dr. Dinakaran**, **Dr. Suthagar, Dr. Sengutuvan**, **Mr. Vinoth Kumar, Mrs. Suganiya, Mrs. Hamsha, Mrs. Nithiya Bharathi, Mrs. Poornima, Mr. Gunasekaran and Mr. Saravan** who made this country like home country and gave me unforgettable memories in my life.

I sincerely thank my dearest friends and relatives Mr. Vadivel, Mr. Karpagaraj, Mr. Vengatesh, Mr. Thirupathi, Mr. Shankar Narayanan, Mr. Ganesh, Mr. Sekar, Mr. Palani, Mr. Sibi, Mr. S. Vengatesan, Mr. G. Balaji, , Mr. Jayaraj, Mr. Padmanathan, Mrs. Padma, Ms. Percy, Mr. Nagarajan, and Mr. Jegadish, for their generous love and support.

Last but certainly not least, I would like to express my most profound gratitude to my parents (**Mr. M.S. Pandiyarajan and Mrs. P. Subbulakshmi**). I would like to express my gratitude to my dear sister **Mrs. Kavitha** and brother in law **S.R. Rajkumar** and family, my dear Father in law **Mr. G. Rajaram** and family, my co-brother **Mr. Sekar** and family and **Mr. Bala Murugan** and family for their great support and encouragement.

Mostly, I would like to pay my heartiest gratitude to lovable wife, **Mrs. Ramya** who sacrifices her life throughout my doctoral studies and also shared the responsibilities for taking care of my child when I was busy in my research. It is not an overemphasis to say that I would not stay far away without her support, motivation, understanding, enthusiasm, love and stand behind in all possible ways to complete this work successfully. I indeed thank from the bottom of my heart to my lovely

daughter (**Ms. Kayazhini**) who do not see my face and after her birth and not getting my love and care. I hope I will make up for the time you spent without me in future.

I would like to thank all those whom I have not mentioned above but helped me in numerous ways to my success. Above all, all prayers and thanks go to God Almighty for giving me the guidance, patience, success and uncountable graces.

M. S. P. Sudhakaran

Contents

CHAPTER -1

Introduction

CHAPTER -2

Materials and methods

CHAPTER -3

Iron-ceria spinel (FeCe$_2$O$_4$) catalyst for dry reforming of propane to inhibit carbon formation

CHAPTER -4

Syngas production via propane dry reforming over SrNiO$_3$ perovskite catalyst

CHAPTER -5

Summary and Recommendations

List of Abbrevations

Al-F	Alumina foam
BE	Binding energy
BET	Brunauer-Emmet-Teller
BJH	Barrett-Joyner-Halenda
CPR	Carbondioxide propane ratio
DW	Distilled water
DRM	Dry reforming methane
DRP	Dry reforming of propane
DRR	Dry reforming reaction
EDS	Energy dispersive X-ray Spectroscopy
FE-SEM	Field-emission scanning electron microscopy
FT	Fischer-Tropsch
FT-IR	Fourier Transform Infrared
GC	Gas chromatography
GHG	Greenhouse gases
GHSV	Gas hourly space velocity
GTL	Gas to liquid
ICDD	International Centre for Diffraction Data
ID	Inner diameter
IR	Infrared
JCPDS	Joint committee on powder diffraction standard
LPG	Liquid petroleum gas
MFC	Mass flow controller
NiF	Nickel foam
NMP	N-methyl-2-pyrrolidinone
OD	Outer diameter

O_L	Lattice oxygen
O_S	Surface oxygen
PPI	Pores per inch
PPQ	PoraPLOT Q
PVDF	Polyvinylidene fluoride
RT	Reaction temperature
RWGS	Reverse water gas shift
SBET	Surface area
SEM	scanning electron microscopy
SMSI	Strong metal-support interactions
Syngas	Synthesis gas
TCD	Thermal conductivity detector
TOS	Time of stream
TPD	Temperature programmed desorption
TPO	Temperature programmed oxidation
TPR	Temperature programmed reduction
Vp	Pore volume
WGSR	Water gas shift reaction
XPS	X-ray photo electron spectroscopy
XRD	X-ray diffraction

List of Tables

List of Figures

Abstract

The light hydrocarbon (C_1-C_4 alkanes) dry reforming process has attracted considerable attention with increasing global gasoline price, for developing sustainable environmentally-compatible synthesis gas (H_2/CO mixtures) production and utilization technologies. Dry reforming of propane (DRP) has been widely investigated, with most studies showing rapid deactivation due to carbon formation and sintering at high elevated temperature. DRP is highly endothermic reactions it acquires high energy. The metallic and bi-metallic catalyst has been showed high performance in DRP. Meanwhile, it has lost their catalytic ability due to sintering and coke formation. These propose demanding to improve catalysts that limit carbon formation and sintering while avoiding structural changes at the elevated temperatures typical of this reaction.

The primary focus of this thesis is that the improving the carbon inhibition and anti-sintering by binary metal oxide in well defined structured such as spinel and perovskite catalyst and their systematic enhancement in the catalytic activity by a various combination of elements. In this work, we have investigated dry reforming of propane on two catalysts. First, the $FeCe_2O_4$ spinel catalyst was synthesized by the sol-gel method to evaluate the catalytic activity and carbon inhibition. A second, the $SrNiO_3$ catalyst was synthesized by a sol-gel method in which rare earth substituted perovskite catalyst. All catalysts were performed DRP, and their physicochemical studies showed that the anti-sintering and minimal carbon formation. Catalysts characterization were measured via various techniques including BET surface area, pore volume, temperature programmed reduction, temperature programmed desorption of H_2 and CO_2. Morphological measurements such as X-ray diffraction, field emission – scanning electron microscopy, scanning electron microscopy-energy dispersive X-ray, Raman, and X-ray photoelectron spectroscopy were analyzed. XRD analysis confirmed the formation of crystallinity of metal oxide by various

synthesis methods and EDS analysis verified the metal dispersion obtained from synthesis. The catalyst evaluation was performed in a fixed-bed reactor of the various temperature range at 550°C to 800°C under atmospheric pressure with stoichiometry ratio of carbon dioxide, and propane (CP) is 3. The catalysts showed the significant activity at elevated temperature. It was found that the conversion and syngas yield increased with increasing temperature. The catalysts exhibited the range of H_2/CO ratio is (0.6 to 0.7), which shows the reaction proceeds through the thermodynamical reaction with different supports and hinders the carbon formation. The catalytic stability of all catalysts was also performed for 50 h time on stream (TOS) for the DRP at the high active reaction temperature. No significant deactivation was observed for the all catalysts at high temperature for a long time. The spent catalysts were characterized by XRD, FE-SEM, Raman, XPS and TPO analysis to understand the morphology of the catalyst and coke deposited on the catalyst. XRD patterns attributed that the carbon formed on each catalyst after 50 h TOS at elevated temperature, mainly low intense graphitic carbon (peak at $2\theta = 26°$) was observed in all catalyst and the crystallinity of catalyst sustain after DRP. The Raman results revealed the form of carbon on the catalyst after DRP, mainly the two peaks were attributed at 1300 ± 50 cm^{-1} and 1500 ± 50 cm^{-1} on all catalyst, which corresponds to the graphite and carbon nanotube respective with an intensity ratio of I_D/I_G. XPS analysis demonstrated the existence of mainly two peaks of carbon species, graphitic (-C-C-), and C-H. An oxidation process performed the quantitative measurement of carbon at 600°C; the deposited carbon reacts with O_2 to CO_2 at 600°C. The results were found that the minimal carbon formation of the catalyst compares with the conventional catalyst. The different lattice compounds showed the limiting of carbon formation and high sustainability due to the immense availability of lattice oxygen and surface oxygen in the crystalline form of catalyst.

CHAPTER -1

1.1 Introduction and literature review

"The production of renewable fuel like hydrogen by conversion of hydrocarbons to synthesis gas (syngas) will play an essential role in the 21st century"[1]. The current crisis of depleting fossil resources with associated environmental disorders encourages massive numbers of researchers around the world to consider alternative routes for fuel production, for example, syngas utilization under gas to liquids (GTL) process. However, since about 50-60% of the cost of this process is based on the raw material (i.e., syngas) [2,3], it is, therefore, a necessity to investigate the possibilities for the production of syngas through hydrocarbons and enhance them. Among these options, dry reforming technology has been recently considered as a potential choice given the revolution in catalyst compounds and reaction operation technologies.

However, the primary challenge that has prevented this process from the commercial application is the severe carbon deposition that deactivates the catalyst, despite the reaction was discovered in earlier 1888 [4] and investigated thoroughly by Fischer and Tropsch in 1928 [4]. However, the process is currently being considered with high potential under the tremendous improvements in catalyst design and reactor operation technologies with the aim to enhance syngas production and reduce carbon deposition. Based on the dry reforming reaction mechanism, carbonaceous residue mainly comes from the hydrocarbon compound decomposition with a slight contribution from a CO disproportionation reaction, which reduces the syngas formation. Carbon formation under such process can be classified into three main types, namely: poisoning, sintering, and coking.

While deactivation by poisoning can be eliminated by pre-treatment of the feedstock [5,6], attention to thermal operating conditions under the various stages of the catalytic reaction system

is a useful approach to reduce the impact of deactivation by sintering [7]. In fact, other factors could improve catalyst attributes for sintering such as the presence of strong metal-support interactions (SMSI), shape and size of the crystallite, support roughness, and pore size, and additives present in either the support or the metal [8]. The primary factor for deactivation is the coke formation whereas the active surface area of the catalyst is lost due to deposition of species obtained from the fluid phase causing blockage of sites and pores [9]. The process occurs typically due to carbon chemical- or physical-sorption leading to encapsulating the metallic active sites with subsequent plugging of the micro- and mesopores of the support. This consequently creates production loss and pressure build-up in the plugged reactor. Hence a costly shutdown is necessarily required to resolve the crisis. In fact, the main features that can be used to diminish coking formation are catalyst structure, surface chemistry, and reaction conditions. This research is generally aimed to improve syngas production in addition to reducing carbon deposition, the primary challenge that prevents this option from proceeding to commercial application. This chapter explores some of the directions discussed in the literature in this context. It initially briefly highlights the first opportunities to produce syngas and the reasons for focusing on the dry reforming process.

1.2 Catalytic Syngas Production from Hydrocarbons

The significant importance of syngas comes from diverse applications by petrochemical industries such as methanol production, ammonia manufacture and the Fischer-Tropsch (FT) reaction as shown in **Figure 1.1.1** Refinery applications along with ammonia production are known as the biggest users of H_2 with increasing demand due to high consumption of fuels and fertilizers [10]. However, fuel production via the FT reaction in the GTL process is the highest consumer of syngas [2]. Consequently, the continuous and feasible supply of the syngas such as

by hydrocarbon reforming is an important issue to fulfill the demand [1]. The conversion of natural gas into fuels can be barely attained because of the high selectivity of syngas production routes [11]. Thus, syngas routes are the preferable option to convert natural gas into liquid fuels, methanol, ammonia and oxygenates [12]. Although the syngas routes are highly efficient, they have been limited by high energy consumption. Currently, the main commercial routes for syngas production from natural gas include steam reforming, partial oxidation and auto-thermal reforming [2]. However, the dry reforming reaction has been receiving growing attention in the last two decades to resolve the severe carbon deposition which is the main problem that is encountered in this route [13-18]. These routes, in general, utilize methane as the hydrocarbon feedstock while light alkanes (C_2-C_4) have started to receive attention in the last few years [19-31]. Indeed, higher hydrocarbons require less energy as the chain length is increased [19]. Hence, the following subsections briefly discuss the routes usually studied for syngas production when using propane as the hydrocarbon feedstock.
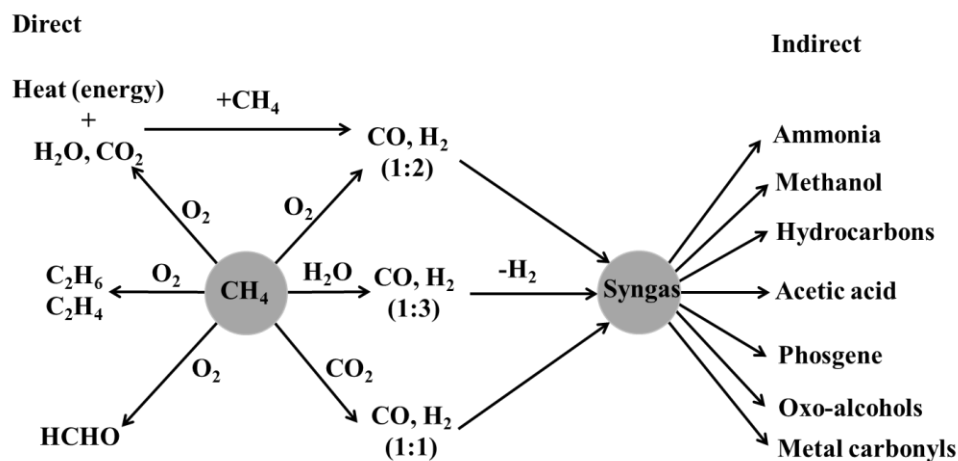
Figure 1.1.1 Various direct and indirect routes to produce useful chemicals from natural gas (adapted from [10]).

1.2.1 Steam reforming

The most favored pathway is probably steam reforming, which is generally given by:

$$C_3H_8 + 3H_2O \rightleftharpoons 3CO + 7H_2 \quad \Delta H_{298}^0 = 499 \; kJ \; mol^{-1} \qquad\qquad \ldots\ldots\ldots (2.1)$$
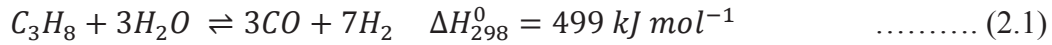
The theoretical syngas ratio for propane steam as seen from Eq. 2.1 is 2.3[32]. In reality, the actual ratio for methane steam reforming is reported to be 5 compared to theoretically 3. This high ratio would be more suitable for the H_2 application rather than the GTL process while adjusting this ratio for the latter involves an extra cost for H_2 separation from steam [2]. Steam reforming involves an additional cost represented by steam generation compared to other routes for syngas such as dry reforming, despite the availability of lower cost water. All these factors, along with the original high energy consumption required for such an endothermic reaction, were anticipated to shift attention towards other routes.

1.2.2 Partial oxidation

Unlike steam reforming, the second route of partial oxidation is an exothermic reaction as expressed [21]:

$$C_3H_8 + \frac{3}{2} O_2 \rightleftharpoons 3CO + 4H_2 \quad \Delta H_{298}^0 = -229 \; kJ \; mol^{-1} \qquad\qquad \ldots\ldots\ldots (2.2)$$
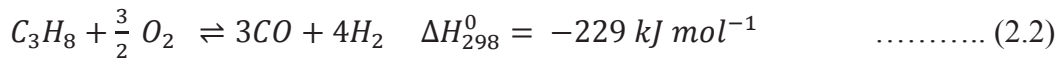
Although the formation of syngas by the catalytic partial oxidation of CH_4 was Initially reported by Prettre et al. [33] in 1946, This reaction needs pure oxygen which costs about 40% of the capital cost of a synthesis gas plant [2]. Regardless of the explosion and flammability risk concerns and the limited secure range for feed mixture, this reaction needs to be heated to 973–1173 K in the absence of a catalyst along with high-temperature recovery and soot [33]. Yet, in the presence of a catalyst, spot formation, and excessive heat, especially at the entrance to the reactor, is still a big challenge which may be considered as the main difficulty in operation, particularly in a large-scale reactor [34,35]. Indeed, De Groote and Froment indicated that the catalyst bed inlet temperature increased up to 1700 K under a reactor temperature of 1223 K, when

simulated by the temperature gradient of a catalyst bed in partial oxidation of methane using the fixed-bed reactor [36]. Moreover, the high potential for further oxidation of the product to CO_2 and H_2O rationalizes the benefits for this reaction. Also, syngas hydrocarbon content is mostly low and slightly challenging to adapt to suit downstream processing requirements [2]. Consequently, these shortcomings diverted general research and further consideration from this reaction. Hence, more attention was paid to adding a small amount of oxygen to steam reforming (Autothermal reforming) [37-41] or focused on dry reforming as reported recently [42-44].

1.2.3 Autothermal reforming

A combination of the routes in subsections 1.1.1 and 1.1.2 would result in utilization of the internal heat generation from the partial oxidation reaction, consequently reducing overall energy consumption. This collective reaction is therefore called autothermal reforming, and its specific enthalpy of formation is subject to the ratio of water and oxygen in the air [45,46]. Under the assumption of using pure oxygen, the reaction and its heat of formation may be given as:

$$C_3H_8 + H_2O + O_2 \rightleftharpoons 3CO + 5H_2 \quad \Delta H_{298}^0 = 15 \; kJ \; mol^{-1} \qquad \ldots\ldots\ldots (2.3)$$
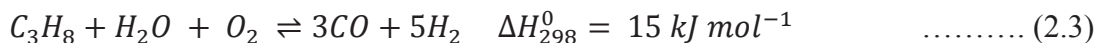
Comparing the heat of formation for Eq. 2.3 with 2.1 shows the advantage of the O_2 addition based on the theoretical thermodynamical perspectives. However, the syngas gas ratio is higher than one, estimated at 1.7 from the previous equation, which means it is not preferred for the GTL process. This reaction was ineffective especially given some of the shortcomings of steam reforming.

1.2.4 Dry reforming

The last main route is known as dry, or carbon dioxide reforming, where CO_2 is utilized to react with hydrocarbons as:

$$C_3H_8 + 3CO_2 \rightleftharpoons 6CO + 4H_2 \quad \Delta H^0_{298} = 644 \ kJ \ mol^{-1} \qquad \text{..........(2.4)}$$
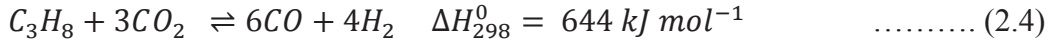
Although this reaction was explored thoroughly by Fischer and Tropsch [47], no commercial application is yet reported [48]. Recently, reaction benefits led to increasing attention under current global considerations [49-58]. This reaction has almost the same energy requirement for steam reforming as may be seen from the thermodynamical aspect. The most important advantage is the syngas ratio of 0.7, which is lower than 1, thus suitable for the GTL process [59-62]. Moreover, the availability of CO_2 from the coal energy process for example, and its lower cost compared to steam generation supports the increased interest. Edwards et al. in 1996 [63] successfully implemented dry reforming of methane in solar energy storage and transport as may be seen from Figure 2.2. Yet, it has been reported that the cost of dry reforming is 20% lower than any other reforming process [59]. This is may be due to the presence of CO_2 as an oxidizing agent, as Michorczyk and Ogonowski reported that under similar conditions the dry reforming temperature is lower than simple propane hydrogenation by 100 K and by 50 K compared to steam reforming [64].
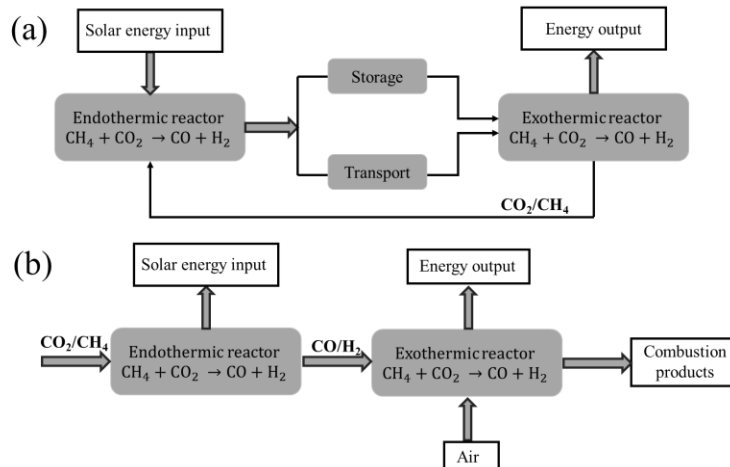
Figure 1.1.2 Concepts for (a) closed and (b) open loop thermochemical heat-pipes based on methane dry reforming and solar energy, adapted from [63].

The CO_2 showed excellent activity as an oxidizing agent compared to H_2 or even O_2, as the latter may alter catalyst characteristics at high temperature [65]. Moreover, some crude natural gas resources may contain up to 30% CO_2 by volume [19,66]. Biogas, which is also considered as an attractive renewable energy source, consists of 50–60% CH_4, 40–50% CO_2, and moisture [67]. Hence, it is more economical to utilize it for syngas production instead of adding costs for separation. Dry reforming is also supported by other advantages such as its suitability for high purity O_2 production as well as usage in chemical energy storage processes [68,69]. Finally, the environmental contribution of this reaction by consuming green-house-gases (GHG), makes dry reforming more preferable under the current concern for global warming [12,70]. In a symposium for strategies for the utilization of fossil fuels in the 21st century, urgent action about CO_2 emissions in addition to other GHGs was recommended [71]. Given these advantages, dry reforming was considered as the primary reaction in this study given the attempt to find outcomes that would help in commercializing this critical process. The commercial application was not viable even with the previous benefits for dry reforming, because of the severe carbon deposition. However, the potential for the process is beginning to be considered in the context of the large developments in catalyst design and reactor operation technologies. The deposited carbon mainly comes from the hydrocarbon substrate decomposition. Hence, the primary routes for the synthesis gas production under each route may be subjected to different hydrocarbon substrates [72-75]. Yet, the commercial application relies on the cost of reactants along with the energy consumption and operational costs for these routes. Under dry reforming, accurate comparison of the prices of hydrocarbon substrates is mainly unfeasible. This is due to fluctuations in the price for natural gas and crude oil, the primary source for light alkanes such as propane, even if it is generally accepted that the cost of propane or liquefied petroleum gas (LPG) is only a small increment.

This study considered propane as the hydrocarbon substrate because the main aim was to design a robust catalyst with high activity for syngas production under diminished carbon deactivation. Propane was expected to produce more surface carbon species compared to natural gas due to a higher carbon atom content, hence, creating an ideal environment for the challenge that needed to be overcome. Moreover, using higher hydrocarbon substrate is preferred as it requires less energy for the bond breakup. Furthermore, higher hydrocarbons are known to have a lower flammability limit which is 5.3–15% for methane and 2.2–9.6% for propane [76]. Therefore, the next section provides insights into this reaction followed by background about catalyst deactivation.

1.3 Propane dry reforming

Several studies in the open literature reported propane dry reforming [23,28,77-84] reflecting the new direction in research by considering higher hydrocarbon substrates, as most of these studies were conducted in the last decade. Therefore, the discussion will sometimes refer to the information published about methane dry reforming with little inspiration from similar reactions such as propane steam reforming. In fact, the propane dry reforming reaction is given by Eq. 2.4 may be represented mainly by two steps: namely propane dehydrogenation to hydrogen, methane and carbonaceous residue (C_xH_{1-x}):

$$C_3H_8 \rightarrow \frac{2}{x} C_xH_{1-x} + CH_4 + \left(\frac{3x-1}{x}\right) H_2 \qquad \ldots\ldots\ldots (2.5)$$
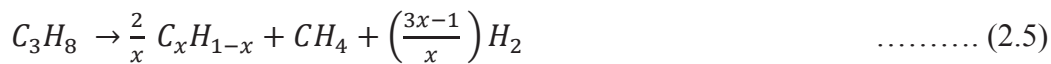
moreover, CO_2 gasification of the carbon deposit via:

$$C_xH_{1-x} + xCO_2 \leftrightarrow 2xCO + \left(\frac{1-x}{2}\right) H_2 \qquad \ldots\ldots\ldots (2.6)$$
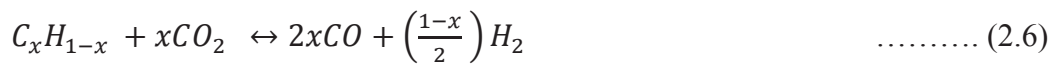
resulting in the overall reaction:

$$C_3H_8 + xCO_2 \leftrightarrow \left(\frac{2}{x} - 1\right) C_xH_{1-x} + 2xCO + CH_4 + \left(\frac{7x-2-x^2}{2x}\right) H_2 \ldots\ldots\ldots \text{(2.7)}$$
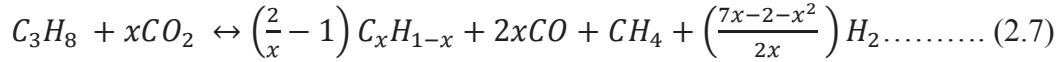
Since this reaction is limited by chemical equilibrium, lower pressures or higher temperatures are essential for higher conversion as per Le Chatelier's principle [64]. Under thermodynamic study for this reaction, Wang et al. showed that this reaction was better to be conducted over a temperature range of 700–1100 K and under atmospheric pressure [85], although, the lower temperature limit seems questionable in this study as the activation temperature is known as 485 K [86]. Yet, higher temperature involves a thermal cracking reaction to coke and sintering particularly for Ni based catalysts [64]. Thus, temperatures higher than 757 K and lower than 972 K may be considered for this reaction under atmospheric pressure. Indeed, the limited studies conducted on propane dry reforming are conducted within this range. Further details such as the reaction mechanism would be provided in the next two subsections followed by an overview of the associated reactions.

1.3.1 Mechanism

Since most of the propane dry reforming studies were conducted recently, most of the published studies in this regard suggested a reaction mechanism based on methane dry reforming. Propane dry reforming possible mechanism described based on the thermodynamic characteristics, Wang et al. [85] suggested the following reaction network:

$$C_3H_8 \rightleftharpoons C_2H_4 + CH_4 \quad \Delta H_{298K} = 89 \; kJ \; mol^{-1} \qquad \ldots\ldots\ldots \text{(2.8)}$$

$$C_2H_4 \rightleftharpoons 2C + 2H_2 \quad \Delta H_{298K} = 52 \; kJ \; mol^{-1} \qquad \ldots\ldots\ldots \text{(2.9)}$$

$$H_2 + CO \rightleftharpoons C + H_2O \quad \Delta H_{298K} = 131 \; kJ \; mol^{-1} \qquad \ldots\ldots\ldots \text{(2.10)}$$

$$CH_4 \rightleftharpoons C + 2H_2 \quad \Delta H_{298K} = 75 \; kJ \; mol^{-1} \qquad \ldots\ldots\ldots \text{(2.11)}$$

$$2CO \rightleftharpoons CO_2 + C \quad \Delta H_{298K} = 172 \: kJ \: mol^{-1}$$ .... (2.12)

$$2H_2 + CO_2 \rightleftharpoons C + 2H_2O \quad \Delta H_{298K} = 90 \: kJ \: mol^{-1}$$ .... (2.13)
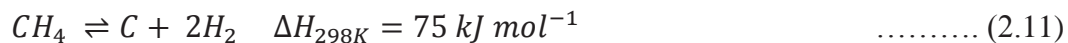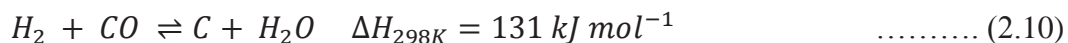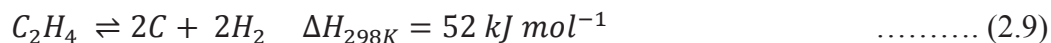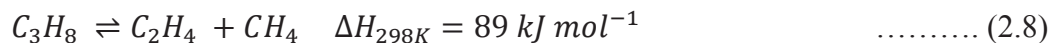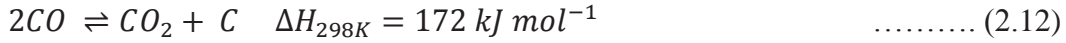
However, the appropriate reaction mechanism should be proposed based on detailed experimental and modeling investigation, as Sutton at al. showed that was unlikely to specify the exact mechanism based on the kinetic data alone [81]. According to their study, modeling for various Langmuir–Hinshelwood mechanisms did not give a defined idea for the mechanism, and the further suggestion was provided by the Mars-van Krevelen mechanism. The following reaction series were proposed as per the Langmuir–Hinshelwood mechanism:

$$C_3H_8 + \odot \rightarrow C_3H_x\odot + (8 - x)H\odot$$ .... (2.13)

$$CO_2 + \odot \rightarrow CO_2\odot$$ .... (2.14)

$$C_3H_x\odot \rightarrow C\odot + xH\odot$$ .... (2.15)

$$CO_2\odot + H\odot \rightleftharpoons CO\odot + OH\odot$$ .... (2.16)

$$C\odot + OH\odot \rightarrow CO + H\odot$$ .... (2.17)

$$2H\odot \rightleftharpoons H_2 + \odot$$ .... (2.18)

$$OH\odot + H\odot \rightleftharpoons H_2O + 2\odot$$ .... (2.19)

$$CH_x\odot + OH\odot \leftrightharpoons CH_xO\odot + H\odot$$ .... (2.20)

$$CH_xO\odot + OH\odot \leftrightharpoons CH_xO\odot + H\odot$$ .... (2.21)

$$CH_xO\odot \rightarrow CO\odot + \frac{x}{2}H_2$$ .... (2.22)

$$CO\odot \leftrightharpoons CO + \odot$$ .... (2.23)
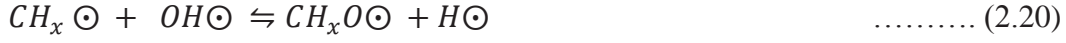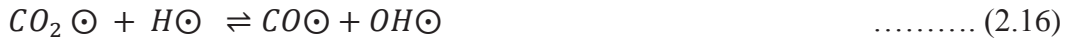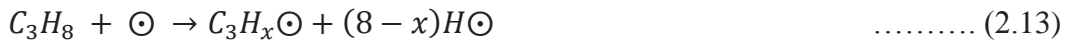
It was suggested that propane could be adsorbed and dissociate to CH$_x$ (C$_{ads}$ and H$_{ads}$) (reactions 2.15 and 2.17) while and carbon dioxide can be adsorbed (reaction 2.16). The latter may consequently react with H$_{ads}$ as in reaction 2.18 to yield CO (in a further step as in reaction 2.23) in addition to the adsorbed hydroxyl group (OH). Subsequently, the adsorbed OH oxides surface carbon to produce CO and H$_2$ at the end (reaction 2.19). Also, it can be utilized to produce moisture through reaction 2.20 or even to generate oxygenated carbon species (CH$_x$O) as in reaction 2.21 which may dissociate (as in reaction 2.22) to adsorbed CO and H. Under this series of reactions, water is proposed (reaction 2.21) although it was not measured experimentally as the alumina support provides enough concentration of acidic and basic sites to produce affinity for the hydroxyl group. Derived from the kinetics observations, dissociation of carbon dioxide was slowest and hence the rate determining step. However, Jensen at al. [87] recently conducted their study over a 1.9wt%Ni/Mg(Al)O catalytic system. Indeed, they have another proposal for the reaction mechanism as:

$$C_3H_{8(g)} + 2^* \rightleftharpoons C_3H_X^* + H^* \qquad \ldots\ldots\ldots (2.24)$$

$$C_3H_7^* + * \rightleftharpoons C_3H_6^* + H^* \qquad \ldots\ldots\ldots (2.25)$$

$$C_3H_7^* + (9-n)^* \rightarrow 3CH_n^* + (7-n)H^* \qquad \ldots\ldots\ldots (2.26)$$

$$CO_{2(g)} + 2^* \rightleftharpoons CO^* + O^* \qquad \ldots\ldots\ldots (2.27)$$

$$H_2O + 2^* \rightleftharpoons HO^* + H^* \qquad \ldots\ldots\ldots (2.28)$$

$$CH_n^* + O^* + n^* \rightleftharpoons CO^* + nH^* + * \qquad \ldots\ldots\ldots (2.29)$$

$$CH_n^* + (4-n)H^* \rightleftharpoons CH_{4(g)} + (5-n)^* \qquad \ldots\ldots\ldots (2.30)$$

$$CO^* \rightleftharpoons CO_g + * \qquad \ldots\ldots\ldots (2.31)$$

$$2H^* \rightleftharpoons H_{2(g)} + * \qquad\qquad\qquad \text{………. (2.32)}$$
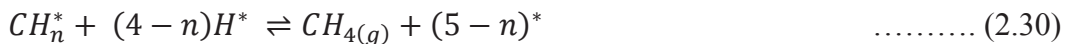
where * are the active sites and $0 \leq x \leq 3$. According to this mechanism, propane dehydrogenated in sequential steps (reactions 2.18–2.20) produce adsorbed surface carbon CH_n which reacted (reaction 2.23) with adsorbed O supplied by CO_2 dissociation (reaction 2.21). Consequently, adsorbed CO (reactions 2.19 and 2.21) and H (in 2.18–2.20, 2.22 and 2.23) may be released to the gas phase as in reactions 2.25 and 2.26. Furthermore, adsorbed surface carbon CH_n may also be hydrogenated by adsorbed H to form methane as in reaction 2.24. However, it seems there is something wrong with reaction 2.22 as the moisture should be generated as a minor contribution of the side reaction; reverse water gas shift (RWGS).

1.3.2 Associated reactions

As seen from the previous section, propane dry reforming reaction is a complex set of reactions in the presence of side reactions such as propane dehydrogenation, reverse-Boudouard and reverse-water-gas-shift reaction (RWGS). These side reactions have various influences on the propane dry reforming reaction path. Thus, this section will provide a brief highlight of each reaction.

1.3.2.1 Propane dehydrogenation

Although propane dehydrogenation may occur in a series of parallel reactions, all of them are slightly endothermic. The most likely reaction to take place is:

$$C_3H_8 \rightarrow CH_4 + 2C + 2H_2, \quad \Delta H_{298K} = 37 \; kJ \; mol^{-1} \qquad \text{……… (2.33)}$$
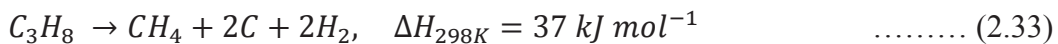
As per the thermodynamic investigation carried out in this study, this reaction is favorable for at higher temperature than 179 K. The importance of this reaction comes from the production of surface carbon that deactivates the catalyst and H_2 in addition to various hydrocarbons. Hence,

the catalyst that has higher resistance to carbon deposition and lower selectivity towards side products would result in higher production of H_2. Therefore, the appropriate catalyst should be selected accordingly. According to the propane dry reforming reaction mechanism, surface carbon is most likely to be oxidized by oxygen from CO_2 or even directly. So, using the catalyst that facilitates CO_2 dissociation should be considered. Also, carbon formation can be kept to a minimum by using some reaction control features such as co-feeding some gases that improve carbon oxidation. Indeed, carbon formation rate is expected to increase with temperature, and hence, temperature range should be selected carefully, although the effect of carbon deposition may be modified due to the presence of other reactions co-occurring.

1.3.2.2 Boudouard reaction

Another side reaction is the Boudouard reaction which also known as CO disproportionation, where CO may dissociate to produce CO_2 and surface carbon as:

$$2CO \rightleftharpoons C + CO_2 \quad \Delta H_{298K} = -172 \; kJ \; mol^{-1} \qquad \ldots\ldots\ldots (2.34)$$
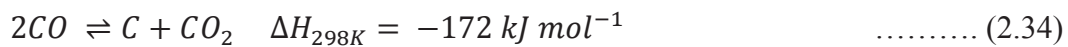
Thermodynamically, this reaction is likely to take place at a reaction temperature lower than 972 K. However, the presence of high concentrations for CO_2 in the system may facilitate keeping the influence of this reaction to a minimum. Also, quicker removal for CO from the system should assist in reducing the effect of this side reaction. Thus, running under a fluidized-bed reactor may help in removing the products (CO and H_2) faster and hence shift the reaction towards the product.

1.3.2.3 Reverse water gas shift

This reaction is at equilibrium and may be expressed as:

$$CO_2 + H_2 \rightleftharpoons CO + H_2O \quad \Delta H_{298K} = 41 \; kJ \; mol^{-1} \qquad \ldots\ldots\ldots (2.35)$$

13

Principally, this reaction is very significant in a system containing an abundant amount of CO_2 and H_2 like propane dry reforming. It is slightly endothermic and is likely to take place at a higher temperature than 1073 K. Likewise, prompt removal of H_2 or CO_2 from the system would lower the contribution of the RWGS reaction. However, since CO_2 is one of the reactants and would be in excess particularly at a higher feed ratio, R, shifting CO_2 towards other steps mentioned under the propane dry reforming mechanism, such as CO_2 dissociation can also help in this matter. Hence, catalyst type selection and other aspects related to catalyst design should be recognized in that context.

1.4 Catalyst deactivation

The severe carbon deposition is the main difficulty that prevented a likely reaction such as propane dry reforming from commercial application. This deposition led to a loss in catalyst activity with time-on-stream in a deactivation process. The impact of deactivation on the lifetime of the catalyst depends on the type of catalytic process. In fact, the impact is limited to the catalyst and often extended to include various consequences that are very important in industries, such as lower production with more inferior quality, further energy requirements and shutdown for catalyst replacement and associated cost of production time loss and catalyst regeneration [5]. Although the challenge of deactivation is not defeated entirely, various solutions are implemented to reduce the impact to a lower level through improving catalyst carbon resilience and using some reactor operational strategies [6]. However, to obtain the optimal solution, it is essential to recognize the nature of the catalyst deactivation process. Hence, this section underlines the main types of catalyst deactivations that generally occur in industrial processes, namely poisoning, sintering (aging) and coking (fouling). After that, this section demonstrates the deactivation sources under propane dry reforming followed by insights into the deactivation mechanism.

1.4.1 Types of deactivations

1.4.1.1 Poisoning

Poisoning is the loss of activity due to impurities from the feed depositing on the active portion leading to a decline in the existing active sites for the primary reaction. Although dry reforming is not yet implemented in the industrial application, the leading cause for poisoning over Ni-based catalyst surface is the adsorption of H_2S, As and HCl under a similar process such as steam reforming [6]. This kind of poisoning is like the trace contaminants in petroleum feedstocks. Poison adsorption, in general, is a fast process, and the influence depends on the nature of the poison and its amount in the feed. While sometimes pre-treatment for the feed may reduce the concentration of the poison to an acceptable level, the strength of adsorption between the poison molecule and catalyst surface may require a higher temperature to crack the interaction [5,6]. Moreover, the tolerance of the metallic active sites for these poisons should be taken into consideration under the exploration for an active catalyst. However, since Ni based catalyst is commonly used for propane dry reforming, which exhibits an excellent tolerance for these catalysts against sulfur among some of the transition metals such as Ru, Co, Fe under the methanation process [5].

1.4.1.2 Sintering

This kind of catalyst deactivation is frequently classified as aging after that structural modification leads to losing catalytic surface and support area. While catalytic surface area loss may occur because of crystalline growth of the catalytic phase, pore collapse could cause loss of support area. It may take place at any stage in the life cycle of a catalyst that requires high-temperature treatment [7]. Hence, the thermal treatment needs to be managed cautiously under these stages which include calcination and reduction during catalyst preparation, reaction operation conditions and regeneration (carbon burn-off). In supported metal catalysts, sintering

제주대학교 중앙도서관
JEJU NATIONAL UNIVERSITY LIBRARY

usually occurs through two models (a) the atomic migration and (b) the crystallites during relocation from a crystallite to the surface of the support. In the second model, crystallite collision and coalescence take place during the migration of crystallites over the surface of the support.
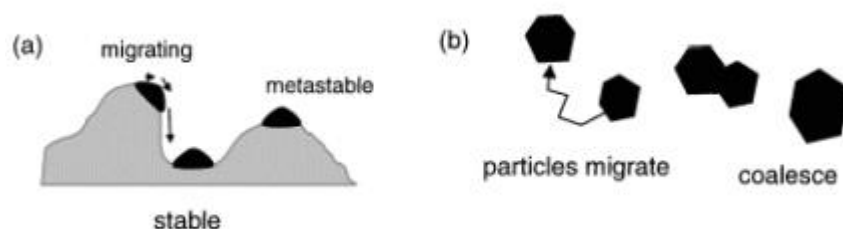
Figure 1.1.3 Theoretical models for crystalline growth under sintering deactivation, (a) the atomic migration and (b) the crystalline migration, adapted from [7].

The main reason behind sintering is conducting catalyst preparation stages or reaction at high temperature for a long time. Apparently, using higher temperatures can lead to a severe decline in the surface area. Since sintering is an outcome of thermal condition variation, control can be achieved by selecting suitable temperature ranges and heating rates under all steps of the catalyst life cycle. Muolijn et al. advised to employ temperature below 0.3-0.5 time the melting point of the metal and support [7]. Conversely, there are other factors that could improve catalyst attributes towards sintering, namely the presence of strong metal-support interactions, shape, and size of the crystallite, support roughness and pore size and additives present in either the support or the metal [6,8]. For instance, Ni has a stronger interaction with Al_2O_3 than with SiO_2 which in turn makes it more thermally stable [8]. Some of the previous studies [88-91] show that Ni particles supported on a highly basic support like lanthanum oxide (La_2O_3), that is carbonated under dry reforming conditions and formed with a thin layer of lanthanum carbonate, which prevents sintering of particles and the extraction of particles from the surface by carbon filaments during the reaction. However, it has been reported that the addition of cerium as a promoter enhances the

basicity of the catalyst [92-96]. This increase in basicity means increasing adsorption in the acidic agent such as CO_2 leading to more carbonate formation which is converted to CO at a higher temperature. Hence, increasing the basicity character of the catalyst leads to a decline in its activity as the more active sites would be shielded by excess carbonate species [97].

1.4.1.3 Coking

This is a physical type of deactivation (also known as fouling) and reflects the loss of the catalyst active surface area due to deposition of species obtained from the fluid phase causing blockage of sites and/or pore [9]. In industrial applications, coking might arise from various materials such as ashes or soots in the combustion processes, asphaltenes in petroleum refineries and carbonaceous deposition in many hydrocracking processes [7]. The carbon lay down is the main complexity that prevented dry reforming from commercial operation. The process can be described, carbon chemisorbed- or physisorbed leading to encapsulating the metallic active sites with subsequent plugging for micro and mesopores of the support. This consequently creates production loss and pressure build-up in the plugged reactor. Hence a costly shutdown is necessarily required to resolve the crisis. Furthermore, the main features that can be used to manage carbon deposition include catalyst structure, surface chemistry, and reaction conditions. Therefore, to obtain a catalyst with high resilience toward coke formation, support selection and treatment should concentrate on maximizing the pore mouth as well as attaining a high surface area. It has been reported that lower catalyst acidity and higher basicity resulted in development in the catalyst spirit against carbon deactivation in the reforming reaction [23,93,98]. It is comprised of many variables such as the concentration of the deposited species, as for example, propane is more carbon enriched than methane, or in the sense of feed ratio in addition to the reaction temperature and pressure or even the operation mode (i.e., fixed, fluidized-bed or

17

membrane, etc.). All these features and variables should be selected to attempt the lowering of carbon deposition.

1.5 Dry reforming catalyst

The common reforming catalyst consists of one or more metallic active clusters located over a support material. The support is usually known as an inert material even though sometimes, metal species may establish a relationship with the support which is often referred to as metal-support interaction. As observed from the earlier discussion, selecting the appropriate support is an important matter to minimize the chance of acquiring sintering deactivation in addition to other factors such as enhancing metal dispersion and creating an economic catalyst. Extensive research by Bradford and Vannice [13], indicated that carbon formation is dependent on numerous parameters, such as the metal, metal crystallite structure, metal–support interactions and support acidity and basicity. This section recapitulates the metals and supports that are typically utilized and reported in the literature, for dry reforming to obtain an active catalyst for this study. The function of using crystalline catalysts under dry reforming and their role in improving catalyst activity towards carbon deposition will be provided. Ultimately, the influence of employing a rare earth metal and alkali earth metal substituted spinel and perovskite as a catalyst to enhance the catalytic performance will also be covered.

1.5.1 Metal catalyst

Table 1.1 displays the most widely used catalysts for dry reforming. It is noticeable that most catalysts used in these studies were mainly based on group VIII of transition metals (Co, Ni, Ru, Rh, Pd, Re, Ir, and Pt). Indeed, most of the transition metals have been recognized as good dry reforming catalysts [99]. Among these, the Ni catalyst was generally preferred commercially for

reforming processes. Alumina (Al_2O_3) was commonly used as the support for nickel catalysts because of its high surface area, low cost and thermal stability [100,101].

Table 1. 1 Previously reported catalysts for dry reforming of methane

Metal	Support	References
Ni	Al_2O_3	[102-104]
	SiO_2, MgO, La_2O_3	[105-111]
	CeO_2, ZrO_2, TiO_2	[112-116]
Co	Al_2O_3	[59], [117,118]
	ZrO_2	[96], [119]
	SiO_2	, [120]
	MgO	[121]
	TiO_2	
Fe	MgO, La_2O_3	[122,123]
Rh	Al_2O_3, SiO_2, La_2O_3, ZrO_2	[100], [123-128]
Pt	Al_2O_3	[124], [129-132]
	SiO_2, MgO	[133,134]
	ZrO_2	,[129],[130-132] [135,136]
	TiO_2	
Ir	Al_2O_3	[137], [124]
	SiO_2, La_2O_3, TiO_2, ZrO_2,	[138]
	MgO	[139]
Pd	Al_2O_3	[42], [140]
Ru	Al_2O_3, ZrO_2, Y_2O_3, SiO_2	[124], [140] [141]
	La_2O_3	[142,143]

Despite the type of metal, it is found that the combination of metal and support influences the resultant catalyst activity. Amongst the first row of group VIII metals (Fe, Co, and Ni), Ni demonstrates the highest activity followed by Co and both are much higher than Fe. Conversely, Rh is a higher element in respect of the high activity and the coking free operation as supported on

Al_2O_3. Solymosi and Tolmacsov [78] studied propane dry reforming over alumina and found that activity decreases in the following order: Rh>Ru>Ir>Pt>Pd using 1wt% metal loading while the order for methane dry reforming was Rh>Pd>Ru>Pt>Ir [144]. Sutton et al. [81] studied propane dry reforming over $1wt\%Ru/Al_2O_3$ and reported that the catalyst has high activity without carbon deposition. On the other hand, Ru may be higher than Rh supported on MgO or SiO_2 [99] [8, 206]. Rhenium supported on alumina was also examined as a catalyst for dry reforming of methane. At higher temperatures, above 973 K, Re was, in fact, more active than Ir for the dry reforming reaction at stoichiometric $CO_2:CH_4$ ratios. However, the activity of Re catalyst decreased severely at lower temperatures. At about 873 K, methane conversion was less than 5% [145]. Apart from group VIII metals, other metal systems were recently used for dry methane reforming with CO_2. A manganese-based catalyst gave high yields of synthesis gas without carbon deposition detected at 1200 K. However; this catalyst has considerably lower activity than the group VIII metals [146].

1.5.2 Bimetallic catalyst

Given the attempt to improve catalyst activity and stability, chemical additives are found to be a useful approach whether applied as a bimetallic or as a promoter. Traditionally, hydrocarbon reforming reactions are carried out over the transition from single metal (also known as monometallic) catalysts. The idea of bimetallic systems to catalysis reforming was initially introduced by Sinfelt [241] were two metal clusters (also identified as crystallites) within a similar metallic group are combined and dispersed on the support and the reaction occurs on these metals as described in **Figure 1.1.4**
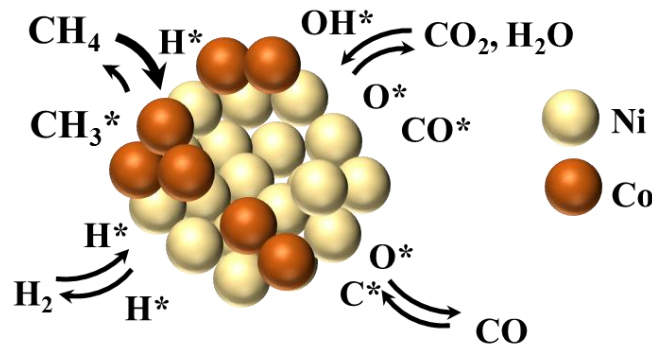
Figure 1.1.4 Schematic diagram for methane dry reforming reaction step over a bimetallic cluster of Co-Ni.

Several studies reported an improvement in catalytic performance and stability by using a bimetallic catalyst in dry reforming reaction compared to monometallic catalysts [48,49,66,147-149]. According to Sinfelt, the number of current metal atoms in a cluster and the dispersion properties of the bimetallic catalysts are comparable to the monometallic catalysts [150]. Different justifications for the role of the second metal in bimetallic catalysts are listed below [151,152]:

- ❖ *Modification of electronic properties of active metal particles.* It was hypothesized that the altered electronic attributes result in weaker bond strength between active species and carbon atom during adsorption of hydrocarbon [153].

- ❖ *Dilution of the active metal surface into smaller entities.* Since carbon deposition is increased in the presence of large clusters, the second metal addition resulted in shrinkage in the metal surface into smaller ensembles whereas the carbon lay-down process slowed [154].

- ❖ *Providing sites for hydrogenation of coke deposits.* It is recognized that some metals display a better tendency for carbon gasification [155,156].

❖ *Decreasing the solubility of carbon within the metal lattice.* The addition of a second metal featured with lower solubility than nickel (e.g., noble metals) minimizes the rate of carbon formation [152].

Likewise, the concept of promoter addition was also utilized to improve catalyst resilience towards deactivation whereas a small quantity (<5wt%) of metal or metal oxide is added to the metal–support matrix. Promoters are often classified into two types: textural or chemical. In general, textural promoters facilitate the preparation of well-dispersed catalytic phases, which are maintained during the reaction. However, chemical promoters employed in the commercial application of reforming, including alkali and alkaline earth metals or metal oxides, improve the activity of reactions [14]. This concept was initially employed under methane dry reforming by Siri et al. [157]. **Table 1.2** shows the conventional additives for a Ni based catalyst under dry reforming reaction to improve syngas production and minimize carbon deposition. Most of the studies were based on Ni catalysts and particularly under alumina support as it is the preferred support for reforming processes.

Table 1. 2 Main promoters of Ni catalyst utilized under dry reforming.

Promoter	Support	References
Ni-K	Al_2O_3	[105], [158]
Ni-Sn	Al_2O_3	[103]
Ni-Mn	Al_2O_3	[103,159]
Ni-Ca	Al_2O_3	[103]
Ni-Co	Al_2O_3	[160,161]
Ni-Ce	Al_2O_3	[162]
Ni-Cu	Al_2O_3	[163]
Ni-Fe	Al_2O_3	[162]
Rh-Ni	Boron nitride	[148]
Ni-Cu	SiO_2	[164,165]
Rh-Ni	SiO_2	[147]
Rh-Ni	MgO	[166]
Rh-Ni	La_2O_3	[167]
Ni-M		[168]

Ni-Ca	M = (Co, Fe, Cu, or Mn)	[169]
Ni-Ce	Al-Mg-O	[170]
Ni-Co	ZrO_2	[171]
Fe-Ni	Mixed oxide	[172,173]
Ni-Sr	CeO_2	[174,175]
	$MgAl_2O_4$	
	SiO_2, Al_2O_3	

1.5.3 Crystalline catalysts

An alternative to conventional supported catalysts is crystalline oxide catalysts. As advantages, a portion of these materials exhibits improved oxygen mobility, which catalyzes the reaction and diminishes carbon deposition. A further advantage of crystalline oxide catalysts is that they regularly inhibit the sintering of active metals isolated in the lattice and some cases require a lower overall concentration of active metals (which reduces overall catalyst cost). Crystalline oxides considered for reforming reactions are spinel, perovskites, pyrochlores, fluorites, and hexaaluminates.

1.5.3.1 Spinel catalyst

The spinel-type oxides (chemical formula: $A^{2+}B^{3+}_2O_4$) have attracted considerable scientific and technological interest due to their unique properties and diverse practical applications [176-178]. where A is generally divalent cations occupying tetrahedral sites, and B are trivalent cations occupying octahedral sites available in the crystal lattice, thereby improving their redox and catalysis properties. In inverse spinel oxides, half of B occupy the tetrahedral sites, and the formula is altered to $B(AB)O_4$. Accordingly, Ni^{2+} ions can be substituted at the A site cation positions.
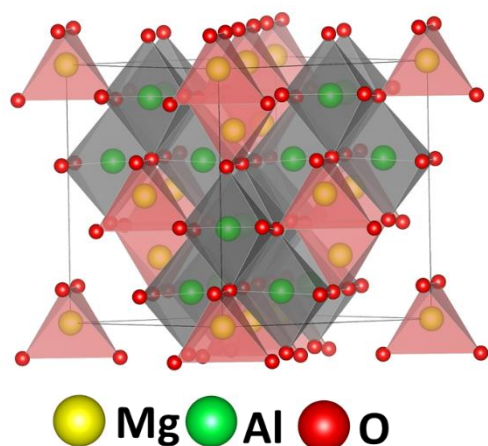
Figure 1.1.5 Crystalline structure of $MgAl_2O_4$ spinel compound. Yellow spheres represent Mg-atom, green spheres represent Al-atoms, and red spheres represent O-atoms.

Table 1. 3 Previous reported spinel catalyst for dry reforming

Spinel	Support	Reference
$MgAl_2O_4$	Al_2O_3	[179]
$CuX_2O_4(X = Fe, Mn, Al, La)$	Al_2O_3	[180]
$CuFe_2O_4$	SiO_2	[181]
$CuFe_2O_4$	Al_2O_3	[182]
$CuAl_2O_4$	Al_2O_3	[183]
$FeAl_2O_4$	SBA-15 silica	[184]
$NiFe_2O_4$	-	[185]
$NiAl_2O_4$	Al_2O_3–YSZ	[186]

Metals located in the A lattice position are 6-coordinate, while B metal is 4-coordinate (see **Figure 1.1.5**). These oxides are arranged in the form of a cubic unit cell in an Fd-3m space group. Several spinel oxides have been synthesized for use as catalysts in the dry reforming reaction $CaAl_2O_4$, $MgAl_2O_4$, $CuAl_2O_4$, $CuFe_2O_4$ and $CuCr_2O_4$ and iron spinel oxides [187]. Guo et al. reported that the $MgAl_2O_4$ spinel layer that formed over Ni/MgO-Al_2O_3 can effectively suppress the phase transformation to form $NiAl_2O_4$ spinel phases and can stabilize the tiny Ni crystallite which exhibits stable performance without any deactivation and stability. Shimoda et al. [182] revealed that the new active phase of Cu–Fe–AlO_4 was formed through the solid-state reaction

24

between $CuFe_2O_4$ spinel and γ-Al_2O_3, prompting the improvement of the catalytic performance. The pre-reduction drives the aluminum molecules migrated to the spinel structure by mean solid-state reactions, and after the new Cu–Fe–AlO_4 spinel phase formed, resulting in the high catalytic activity. Benrabaa et al. detailed that the nickel ferrite ($NiFe_2O_4$) spinel catalyst demonstrated the significant activity and restrained the carbon formation due to the formation Ni-Fe alloy by decomposition of the spinel structure. The Ni metallic species in this alloy could prevent their surface sintering and prevent the coke formation. Ye et al. and Valente et al. [188,189] respectively have synthesized Mg-M-Al (M = Fe, Cu, Ni) catalysts acquired from hydrotalcites as precursors. After calcination of the catalyst to obtain spinel oxides, the properties of the oxides, such as high metal dispersion, extensive surface area and porosity, and excellent thermal stability, resulted in better catalytic behaviors. Andressa et al. [184] examined the nanostructured MAl_2O_4 with the substitution of various metals M = Cu, Ni, Fe or Mg of spinel for dehydrogenation of ethylbenzene with CO_2. The results demonstrate that the $FeAl_2O_4$ catalyst provides the best catalytic activity among others due to the continuous oxidation of Fe^{3+} sites by the CO_2 from the reaction.

1.5.3.2 Perovskite catalyst

The Perovskite-types are ABO_3 type crystal structured materials with alkaline earth or rare earth metal at the A-site and a transition metal at the B-site [190]. In the perfect frame, the crystal structure of cubic ABX_3 perovskite can be described as consisting of corner-sharing $[BX_6]$ octahedra with the A cation occupying the 12-fold coordination site formed in the middle of the cube of eight such octahedra. These have some energizing chemical and physical properties, e.g., high thermal stability, the excellent reactivity of lattice oxygen, low cost and abundant resources [191]. A-site replacement with alkaline earth metal is expected to enhance the carbon susceptible

and thermal stability, and the B-site alteration is expected to increase the activity of the catalyst [192,193].
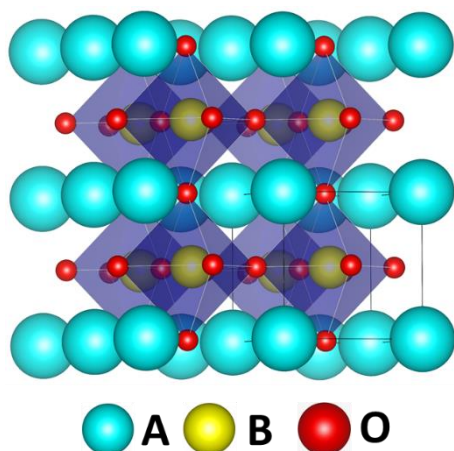
Figure 1.1.6 Crystal structure of perfect perovskite compound. Blue spheres represent A-cation, yellow spheres represent B-cation, and red spheres represent O-atoms.

In last decade, numerous researchers have been broadly reported $LaNiO_3$, [194-196] $LaFeO_3$, [197] $SmCoO_3$ [198]and likewise partial substitution of B- site perovskite catalysts demonstrate the higher activity, stability, and resistance to coke formation even at elevated temperature. It increases the syngas production in dry reforming reaction [199-201]. Batiot-Dupeyrat et al.[202] used $LaNiO_3$ as catalyst precursor for the CO_2 reforming of methane. The reaction was studied by a pulse technique using a CH_4/CO_2 ratio close to unity. The author proposed the mechanism involving the partial re-oxidation of La_2O_3 and Ni^0 by CO_2 followed by reduction back to La_2O_3 and Ni^0 by CH_4. Goldwasser et al. [199] studied $Ln_{1-x}Ca_xRu_{0.8}Ni_{0.2}O_3$ (Ln = La, Sm, Nd) perovskites synthesized by a modified citrate method. These perovskites were first reduced at 700 °C, to obtain nominal compositions of (Ru, Ni)/CaO and La_2O_3, Sm_2O_3, Nd_2O_3, before the catalytic tests. The authors observed Sm containing perovskites to be the best among the lanthanide series. In the case of Sr-substituted $LaNiO_3$ perovskites synthesized by the auto combustion method, it was observed that catalytic activity depends on Sr content

26

($LaNiO_3$>$La_{0.6}Sr_{0.4}NiO_3$>Ni(5 %)/La_2O_3>$La_{0.9}Sr_{0.1}NiO_3$). The $SrCO_3$ and $La_2O_2CO_3$ phases formed during the reaction were proposed to be responsible for the lack of carbon deposition. These studies were performed using the pulse technique[201].

1.6 Catalyst support

1.6.1 Effect of support

Choosing the right support in heterogeneous catalysis in industrial applications is an essential concern in order to avoid deactivation by sintering, though protecting the catalyst structure from damage at the high temperature required for reforming processes [223]. **Table 1.4** demonstrates the effect of support on the catalytic activity under dry reforming reaction. Also, it can be seen that most of the support comparative studies were conducted for Group VIII metals. For noble metals, it is generally accepted that alumina provides excellent support under dry reforming. Nakamura et al. reported that the impact of support on catalytic selectivity was in the following order: Al_2O_3>TiO_2>SiO_2 in perspective of CH_4 and CO_2 conversion. The researchers considered that the significant effect of support might be a direct result of an activation of CH_4 or CO_2 by metal oxides and the variation of particle size of the metal. As well, Rh metals over various supports were examined for propane dry reforming by Solymosi et al. [66]; they reported that the activity order decreased as Al_2O_3>TiO_2>MgO>SiO_2 while it was verified by several authors [76][203] that a Ni catalyst based on Al_2O_3 is more active than when supported on SiO_2, Swaan et al. [204] indicated that the activity order for Ni based catalyst deceased as supported by SiO_2>ZrO_2>La_2O_3>MgO>TiO_2. Consequently, it can be concluded that alumina is favored support for a Ni catalyst. Notwithstanding, for a bimetallic catalyst such as Ni-Pd the strength of reactivity was positioned according to the support used followed by the decreasing order ZrO_2–La_2O_3, La_2O_3 >ZrO_2>SiO_2>Al_2O_3>TiO_2 [49]. On the other hand, Nakagawa et al. [205] investigated the effect

of support material in nickel-based catalysts for steam reforming of CH_4. The methane conversion in decreasing order is Al_2O_3>oxidized diamond Y_2O_3>TiO_2>MgO>SiO_2>La_2O_3.

Table 1. 4 Effect of support on catalyst activity for dry reforming

Activity Order	Temperature (K)	Metal loading (Wt%)	Reference
Ru			
Al_2O_3>TiO_2>SiO_2	893	0.5	[139]
Pd			
TiO_2>Al_2O_3>NaY>SiO_2>			
MgO>Na-ZSM-5	773	5	[206]
TiO_2>Al_2O_3>SiO_2>MgO	773	1	[207]
Rh			
Al_2O_3>TiO_2>MgO>SiO_2	923	1	[79]
Ni			
Al_2O_3>SiO_2	800-1000	40	[208]
NaY>Al_2O_3>SiO_2	873	2	[203]
SiO_2>ZrO_2>La_2O_3>MgO>TiO_2	823	4	[204]

Alumina generally has a higher thermal and mechanical stability and rich chemistry. The oxides of alumina exist in different structures, but only three phases are of interest; namely the non-porous, crystallographically ordered α-Al_2O_3 and the porous amorphous n and γ-Al_2O_3 [223]. The most typical catalyst for the reforming reaction is Ni/Al_2O_3 due to its low cost and high turnover frequency [209]. Although, Al_2O_3 has some limitations in application. It is available in the form of pellets. These offer significant mass transfer limitations due to the relatively large size of the packing bodies (typically 1-10 mm). Generally, these sizes cannot be smaller otherwise the reactor would suffer essential pressure drops. Moreover, the chaotic distribution of the liquid in the void space of the catalytic bed might create dead zones, channeling and/or flow maldistribution which can directly affect conversion and selectivity. However, the catalyst loading can be very high, leading to high reaction rates per volume reactor [2, 18].

1.6.2 Structured support

To circumvent the disadvantages of the conventional reactors, structured catalytic systems at both micro- and meso- levels rise as an excellent alternative. Structured reactors not only enhance the reaction rates by suppressing mass and heat transfer limitations but also simplify the fluid mechanics and the scaling up [210].

(A)   **(B)**
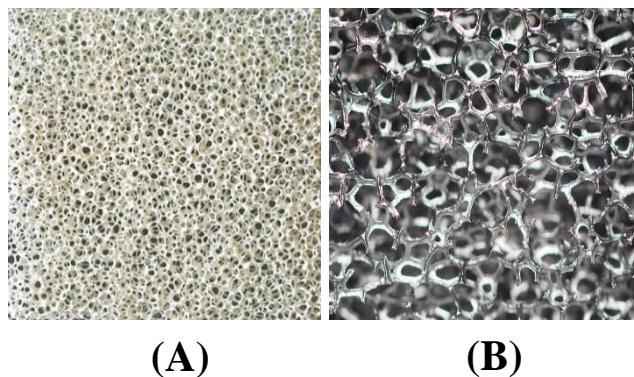
Figure 1.1.7 Photographic images of commercial foam (A) alumina foam (B) nickel foam

Solid foams consist of three-dimensional networks of connected strands containing interconnected pores (**Figure 1.1.7**). This material mimics to some degree the inverse structure of packed bed made of dense spheres [210]. Strictly speaking, foams are not structured reactors since they do not present regularity. However, they exhibit features that are typical for those types of the reactor such as high and uniform accessibility to the catalytic active sites, and low pressure drops. Recently, the use of solid foams has increased due to their different possible applications as heat exchangers, chemical inert packings, and catalyst support [211]. They can be made of a wide variety of materials, namely, ceramics, metals, carbon and silicon carbide. Foams exhibit a very high porosity (97-98%) but low specific surface areas, which are similar to those of monoliths (lower than 4 $m^2 . g^{-1}$). Hence, in this work, the alumina foam and nickel foam were used as catalyst support for DRP.

1.7 The scope of this present work

As a result, the principal goal of this study was to improve the dry reforming process through two main strategies, namely: design of a crystalline catalyst for carbon-resilient, and reactor operations to minimize online catalyst activity decay. The catalyst of choice was Fe and Sr based crystalline compound while C_3H_8 was the hydrocarbon substrate. The selection was motivated by the need to ensure that any benefits arising from the new initiative would have immediate commercial appeal, since crystalline catalyst is the key ingredient in industrial reforming catalysts, while C_3H_8 is a major constituent of natural gas and gaseous effluents from petroleum processing, offering a higher propensity to carbon deposition than CH_4 under typical reforming conditions. According to the literature survey, rare earth crystalline oxides widely utilized that are generally preferred for reforming reaction, due to acceptable activity combined with low price and availability. Also, alumina (Al_2O_3) was commonly used as the support for catalysts because of its high surface area, low cost, and thermal stability. In the attempt to improve this catalyst, the synthesis of spinel catalyst such as iron ceriate could have excellent anti-coking buoyancy and stability and could enhance the thermal attributes of support.

Specifically, the objectives of this thesis are as follows:

❖ To synthesis novel crystalline spinel and perovskite catalysts ($FeCe_2O_4$ and $SrNiO_3$) by sol-gel method citric acid as a chelating agent.

❖ The $FeCe_2O_4$ spinel crystalline catalyst of alumina foam used as a catalyst in dry reforming reaction. To prepared $SrNiO_3$ with Al_2O_3 and nickel foam catalyst for dry reforming propane.

❖ To investigate and analyze the crystalline phase analysis, surface morphology and elemental identifications of prepared samples by the X-ray diffraction (XRD), Raman

spectroscopy, X-ray photoelectron spectroscopy (XPS) and Field emission electron microscopy (FE-SEM).

❖ To characterize the catalysts, structural properties of prepared samples for the surface area using Brunauer Emmett Teller (BET) method, for bulk metallic reduction using Temperature programmed reduction (TPR) and for surface activity using temperature programmed desorption (TPD).

❖ To examine the effect of spinel and perovskite catalyst with mesopores supports to understand the variation in physicochemical attributes, the crystallite of spinel and perovskite features

❖ Investigate the effect of $FeCe_2O_4$ and $SrNiO_3$ on syngas production and carbon formation under propane dry reforming reaction in a fixed-bed reactor.

❖ Examine the beneficial of $FeCe_2O_4$ and $SrNiO_3$ promotion through deactivation of catalyst studies over longevity runs to examine the carbon inhibition.

❖ To conduct post-mortem characterizations for spent catalysts, performed to identify and match the variations in the catalysts with observed reaction characteristics. Study the influence of propane dry reforming on the production of syngas and catalyst deactivation.

❖ To characterize the carbon deposited on the surface of catalysts after dry reforming propane by XPS, Raman, FE-SEM, and Temperature programmed oxidation(TPO).

1.8 Reference

1. Rostrup-Nielsen, J.R. New aspects of syngas production and use. *Catalysis Today* **2000**, *63*, 159-164.
2. Wilhelm, D.J.; Simbeck, D.R.; Karp, A.D.; Dickenson, R.L. Syngas production for gas-to-liquids applications: Technologies, issues and outlook. *Fuel Processing Technology* **2001**, *71*, 139-148.
3. Pen˜a, M.A.; Gómez, J.P.; Fierro, J.L.G. New catalytic routes for syngas and hydrogen production. *Applied Catalysis A: General* **1996**, *144*, 7-57.
4. Fischer, F.; Tropsch, H. Conversion of methane into hydrogen and carbon monoxide. *Brennst. Chem.* **1928**, *3*.

5. Bartholomew, C.H. Mechanisms of catalyst deactivation. *Applied Catalysis A: General* **2001**, *212*, 17-60.

6. Forzatti, P.; Lietti, L. Catalyst deactivation. *Catalysis Today* **1999**, *52*, 165-181.

7. Moulijn, J.A.; van Diepen, A.E.; Kapteijn, F. Catalyst deactivation: Is it predictable?: What to do? *Applied Catalysis A: General* **2001**, *212*, 3-16.

8. Bartholomew, C.H.; Pannell, R.B.; Fowler, R.W. Sintering of alumina-supported nickel and nickel bimetallic methanation catalysts in H_2H_2O atmospheres. *Journal of Catalysis* **1983**, *79*, 34-46.

9. Furimsky, E.; Massoth, F.E. Deactivation of hydroprocessing catalysts. *Catalysis Today* **1999**, *52*, 381-495.

10. Ross, J.R.H.; van Keulen, A.N.J.; Hegarty, M.E.S.; Seshan, K. The catalytic conversion of natural gas to useful products. *Catalysis Today* **1996**, *30*, 193-199.

11. Rostrup-Nielsen, J.R. Linking science, and industrial catalysis. *Topics in Catalysis* **1994**, *1*, 377-382.

12. Wurzel, T.; Malcus, S.; Mleczko, L. Reaction engineering investigations of CO_2 reforming in a fluidized-bed reactor. *Chemical Engineering Science* **2000**, *55*, 3955-3966.

13. Bradford, M.C.J.; Vannice, M.A. CO_2 reforming of CH_4. *Catalysis Reviews* **1999**, *41*, 1-42.

14. Fan, M.S.; Abdullah Ahmad, Z.; Bhatia, S. Catalytic technology for carbon dioxide reforming of methane to synthesis gas. *ChemCatChem* **2009**, *1*, 192-208.

15. Budiman, A.W.; Song, S.-H.; Chang, T.-S.; Shin, C.-H.; Choi, M.-J. Dry reforming of methane over cobalt catalysts: A literature review of catalyst development. *Catalysis Surveys from Asia* **2012**, *16*, 183-197.

16. Serrano-Lotina, A.; Daza, L. Long-term stability test of Ni-based catalyst in carbon dioxide reforming of methane. *Applied Catalysis A: General* **2014**, *474*, 107-113.

17. Frontera, P.; Macario, A.; Aloise, A.; Crea, F.; Antonucci, P.L.; Nagy, J.B.; Frusteri, F.; Giordano, G. Catalytic dry-reforming on Ni–zeolite supported catalyst. *Catalysis Today* **2012**, *179*, 52-60.

18. Wang, N.; Shen, K.; Huang, L.; Yu, X.; Qian, W.; Chu, W. Facile route for synthesizing ordered mesoporous Ni–Ce–Al oxide materials and their catalytic performance for methane dry reforming to hydrogen and syngas. *ACS Catalysis* **2013**, *3*, 1638-1651.

19. Olafsen, A.; Daniel, C.; Schuurman, Y.; Råberg, L.B.; Olsbye, U.; Mirodatos, C. Light alkanes CO_2 reforming to synthesis gas over ni based catalysts. *Catalysis Today* **2006**, *115*, 179-185.

20. Pino, L.; Vita, A.; Cipitì, F.; Laganà, M.; Recupero, V. Performance of Pt/CeO_2 catalyst for propane oxidative steam reforming. *Applied Catalysis A: General* **2006**, *306*, 68-77.

21. Faria, W.L.S.; Dieguez, L.C.; Schmal, M. Autothermal reforming of propane for hydrogen production over Pd/CeO_2/Al_2O_3 catalysts. *Applied Catalysis B: Environmental* **2008**, *85*, 77-85.

22. Hardiman, K.M.; Ying, T.T.; Adesina, A.A.; Kennedy, E.M.; Dlugogorski, B.Z. Performance of a Co-Ni catalyst for propane reforming under low steam-to-carbon ratios. *Chemical Engineering Journal* **2004**, *102*, 119-130.

23. Råberg, L.B.; Jensen, M.B.; Olsbye, U.; Daniel, C.; Haag, S.; Mirodatos, C.; Sjåstad, A.O. Propane dry reforming to synthesis gas over Ni-based catalysts: Influence of support and operating parameters on catalyst activity and stability. *Journal of Catalysis* **2007**, *249*, 250-260.

24. Mok, Y.S.; Jwa, E.; Hyun, Y.J. Regeneration of C_4H_{10} dry reforming catalyst by nonthermal plasma. *Journal of Energy Chemistry* **2013**, *22*, 394-402.

25. Laosiripojana, N.; Sangtongkitcharoen, W.; Assabumrungrat, S. Catalytic steam reforming of ethane and propane over CeO_2-doped Ni/Al_2O_3 at SOFC temperature: Improvement of resistance toward carbon formation by the redox property of doping CeO_2. *Fuel* **2006**, *85*, 323-332.

26. Zyryanova, M.M.; Snytnikov, P.V.; Shigarov, A.B.; Belyaev, V.D.; Kirillov, V.A.; Sobyanin, V.A. Low-temperature catalytic steam reforming of propane–methane mixture into methane-rich gas: Experiment and macrokinetic modeling. *Fuel* **2014**, *135*, 76-82.

27. Moon, K.; Kale, G.R. Energy analysis in combined reforming of propane. *Journal of Engineering* **2013**, *2013*, 1-10.

28. Karuppiah, J.; Mok, Y.S. Plasma-reduced Ni/γ–Al_2O_3, and CeO_2–Ni/γ–Al_2O_3 catalysts for improving dry reforming of propane. *International Journal of Hydrogen Energy* **2014**, *39*, 16329-16338.

29. Shah, Y.T.; Gardner, T.H. Dry reforming of hydrocarbon feedstocks. *Catalysis Reviews* **2014**, *56*, 476-536.

30. Siahvashi, A.; Chesterfield, D.; Adesina, A.A. Propane CO_2 (dry) reforming over bimetallic Mo–Ni/Al$_2$O$_3$ catalyst. *Chemical Engineering Science* **2013**, *93*, 313-325.

31. Althenayan, F.M.; Yei Foo, S.; Kennedy, E.M.; Dlugogorski, B.Z.; Adesina, A.A. Bimetallic Co–Ni/Al$_2$O$_3$ catalyst for propane dry reforming: Estimation of reaction metrics from longevity runs. *Chemical Engineering Science* **2010**, *65*, 66-73.

32. Rakib, M.A.; Grace, J.R.; Lim, C.J.; Elnashaie, S.S.E.H.; Ghiasi, B. Steam reforming of propane in a fluidized bed membrane reactor for hydrogen production. *International Journal of Hydrogen Energy* **2010**, *35*, 6276-6290.

33. Prettre, M.; Eichner, C.; Perrin, M. The catalytic oxidation of methane to carbon monoxide and hydrogen. *Transactions of the Faraday Society* **1946**, *42*, 335b-339.

34. Dias, J.A.C.; Assaf, J.M. Autothermal reforming of methane over Ni/γ-Al$_2$O$_3$ promoted with pd: The effect of the Pd source in activity, temperature profile of reactor and in ignition. *Applied Catalysis A: General* **2008**, *334*, 243-250.

35. Gao, J.; Guo, J.; Liang, D.; Hou, Z.; Fei, J.; Zheng, X. Production of syngas via autothermal reforming of methane in a fluidized-bed reactor over the combined CeO$_2$–ZrO$_2$/SiO$_2$ supported ni catalysts. *International Journal of Hydrogen Energy* **2008**, *33*, 5493-5500.

36. De Groote, A.M.; Froment, G.F. Simulation of the catalytic partial oxidation of methane to synthesis gas. *Applied Catalysis A: General* **1996**, *138*, 245-264.

37. Lim, S.-S.; Lee, H.-J.; Moon, D.-J.; Kim, J.-H.; Park, N.-C.; Shin, J.-S.; Kim, Y.-C. Autothermal reforming of propane over ce modified Ni/LaAlO$_3$ perovskite-type catalysts. *Chemical Engineering Journal* **2009**, *152*, 220-226.

38. Zeng, G.; Tian, Y.; Li, Y. Thermodynamic analysis of hydrogen production for fuel cell via oxidative steam reforming of propane. *International Journal of Hydrogen Energy* **2010**, *35*, 6726-6737.

39. Rafiq, M.H.; Hustad, J.E. Biosyngas production by autothermal reforming of waste cooking oil with propane using a plasma-assisted gliding arc reactor. *International Journal of Hydrogen Energy* **2011**, *36*, 8221-8233.

40. Burra, K.G.; Gupta, A.K. Sorption enhanced steam reforming of propane using calcium looping. **2017**, V001T004A046.

41. Çağlayan, B.S.; Avcı, A.K.; Önsan, Z.İ.; Aksoylu, A.E. Production of hydrogen over bimetallic Pt–Ni/δ-Al$_2$O$_3$: I. Indirect partial oxidation of propane. *Applied Catalysis A: General* **2005**, *280*, 181-188.

42. Nematollahi, B.; Rezaei, M.; Khajenoori, M. Combined dry reforming and partial oxidation of methane to synthesis gas on noble metal catalysts. *International Journal of Hydrogen Energy* **2011**, *36*, 2969-2978.

43. Tsyganok, A.I.; Inaba, M.; Tsunoda, T.; Suzuki, K.; Takehira, K.; Hayakawa, T. Combined partial oxidation and dry reforming of methane to synthesis gas over noble metals supported on Mg–Al mixed oxide. *Applied Catalysis A: General* **2004**, *275*, 149-155.

44. Wang, W.; Stagg-Williams, S.M.; Noronha, F.B.; Mattos, L.V.; Passos, F.B. Partial oxidation and combined reforming of methane on Ce-promoted catalysts. *Catalysis Today* **2004**, *98*, 553-563.

45. Ayabe, S.; Omoto, H.; Utaka, T.; Kikuchi, R.; Sasaki, K.; Teraoka, Y.; Eguchi, K. Catalytic autothermal reforming of methane and propane over supported metal catalysts. *Applied Catalysis A: General* **2003**, *241*, 261-269.

46. Crisafulli, C.; Scirè, S.; Maggiore, R.; Minicò, S.; Galvagno, S. CO_2 reforming of methane over ni–ru and Ni–Pd bimetallic catalysts. *Catalysis Letters* **1999**, *59*, 21-26.

47. Dry, M.E. The fischer–tropsch process: 1950–2000. *Catalysis Today* **2002**, *71*, 227-241.

48. Hu, Y.H. Advances in catalysts for CO_2 reforming of methane. In *Advances in CO$_2$ conversion and utilization*, American Chemical Society: 2010; Vol. 1056, pp 155-174.

49. Steinhauer, B.; Kasireddy, M.R.; Radnik, J.; Martin, A. Development of ni-pd bimetallic catalysts for the utilization of carbon dioxide and methane by dry reforming. *Applied Catalysis A: General* **2009**, *366*, 333-341.

50. Qian, L.; Yue, B.; Pei, S.; Zhang, L.; Ye, L.; Cheng, J.; Tsang Shik, C.; He, H. Reforming of CH_4 with CO_2 over Rh/H-beta: Effect of rhodium dispersion on the catalytic activity and coke resistance. *Chinese Journal of Chemistry* **2010**, *28*, 1864-1870.

51. Corthals, S.; Van Nederkassel, J.; De Winne, H.; Geboers, J.; Jacobs, P.; Sels, B. Design of active and stable $NiCeO_2ZrO_2MgAl_2O_4$ dry reforming catalysts. *Applied Catalysis B: Environmental* **2011**, *105*, 263-275.

52. Ağbaba, M.; Levent, M.; Şahin, Y. Production of synthesis gases from catalytic steam reforming of ethanol and propane processes. In *Progress in clean energy, volume 2: Novel systems and applications*, Dincer, I.; Colpan, C.O.; Kizilkan, O.; Ezan, M.A., Eds. Springer International Publishing: Cham, 2015; pp 525-538.

53. Goula, M.A.; Charisiou, N.D.; Papageridis, K.N.; Delimitis, A.; Pachatouridou, E.; Iliopoulou, E.F. Nickel on alumina catalysts for the production of hydrogen rich mixtures via the biogas dry reforming reaction: Influence of the synthesis method. *International Journal of Hydrogen Energy* **2015**, *40*, 9183-9200.

54. Charisiou, N.D.; Siakavelas, G.; Papageridis, K.N.; Baklavaridis, A.; Tzounis, L.; Avraam, D.G.; Goula, M.A. Syngas production via the biogas dry reforming reaction over nickel supported on modified with CeO_2 and/or La_2O_3 alumina catalysts. *Journal of Natural Gas Science and Engineering* **2016**, *31*, 164-183.

55. Wang, F.; Xu, L.; Zhang, J.; Zhao, Y.; Li, H.; Li, H.X.; Wu, K.; Xu, G.Q.; Chen, W. Tuning the metal-support interaction in catalysts for highly efficient methane dry reforming reaction. *Applied Catalysis B: Environmental* **2016**, *180*, 511-520.

56. Sumrunronnasak, S.; Tantayanon, S.; Kiatgamolchai, S.; Sukonket, T. Improved hydrogen production from dry reforming reaction using a catalytic packed-bed membrane reactor with Ni-based catalyst and dense PdAgCu alloy membrane. *International Journal of Hydrogen Energy* **2016**, *41*, 2621-2630.

57. Benguerba, Y.; Dehimi, L.; Virginie, M.; Dumas, C.; Ernst, B. Numerical investigation of the optimal operative conditions for the dry reforming reaction in a fixed-bed reactor: Role of the carbon deposition and gasification reactions. *Reaction Kinetics, Mechanisms and Catalysis* **2015**, *115*, 483-497.

58. Usman, M.; Wan Daud, W.M.A.; Abbas, H.F. Dry reforming of methane: Influence of process parameters—a review. *Renewable and Sustainable Energy Reviews* **2015**, *45*, 710-744.

59. Ruckenstein, E.; Wang, H.Y. Carbon dioxide reforming of methane to synthesis gas over supported cobalt catalysts. *Applied Catalysis A: General* **2000**, *204*, 257-263.

60. Farina, G.L.; Supp, E. Produce syngas for methanol. *Hydrocarbon Processing* **1992**, *71*, 77-79.

61. Mondal, K.; Sasmal, S.; Badgandi, S.; Chowdhury, D.R.; Nair, V. Dry reforming of methane to syngas: A potential alternative process for value added chemicals—a techno-economic perspective. *Environmental Science and Pollution Research* **2016**, *23*, 22267-22273.

62. Portillo, M.A.; Perales, A.L.V.; Vidal-Barrero, F.; Campoy, M. A kinetic model for the synthesis of ethanol from syngas and methanol over an alkali-Co doped molybdenum sulfide catalyst: Model building and validation at bench scale. *Fuel Processing Technology* **2016**, *151*, 19-30.

63. Edwards, J.H.; Do, K.T.; Maitra, A.M.; Schuck, S.; Fok, W.; Stein, W. The use of solar-based CO_2/CH_4 reforming for reducing greenhouse gas emissions during the generation of electricity and process heat. *Energy Conversion and Management* **1996**, *37*, 1339-1344.

64. Michorczyk, P.; Ogonowski, J. Dehydrogenation of propane in the presence of carbon dioxide over oxide-based catalysts. *Reaction Kinetics and Catalysis Letters* **2003**, *78*, 41-47.

65. Alenazey, F.; Cooper, C.G.; Dave, C.B.; Elnashaie, S.S.E.H.; Susu, A.A.; Adesina, A.A. Coke removal from deactivated Co–Ni steam reforming catalyst using different gasifying agents: An analysis of the gas–solid reaction kinetics. *Catalysis Communications* **2009**, *10*, 406-411.

66. San-José-Alonso, D.; Juan-Juan, J.; Illán-Gómez, M.J.; Román-Martínez, M.C. Ni, Co and bimetallic Ni–Co catalysts for the dry reforming of methane. *Applied Catalysis A: General* **2009**, *371*, 54-59.

67. Kim, D.K.; Maier, W.F. Combinatorial discovery of new autoreduction catalysts for the CO_2 reforming of methane. *Journal of Catalysis* **2006**, *238*, 142-152.

68. Cimenti, M.; Hill, J.M. Thermodynamic analysis of solid oxide fuel cells operated with methanol and ethanol under direct utilization, steam reforming, dry reforming or partial oxidation conditions. *Journal of Power Sources* **2009**, *186*, 377-384.

69. Lanzini, A.; Leone, P.; Guerra, C.; Smeacetto, F.; Brandon, N.P.; Santarelli, M. Durability of anode supported solid oxides fuel cells (SOFC) under direct dry-reforming of methane. *Chemical Engineering Journal* **2013**, *220*, 254-263.

70. Qian, L.; Yan, Z.F. *Studies on adsorption and dissociation of methane and carbon dioxide on nickel catalyst*. 2002; Vol. 11, p 151-158.

71. Guo, J.; Hou, Z.; Zheng, X. Autothermal reforming of CH_4 and C_3H_8 to syngas in a fluidized-bed reactor. *Chinese Journal of Catalysis* **2010**, *31*, 1115-1121.

72. Souza, M.d.M.V.M.; Clavé, L.; Dubois, V.; Perez, C.A.C.; Schmal, M. Activation of supported nickel catalysts for carbon dioxide reforming of methane. *Applied Catalysis A: General* **2004**, *272*, 133-139.

73. Liu, S.; Xiong, G.; Yang, W.; Xu, L.; Xiong, G.; Li, C. Partial oxidation of ethane to syngas over nickel-based catalysts modified by alkali metal oxide and rare earth metal oxide. *Catalysis Letters* **1999**, *63*, 167-171.

74. Sehested, J. Four challenges for nickel steam-reforming catalysts. *Catalysis Today* **2006**, *111*, 103-110.

75. Lebouvier, A.; Iwarere, S.A.; d'Argenlieu, P.; Ramjugernath, D.; Fulcheri, L. Assessment of carbon dioxide dissociation as a new route for syngas production: A comparative review and potential of plasma-based technologies. *Energy & Fuels* **2013**, *27*, 2712-2722.

76. <perrys.Chemical.Engineers.Handbook.7th.Ed.Eboo.Pdf>.

77. Olafsen, A.; Slagtern, Å.; Dahl, I.M.; Olsbye, U.; Schuurman, Y.; Mirodatos, C. Mechanistic features for propane reforming by carbon dioxide over a Ni/Mg(Al)O hydrotalcite-derived catalyst. *Journal of Catalysis* **2005**, *229*, 163-175.

78. Solymosi, F.; Tolmacsov, P. Decomposition of propane and its reactions with CO_2 over alumina-supported Pt metals. *Catalysis Letters* **2002**, *83*, 183-186.

79. Solymosi, F.; Tolmacsov, P.; Kedves, K. CO_2 reforming of propane over supported Rh. *Journal of Catalysis* **2003**, *216*, 377-385.

80. Solymosi, F.; Tolmacsov, P.; Zakar, T.S. Dry reforming of propane over supported Re catalyst. *Journal of Catalysis* **2005**, *233*, 51-59.

81. Sutton, D.; Moisan, J.-F.; Ross, J.R.H. Kinetic study of CO_2 reforming of propane over Ru/Al_2O_3. *Catalysis Letters* **2001**, *75*, 175-181.

82. Karuppiah, J.; Linga Reddy, E.; Mok, Y. Anodized aluminum oxide supported $NiO-CeO_2$ catalyst for dry reforming of propane. *Catalysts* **2016**, *6*, 154.

83. Malaibari, Z.O.; Croiset, E.; Amin, A.; Epling, W. Effect of interactions between ni and mo on catalytic properties of a bimetallic $Ni-Mo/Al_2O_3$ propane reforming catalyst. *Applied Catalysis A: General* **2015**, *490*, 80-92.

84. Siahvashi, A.; Adesina, A.A. Synthesis gas production via propane dry (CO_2) reforming: Influence of potassium promotion on bimetallic $Mo-Ni/Al_2O_3$. *Catalysis Today* **2013**, *214*, 30-41.

85. Wang, X.; Wang, N.; Zhao, J.; Wang, L. Thermodynamic analysis of propane dry and steam reforming for synthesis gas or hydrogen production. *International Journal of Hydrogen Energy* **2010**, *35*, 12800-12807.

86. <(chemical engineers handbook) don green, robert perry-perry's chemical engineers' handbook-mcgraw-hill professional (2007).Pdf>.

87. Jensen, M.B.; Råberg, L.B.; Olafsen Sjåstad, A.; Olsbye, U. Mechanistic study of the dry reforming of propane to synthesis gas over a Ni/Mg(Al)O catalyst. *Catalysis Today* **2009**, *145*, 114-120.

88. Slagtern, A.; Schuurman, Y.; Leclercq, C.; Verykios, X.; Mirodatos, C. Specific features concerning the mechanism of methane reforming by carbon dioxide over Ni/La_2O_3 catalyst. *Journal of Catalysis* **1997**, *172*, 118-126.

89. Tsipouriari, V.A.; Verykios, X.E. Kinetic study of the catalytic reforming of methane with carbon dioxide to synthesis gas over Ni/La_2O_3 catalyst. *Catalysis Today* **2001**, *64*, 83-90.

90. Verykios, X.E. Catalytic dry reforming of natural gas for the production of chemicals and hydrogen. *International Journal of Hydrogen Energy* **2003**, *28*, 1045-1063.

91. Li, X.; Li, D.; Tian, H.; Zeng, L.; Zhao, Z.-J.; Gong, J. Dry reforming of methane over Ni/La_2O_3 nanorod catalysts with stabilized ni nanoparticles. *Applied Catalysis B: Environmental* **2017**, *202*, 683-694.

92. Daza, C.E.; Gallego, J.; Mondragón, F.; Moreno, S.; Molina, R. High stability of Ce-promoted Ni/Mg–Al catalysts derived from hydrotalcites in dry reforming of methane. *Fuel* **2010**, *89*, 592-603.

93. Pechimuthu, N.A.; Pant, K.K.; Dhingra, S.C.; Bhalla, R. Characterization and activity of k, CeO_2, and mn promoted Ni/Al_2O_3 catalysts for carbon dioxide reforming of methane. *Industrial & Engineering Chemistry Research* **2006**, *45*, 7435-7443.

94. Amin, R.; Liu, B.S.; Zhao, Y.C.; Huang, Z.B. Hydrogen production by corncob/CO_2 dry reforming over CeO_2 modified Ni-based MCM-22 catalysts. *International Journal of Hydrogen Energy* **2016**, *41*, 12869-12879.

95. Hassani Rad, S.J.; Haghighi, M.; Alizadeh Eslami, A.; Rahmani, F.; Rahemi, N. Sol–gel vs. Impregnation preparation of MgO and CeO_2 doped Ni/Al_2O_3 nanocatalysts used in dry reforming of methane: Effect of process conditions, synthesis method and support composition. *International Journal of Hydrogen Energy* **2016**, *41*, 5335-5350.

96. Abasaeed, A.E.; Al-Fatesh, A.S.; Naeem, M.A.; Ibrahim, A.A.; Fakeeha, A.H. Catalytic performance of CeO_2 and ZrO_2 supported Co catalysts for hydrogen production via dry reforming of methane. *International Journal of Hydrogen Energy* **2015**, *40*, 6818-6826.

97. Inui, T. Reforming of CH_4 by CO_2, O_2 and/or H_2O. In *Catalysis: Volume 16*, Spivey, J.J., Ed. The Royal Society of Chemistry: 2002; Vol. 16, pp 133-154.

98. Wang, S.; Lu, G.Q. Role of CeO_2 in Ni/CeO_2–Al_2O_3 catalysts for carbon dioxide reforming of methane. *Applied Catalysis B: Environmental* **1998**, *19*, 267-277.

99. Rostrupnielsen, J.R.; Hansen, J.H.B. CO_2-reforming of methane over transition metals. *Journal of Catalysis* **1993**, *144*, 38-49.

100. Tsipouriari, V.A.; Efstathiou, A.M.; Verykios, X.E. Transient kinetic study of the oxidation and hydrogenation of carbon species formed during CH_4/He, CO_2/He, and CH_4/CO_2 reactions over Rh/Al_2O_3 catalyst. *Journal of Catalysis* **1996**, *161*, 31-42.

101. Kim, J.-H.; Suh, D.J.; Park, T.-J.; Kim, K.-L. Effect of metal particle size on coking during CO_2 reforming of CH_4 over Ni–alumina aerogel catalysts. *Applied Catalysis A: General* **2000**, *197*, 191-200.

102. Cui, Y.; Zhang, H.; Xu, H.; Li, W. Kinetic study of the catalytic reforming of CH_4 with CO_2 to syngas over Ni/α-Al_2O_3 catalyst: The effect of temperature on the reforming mechanism. *Applied Catalysis A: General* **2007**, *318*, 79-88.

103. Castro Luna, A.E.; Iriarte, M.E. Carbon dioxide reforming of methane over a metal modified Ni-Al_2O_3 catalyst. *Applied Catalysis A: General* **2008**, *343*, 10-15.

104. Barroso-Quiroga, M.M.; Castro-Luna, A.E. Catalytic activity and effect of modifiers on Ni-based catalysts for the dry reforming of methane. *International Journal of Hydrogen Energy* **2010**, *35*, 6052-6056.

105. Juan-Juan, J.; Román-Martínez, M.C.; Illán-Gómez, M.J. Effect of potassium content in the activity of K-promoted Ni/Al_2O_3 catalysts for the dry reforming of methane. *Applied Catalysis A: General* **2006**, *301*, 9-15.

106. Juan-Juan, J.; Román-Martínez, M.C.; Illán-Gómez, M.J. Nickel catalyst activation in the carbon dioxide reforming of methane: Effect of pretreatments. *Applied Catalysis A: General* **2009**, *355*, 27-32.

107. Wang, S.; Lu, G.Q. Catalytic activities and coking characteristics of oxides-supported Ni catalysts for CH_4 reforming with carbon dioxide. *Energy & Fuels* **1998**, *12*, 248-256.

108. Tsipouriari, V.A.; Verykios, X.E. Carbon and oxygen reaction pathways of CO_2 reforming of methane over Ni/La_2O_3 and Ni/Al_2O_3 catalysts studied by isotopic tracing techniques. *Journal of Catalysis* **1999**, *187*, 85-94.

109. Zhang, Z.; Verykios, X.E.; MacDonald, S.M.; Affrossman, S. Comparative study of carbon dioxide reforming of methane to synthesis gas over Ni/La_2O_3 and conventional nickel-based catalysts. *The Journal of Physical Chemistry* **1996**, *100*, 744-754.
110. Gronchi, P.; Centola, P.; Rosso, R.D. Dry reforming of CH_4 with ni and rh metal catalysts supported on SiO_2 and La_2O_3. *Applied Catalysis A: General* **1997**, *152*, 83-92.
111. Ruckenstein, E.; Hu, Y.H. Interactions between ni and La_2O_3 in Ni/La_2O_3 catalysts prepared using different ni precursors. *Journal of Catalysis* **1996**, *161*, 55-61.
112. Valentini, A.; Carreño, N.L.V.; Probst, L.F.D.; Barison, A.; Ferreira, A.G.; Leite, E.R.; Longo, E. $Ni:CeO_2$ nanocomposite catalysts prepared by polymeric precursor method. *Applied Catalysis A: General* **2006**, *310*, 174-182.
113. Pompeo, F.; Nichio, N.N.; Souza, M.M.V.M.; Cesar, D.V.; Ferretti, O.A.; Schmal, M. Study of ni and pt catalysts supported on $\alpha-Al_2O_3$ and ZrO_2 applied in methane reforming with CO_2. *Applied Catalysis A: General* **2007**, *316*, 175-183.
114. Rezaei, M.; Alavi, S.M.; Sahebdelfar, S.; Yan, Z.-F. Nanocrystalline zirconia as support for nickel catalyst in methane reforming with CO_2. *Energy & Fuels* **2006**, *20*, 923-929.
115. Zhang, Q.-H.; Li, Y.; Xu, B.-Q. Reforming of methane and coalbed methane over nanocomposite Ni/ZrO_2 catalyst. *Catalysis Today* **2004**, *98*, 601-605.
116. Ruckenstein, E.; Hang Hu, Y. Role of support in CO_2 reforming of CH_4 to syngas over Ni catalysts. *Journal of Catalysis* **1996**, *162*, 230-238.
117. Hao, Z.; Zhu, Q.; Jiang, Z.; Li, H. Fluidization characteristics of aerogel Co/Al_2O_3 catalyst in a magnetic fluidized bed and its application to $CH_4–CO_2$ reforming. *Powder Technology* **2008**, *183*, 46-52.
118. Hou, Z.; Yashima, T. Supported Co catalysts for methane reforming with CO_2. *Reaction Kinetics and Catalysis Letters* **2004**, *81*, 153-159.
119. Bouarab, R.; Cherifi, O.; Auroux, A. Reforming of methane by CO_2 in presence of cobalt- based catalysts. *Green Chemistry* **2003**, *5*, 209-212.
120. Wang, H.Y.; Ruckenstein, E. CO_2 reforming of CH_4 over Co/MgO solid solution catalysts — effect of calcination temperature and Co loading. *Applied Catalysis A: General* **2001**, *209*, 207-215.
121. Nagaoka, K.; Takanabe, K.; Aika, K.-i. Influence of the reduction temperature on catalytic activity of Co/TiO_2 (anatase-type) for high pressure dry reforming of methane. *Applied Catalysis A: General* **2003**, *255*, 13-21.
122. Djaidja, A.; Messaoudi, H.; Kaddeche, D.; Barama, A. Study of Ni–M/MgO and Ni–M–Mg/Al (M=Fe or Cu) catalysts in the $CH_4–CO_2$ and $CH_4–H_2O$ reforming. *International Journal of Hydrogen Energy* **2015**, *40*, 4989-4995.
123. Tsoukalou, A.; Imtiaz, Q.; Kim, S.M.; Abdala, P.M.; Yoon, S.; Müller, C.R. Dry-reforming of methane over bimetallic $Ni–M/La_2O_3$ (M=Co,Fe): The effect of the rate of $La_2O_2Co_3$ formation and phase stability on the catalytic activity and stability. *Journal of Catalysis* **2016**, *343*, 208-214.
124. Hou, Z.; Chen, P.; Fang, H.; Zheng, X.; Yashima, T. Production of synthesis gas via methane reforming with CO_2 on noble metals and small amount of noble-(Rh-) promoted Ni catalysts. *International Journal of Hydrogen Energy* **2006**, *31*, 555-561.
125. Stevens, R.W.; Chuang, S.S.C. In situ ir study of transient CO_2 reforming of CH_4 over Rh/Al_2O_3. *The Journal of Physical Chemistry B* **2004**, *108*, 696-703.
126. Verykios, X.E. Mechanistic aspects of the reaction of CO_2 reforming of methane over Rh/Al_2O_3 catalyst. *Applied Catalysis A: General* **2003**, *255*, 101-111.
127. Yokota, S.; Okumura, K.; Niwa, M. Strong inhibition effect of sulfur impurities in alumina supports on the catalytic activity of rh in the $CH_4–CO_2$ reforming reaction. *Applied Catalysis A: General* **2006**, *310*, 122-126.
128. Múnera, J.F.; Irusta, S.; Cornaglia, L.M.; Lombardo, E.A.; Vargas Cesar, D.; Schmal, M. Kinetics and reaction pathway of the CO_2 reforming of methane on Rh supported on lanthanum-based solid. *Journal of Catalysis* **2007**, *245*, 25-34.

129. Ballarini, A.D.; de Miguel, S.R.; Jablonski, E.L.; Scelza, O.A.; Castro, A.A. Reforming of CH₄ with CO₂ on Pt-supported catalysts: Effect of the support on the catalytic behaviour. *Catalysis Today* **2005**, *107-108*, 481-486.

130. Mattos, L.V.; Rodino, E.; Resasco, D.E.; Passos, F.B.; Noronha, F.B. Partial oxidation and CO₂ reforming of methane on Pt/Al₂O₃, Pt/ZrO₂, and Pt/Ce–ZrO₂ catalysts. *Fuel Processing Technology* **2003**, *83*, 147-161.

131. O'Connor, A.M.; Schuurman, Y.; Ross, J.R.H.; Mirodatos, C. Transient studies of carbon dioxide reforming of methane over Pt/ZrO₂ and Pt/Al₂O₃. *Catalysis Today* **2006**, *115*, 191-198.

132. Souza, M.M.V.M.; Aranda, D.A.G.; Schmal, M. Coke formation on Pt/ZrO₂/Al₂O₃ catalysts during CH₄ reforming with CO₂. *Industrial & Engineering Chemistry Research* **2002**, *41*, 4681-4685.

133. Bradford, M.C.J.; Vannice, M.A. CO₂ reforming of CH₄ over supported pt catalysts. *Journal of Catalysis* **1998**, *173*, 157-171.

134. Yang, M.; Papp, H. CO₂ reforming of methane to syngas over highly active and stable Pt/MgO catalysts. *Catalysis Today* **2006**, *115*, 199-204.

135. Bitter, J.H.; Seshan, K.; Lercher, J.A. The state of zirconia supported platinum catalysts for CO₂/CH₄ reforming. *Journal of Catalysis* **1997**, *171*, 279-286.

136. van Keulen, A.N.J.; Seshan, K.; Hoebink, J.H.B.J.; Ross, J.R.H. Tap investigations of the CO₂ reforming of CH₄ over Pt/ZrO₂. *Journal of Catalysis* **1997**, *166*, 306-314.

137. Mark, M.F.; Maier, W.F. CO₂-reforming of methane on supported Rh and Ir catalysts. *Journal of Catalysis* **1996**, *164*, 122-130.

138. Mark Michael, F.; Maier Wilhelm, F.; Mark, F. Reaction kinetics of the CO₂ reforming of methane. *Chemical Engineering & Technology* **2004**, *20*, 361-370.

139. Nakagawa, K.; Anzai, K.; Matsui, N.; Ikenaga, N.; Suzuki, T.; Teng, Y.; Kobayashi, T.; Haruta, M. Effect of support on the conversion of methane to synthesis gas over supported iridium catalysts. *Catalysis Letters* **1998**, *51*, 163-167.

140. Schulz, P.G.; Gonzalez, M.G.; Quincoces, C.E.; Gigola, C.E. Methane reforming with carbon dioxide. The behavior of Pd/α-Al₂O₃ and Pd−CeOₓ/α-Al₂O₃ catalysts. *Industrial & Engineering Chemistry Research* **2005**, *44*, 9020-9029.

141. Matsui, N.-o.; Anzai, K.; Akamatsu, N.; Nakagawa, K.; Ikenaga, N.-o.; Suzuki, T. Reaction mechanisms of carbon dioxide reforming of methane with Ru-loaded lanthanum oxide catalyst. *Applied Catalysis A: General* **1999**, *179*, 247-256.

142. Ferreira-Aparicio, P.; Rodríguez-Ramos, I.; Anderson, J.A.; Guerrero-Ruiz, A. Mechanistic aspects of the dry reforming of methane over ruthenium catalysts. *Applied Catalysis A: General* **2000**, *202*, 183-196.

143. Carrara, C.; Múnera, J.; Lombardo, E.A.; Cornaglia, L.M. Kinetic and stability studies of Ru/La₂O₃ used in the dry reforming of methane. *Topics in Catalysis* **2008**, *51*, 98-106.

144. Solymosi, F.; Kutsán, G.; Erdöhelyi, A. Catalytic reaction of CH₄ with CO₂ over alumina-supported pt metals. *Catalysis Letters* **1991**, *11*, 149-156.

145. Claridge, J.B.; Green, M.L.H.; Tsang, S.C. Methane conversion to synthesis gas by partial oxidation and dry reforming over rhenium catalysts. *Catalysis Today* **1994**, *21*, 455-460.

146. Mirzabekova, S.R.; Mamedov, A.K.; Aliev, V.S.; Krylov, O.V. Conversion of C₁−C₂ alkanes over manganese catalysts reoxidized by carbon dioxide and oxygen. *Reaction Kinetics and Catalysis Letters* **1992**, *47*, 159-166.

147. Jóźwiak, W.K.; Nowosielska, M.; Rynkowski, J. Reforming of methane with carbon dioxide over supported bimetallic catalysts containing Ni and noble metal: I. Characterization and activity of SiO₂ supported Ni–Rh catalysts. *Applied Catalysis A: General* **2005**, *280*, 233-244.

148. Wu, J.C.S.; Chou, H.-C. Bimetallic Rh–Ni/BN catalyst for methane reforming with CO₂. *Chemical Engineering Journal* **2009**, *148*, 539-545.

149. Zhang, J.; Wang, H.; Dalai, A.K. Effects of metal content on activity and stability of Ni-Co bimetallic catalysts for CO₂ reforming of CH₄. *Applied Catalysis A: General* **2008**, *339*, 121-129.

150. Sinfelt, J.H. Role of surface science in catalysis. *Surface Science* **2002**, *500*, 923-946.

151. Macleod, N.; Fryer, J.R.; Stirling, D.; Webb, G. Deactivation of bi- and multimetallic reforming catalysts: Influence of alloy formation on catalyst activity. *Catalysis Today* **1998**, *46*, 37-54.

152. Bartholomew, C.H.; Weatherbee, G.D.; Jarvi, G.A. Effects of carbon deposits on the specific activity of nickel and nickel bimetallic catalysts. *Chemical Engineering Communications* **1980**, *5*, 125-134.

153. Burch, R.; Garla, L.C. Platinum-tin reforming catalysts: II. Activity and selectivity in hydrocarbon reactions. *Journal of Catalysis* **1981**, *71*, 360-372.

154. Coq, B.; Figueras, F. Conversion of methylcyclopentane on platinum-tin reforming catalysts. *Journal of Catalysis* **1984**, *85*, 197-205.

155. Parera, J.M.; Beltramini, J.N. Stability of bimetallic reforming catalysts. *Journal of Catalysis* **1988**, *112*, 357-365.

156. Carter, J.L.; McVinker, G.B.; Weissman, W.; Kmak, M.S.; Sinfelt, J.H. Bimetallic catalysts; application in catalytic reforming. *Applied Catalysis* **1982**, *3*, 327-346.

157. Siri, G.J.; Marchetti, G.S.; Ferretti, O.A.; Gonzalez, M.G. Sulfur poisoning of Mo-promoted ni catalysts. In *Studies in surface science and catalysis*, Bartholomew, C.H.; Butt, J.B., Eds. Elsevier: 1991; Vol. 68, pp 531-537.

158. Osaki, T.; Mori, T. Role of potassium in carbon-free CO_2 reforming of methane on K-promoted Ni/Al_2O_3 catalysts. *Journal of Catalysis* **2001**, *204*, 89-97.

159. Fakeeha, A.H.; Naeem, M.A.; Khan, W.U.; Abasaeed, A.E.; Al-Fatesh, A.S. Reforming of methane by CO_2 over bimetallic Ni-Mn/γ-Al_2O_3 catalyst. *Chinese Journal of Chemical Physics* **2014**, *27*, 214-220.

160. Djinović, P.; Osojnik Črnivec, I.G.; Erjavec, B.; Pintar, A. Influence of active metal loading and oxygen mobility on coke-free dry reforming of Ni–Co bimetallic catalysts. *Applied Catalysis B: Environmental* **2012**, *125*, 259-270.

161. Foo, S.Y.; Cheng, C.K.; Nguyen, T.-H.; Adesina, A.A. Kinetic study of methane CO_2 reforming on Co–Ni/Al_2O_3 and Ce–Co–Ni/Al_2O_3 catalysts. *Catalysis Today* **2011**, *164*, 221-226.

162. Halliche, D.; Bouarab, R.; Cherifi, O.; Bettahar, M.M. Carbon dioxide reforming of methane on modified Ni/α-$A1_2O_3$ catalysts. *Catalysis Today* **1996**, *29*, 373-377.

163. Tuan, A.L.; Luong, T.N.; Ishihara, N.K. Low-temperature catalytic performance of Ni-Cu/Al_2O_3 catalysts for gasoline reforming to produce hydrogen applied in spark ignition engines. *Catalysts* **2016**, *6*.

164. Michalkiewicz, B.; Sreńscek-Nazzal, J.; Ziebro, J. Optimization of synthesis gas formation in methane reforming with carbon dioxide. *Catalysis Letters* **2009**, *129*, 142-148.

165. Carrero, A.; Calles, A.J.; García-Moreno, L.; Vizcaíno, J.A. Production of renewable hydrogen from glycerol steam reforming over bimetallic Ni-(Cu,Co,Cr) catalysts supported on SBA-15 silica. *Catalysts* **2017**, *7*.

166. Chen, Y.-g.; Tomishige, K.; Yokoyama, K.; Fujimoto, K. Promoting effect of Pt, Pd and Rh noble metals to the $Ni_{0.03}Mg_{0.97}O$ solid solution catalysts for the reforming of CH_4 with CO_2. *Applied Catalysis A: General* **1997**, *165*, 335-347.

167. Irusta, S.; Cornaglia, L.M.; Lombardo, E.A. Hydrogen production using Ni–Rh on La_2O_3 as potential low-temperature catalysts for membrane reactors. *Journal of Catalysis* **2002**, *210*, 7-16.

168. Zhang, J.; Wang, H.; Dalai, A.K. Development of stable bimetallic catalysts for carbon dioxide reforming of methane. *Journal of Catalysis* **2007**, *249*, 300-310.

169. Liu, H.; Li, S.; Zhang, S.; Wang, J.; Zhou, G.; Chen, L.; Wang, X. Catalytic performance of novel Ni catalysts supported on SiC monolithic foam in carbon dioxide reforming of methane to synthesis gas. *Catalysis Communications* **2008**, *9*, 51-54.

170. Kim, D.K.; Stöwe, K.; Müller, F.; Maier, W.F. Mechanistic study of the unusual catalytic properties of a new nice mixed oxide for the CO_2 reforming of methane. *Journal of Catalysis* **2007**, *247*, 101-111.

171. Luisetto, I.; Tuti, S.; Di Bartolomeo, E. Co and Ni supported on CeO_2 as selective bimetallic catalyst for dry reforming of methane. *International Journal of Hydrogen Energy* **2012**, *37*, 15992-15999.

172. Theofanidis, S.A.; Galvita, V.V.; Poelman, H.; Marin, G.B. Enhanced carbon-resistant dry reforming Fe-Ni catalyst: Role of Fe. *ACS Catalysis* **2015**, *5*, 3028-3039.

173. Medeiros, R.L.B.A.; Macedo, H.P.; Melo, V.R.M.; Oliveira, Â.A.S.; Barros, J.M.F.; Melo, M.A.F.; Melo, D.M.A. Ni supported on Fe-doped $MgAl_2O_4$ for dry reforming of methane: Use of factorial design to optimize H_2 yield. *International Journal of Hydrogen Energy* **2016**, *41*, 14047-14057.

174. Jing, Q.S.; Fei, J.H.; Lou, H.; Mo, L.Y.; Zheng, X.M. Effective reforming of methane with CO_2 and O_2 to low H_2/CO ratio syngas over $Ni/MgO–SiO_2$ using fluidized bed reactor. *Energy Conversion and Management* **2004**, *45*, 3127-3137.

175. Ibrahim, A.A.; Fakeeha, A.H.; Al-Fatesh, A.S. Enhancing hydrogen production by dry reforming process with strontium promoter. *International Journal of Hydrogen Energy* **2014**, *39*, 1680-1687.

176. Sun, G.; Sun, L.; Wen, H.; Jia, Z.; Huang, K.; Hu, C. From layered double hydroxide to spinel nanostructures: Facile synthesis and characterization of nanoplatelets and nanorods. *The Journal of Physical Chemistry B* **2006**, *110*, 13375-13380.

177. Fierro, G.; Ferraris, G.; Dragone, R.; Lo Jacono, M.; Faticanti, M. H_2 reduction behavior and NO/N_2O abatement catalytic activity of manganese based spinels doped with copper, cobalt and iron ions. *Catalysis Today* **2006**, *116*, 38-49.

178. Muraleedharan Nair, M.; Kaliaguine, S. Structured catalysts for dry reforming of methane. *New J. Chem.* **2016**, *40*, 4049-4060.

179. Guo, J.; Lou, H.; Zhao, H.; Zheng, X. Improvement of stability of out-layer $MgAl_2O_4$ spinel for a $Ni/MgAl_2O_4/Al_2O_3$ catalyst in dry reforming of methane. *Reaction Kinetics and Catalysis Letters* **2005**, *84*, 93-100.

180. Huang, Y.-H.; Wang, S.-F.; Tsai, A.-P.; Kameoka, S. Reduction behaviors and catalytic properties for methanol steam reforming of Cu-based spinel compounds CuX_2O_4 (X=Fe, Mn, Al, La). *Ceramics International* **2014**, *40*, 4541-4551.

181. Kameoka, S.; Tanabe, T.; Tsai, A.P. Self-assembled porous nano-composite with high catalytic performance by reduction of tetragonal spinel $CuFe_2O_4$. *Applied Catalysis A: General* **2010**, *375*, 163-171.

182. Shimoda, N.; Faungnawakij, K.; Kikuchi, R.; Fukunaga, T.; Eguchi, K. Catalytic performance enhancement by heat treatment of $CuFe_2O_4$ spinel and γ-alumina composite catalysts for steam reforming of dimethyl ether. *Applied Catalysis A: General* **2009**, *365*, 71-78.

183. Matsukata, M.; Uemiya, S.; Kikuchi, E. Copper–alumina spinel catalysts for steam reforming of methanol. *Chemistry Letters* **1988**, *17*, 761-764.

184. Batista, A.H.d.M.; Ramos, F.S.O.; Braga, T.P.; Lima, C.L.; de Sousa, F.F.; Barros, E.B.D.; Filho, J.M.; Oliveira, A.S.d.; Sousa, J.R.d.; Valentini, A.*, et al.* Mesoporous MAl_2O_4 (M=Cu, Ni, Fe or Mg) spinels: Characterisation and application in the catalytic dehydrogenation of ethylbenzene in the presence of CO_2. *Applied Catalysis A: General* **2010**, *382*, 148-157.

185. Chamoumi, M.; Abatzoglou, N. $NiFe_2O_4$ production from $α-Fe_2O_3$ via improved solid state reaction: Application as catalyst in CH_4 dry reforming. *The Canadian Journal of Chemical Engineering* **2016**, *94*, 1801-1808.

186. Achouri, I.E.; Abatzoglou, N.; Fauteux-Lefebvre, C.; Braidy, N. Diesel steam reforming: Comparison of two nickel aluminate catalysts prepared by wet-impregnation and co-precipitation. *Catalysis Today* **2013**, *207*, 13-20.

187. Benrabaa, R.; Boukhlouf, H.; Löfberg, A.; Rubbens, A.; Vannier, R.N.; Bordes-Richard, E.; Barama, A. Nickel ferrite spinel as catalyst precursor in the dry reforming of methane: Synthesis, characterization and catalytic properties. *Journal of Natural Gas Chemistry* **2012**, *21*, 595-604.

188. Ye, X.; Ma, N.; Hua, W.; Yue, Y.; Miao, C.; Xie, Z.; Gao, Z. Dehydrogenation of ethylbenzene in the presence of CO_2 over catalysts prepared from hydrotalcite-like precursors. *Journal of Molecular Catalysis A: Chemical* **2004**, *217*, 103-108.

189. Valente, J.S.; Hernandez-Cortez, J.; Cantu, M.S.; Ferrat, G.; López-Salinas, E. Calcined layered double hydroxides Mg–Me–Al (Me: Cu, Fe, Ni, Zn) as bifunctional catalysts. *Catalysis Today* **2010**, *150*, 340-345.

190. Crystallography and chemistry of perovskites. In *Handbook of magnetism and advanced magnetic materials*.

191. Yamazoe, N.; Teraoka, Y. Oxidation catalysis of perovskites --- relationships to bulk structure and composition (valency, defect, etc.). *Catalysis Today* **1990**, *8*, 175-199.

192. Mawdsley, J.R.; Krause, T.R. Rare earth-first-row transition metal perovskites as catalysts for the autothermal reforming of hydrocarbon fuels to generate hydrogen. *Applied Catalysis A: General* **2008**, *334*, 311-320.

193. Dinka, P.; Mukasyan, A.S. Perovskite catalysts for the auto-reforming of sulfur containing fuels. *Journal of Power Sources* **2007**, *167*, 472-481.

194. Gallego, G.S.; Mondragón, F.; Barrault, J.; Tatibouët, J.-M.; Batiot-Dupeyrat, C. CO_2 reforming of CH_4 over La–Ni based perovskite precursors. *Applied Catalysis A: General* **2006**, *311*, 164-171.

195. Chawl, S.K.; George, M.; Patel, F.; Patel, S. Production of synthesis gas by carbon dioxide reforming of methane over nickel based and perovskite catalysts. *Procedia Engineering* **2013**, *51*, 461-466.

196. Nair, M.M.; Kaliaguine, S.; Kleitz, F. Nanocast $LaNiO_3$ perovskites as precursors for the preparation of coke-resistant dry reforming catalysts. *ACS Catalysis* **2014**, *4*, 3837-3846.

197. Kondakindi, R.R.; Kundu, A.; Karan, K.; Peppley, B.A.; Qi, A.; Thurgood, C.; Schurer, P. Characterization and activity of perovskite catalysts for autothermal reforming of dodecane. *Applied Catalysis A: General* **2010**, *390*, 271-280.

198. Osazuwa, O.U.; Setiabudi, H.D.; Rasid, R.A.; Cheng, C.K. Syngas production via methane dry reforming: A novel application of $SmCoO_3$ perovskite catalyst. *Journal of Natural Gas Science and Engineering* **2017**, *37*, 435-448.

199. Goldwasser, M.R.; Rivas, M.E.; Pietri, E.; Pérez-Zurita, M.J.; Cubeiro, M.L.; Gingembre, L.; Leclercq, L.; Leclercq, G. Perovskites as catalysts precursors: CO_2 reforming of CH_4 on $Ln_{1-x}Ca_x Ru_{0.8}Ni_{0.2}O_3$ (Ln = La, Sm, Nd). *Applied Catalysis A: General* **2003**, *255*, 45-57.

200. Pichas, C.; Pomonis, P.; Petrakis, D.; Ladavos, A. Kinetic study of the catalytic dry reforming of CH_4 with CO_2 over $La_{2-x}Sr_xNiO_4$ perovskite-type oxides. *Applied Catalysis A: General* **2010**, *386*, 116-123.

201. Valderrama, G.; Kiennemann, A.; Goldwasser, M.R. La-Sr-Ni-Co-O based perovskite-type solid solutions as catalyst precursors in the CO_2 reforming of methane. *Journal of Power Sources* **2010**, *195*, 1765-1771.

202. Batiot-Dupeyrat, C.; Gallego, G.A.S.; Mondragon, F.; Barrault, J.; Tatibouët, J.-M. CO_2 reforming of methane over $LaNiO_3$ as precursor material. *Catalysis Today* **2005**, *107-108*, 474-480.

203. Kim, G.J.; Cho, D.-S.; Kim, K.-H.; Kim, J.-H. The reaction of CO_2 with CH_4 to synthesize H_2 and co over nickel-loaded y-zeolites. *Catalysis Letters* **1994**, *28*, 41-52.

204. Swaan, H.M.; Kroll, V.C.H.; Martin, G.A.; Mirodatos, C. Deactivation of supported nickel catalysts during the reforming of methane by carbon dioxide. *Catalysis Today* **1994**, *21*, 571-578.

205. Nakagawa, K.; Kajita, C.; Ikenaga, N.-o.; Nishitani-Gamo, M.; Ando, T.; Suzuki, T. Dehydrogenation of light alkanes over oxidized diamond-supported catalysts in the presence of carbon dioxide. *Catalysis Today* **2003**, *84*, 149-157.

206. Masai, M.; Kado, H.; Miyake, A.; Nishiyama, S.; Tsuruya, S. Methane reforming by carbon dioxide and steam over supported Pd, Pt, and Rh catalysts. In *Studies in surface science and catalysis*, Bibby, D.M.; Chang, C.D.; Howe, R.F.; Yurchak, S., Eds. Elsevier: 1988; Vol. 36, pp 67-71.

207. Erdöhelyi, A.; Cserényi, J.; Papp, E.; Solymosi, F. Catalytic reaction of methane with carbon dioxide over supported palladium. *Applied Catalysis A: General* **1994**, *108*, 205-219.

208. Takano, A.; Tagawa, T.; Goto, S. Carbon dioxide reforming of methane on supported nickel catalysts. *JOURNAL OF CHEMICAL ENGINEERING OF JAPAN* **1994**, *27*, 727-731.

209. Zhang, Y.; Xiong, G.; Sheng, S.; Yang, W. Deactivation studies over $NiO/\gamma-Al_2O_3$ catalysts for partial oxidation of methane to syngas. *Catalysis Today* **2000**, *63*, 517-522.

210. Gascon, J.; van Ommen, J.R.; Moulijn, J.A.; Kapteijn, F. Structuring catalyst and reactor - an inviting avenue to process intensification. *Catalysis Science & Technology* **2015**, *5*, 807-817.

211. Zhang, W.; Zhang, B.; Shi, Z. Study on hydrodynamic performance and mass transfer efficiency of nickel foam packing. *Procedia Engineering* **2011**, *18*, 271-276.

CHAPTER -2

Materials and methods

2.1 Introduction

This chapter narrates a list of chemicals, gases, experimental methods and the characterization techniques, which are adapted for the present investigation. To achieve research objective, the experimental work was done in the laboratory, followed by physicochemical characterization and evaluation of the catalytic properties of the obtained materials.

2.2 Materials

2.2.1 Chemicals

Table 2.1 displays the list of chemicals used in this study along with respective grades and were used without any further purification and their applications.

Table 2. 1 Specifications of chemicals used in this study

Chemical	Formula	Grade/Purity/ Conc.	Application	Supplier
γ-alumina	Al_2O_3		Catalysts preparation	Alfa-Aser
α – alumina	Al_2O_3	Industrial	Catalysts preparation	
Nickel foam	Ni	-	Catalysts preparation	MTI Crop., Ltd., Korea
Nickel Nitrate hexahydrate	$Ni(NO_3)_2 \cdot 6H2O$	> 98 %	Catalysts preparation	Daejung Chemicals & Metals Co. Ltd, Korea
Iron nitrate monohydrate	$Fe(NO_3)_2 \cdot 9H_2O$	> 98 %	Catalysts preparation	Daejung Chemicals & Metals Co. Ltd, Korea
Cerium nitrate hexahydrate	$Ce(NO_3)_2 \cdot 9H_2O$	> 98 %	Catalysts preparation	Junsei Chemical Co. Ltd. Japan
Strontium nitrate	$Sr(NO_3)_2$	> 99 %	Catalysts preparation	Junsei Chemical Co. Ltd. Japan
Citric acid	$C_6H_8O_7$	> 98 %	Catalysts preparation	Daejung Chemicals & Metals Co. Ltd, Korea
Hydrochloric acid	HCl	35%	Catalysts preparation	Daejung Chemicals & Metals Co. Ltd, Korea

제주대학교 중앙도서관
JEJU NATIONAL UNIVERSITY LIBRARY

Polyvinylidene fluoride (PVDF)	$(CH_2CF_2)n$	-	Catalysts preparation	Sigma Aldrich
N-Methyl-2-pyrrolidinone (NMP)	C_5H_9NO	99.7%	Catalysts preparation	Daejung Chemicals & Metals Co. Ltd, Korea
Ethanol	CH_3CH_2OH	99.9%	Catalysts preparation	Fisher Scientific
Acetone	C_3H_6O	99.8%	Catalysts preparation	Fisher Scientific

2.2.2 Gases

Gases used in the investigation, including their purities and applications, are tabulated in Table 3.2. All gases were supplied by Coregas (Australia) gases, except propane which was provided by BOC (Australia).

Table 2. 2 Specifications and applications of gases

Gas	Purity	Application
C_3H_8	99.9%	Reactant & GC calibration
CO_2	99.0%	Reactant & GC calibration
Ar	99.99%	Carrier gas for DRP, H_2-TPD, H_2-TPR
N_2	99.99%	Carrier gas for O_2-TPO
O_2	99.99%	Reactant gas for O_2-TPO
Ar	99.999%	GC carrier gas
He	99.999%	GC carrier gas
H_2	99.99%	GC calibration, reactant gas for H_2-TPR & reduction
10%H_2/Ar	10% H_2 in Ar balance	H_2-TPR, H_2-TPD, and reduction
10%O_2/N_2	10% O_2 in N_2 balance	TPO
10%C_3H_8/30%CO_2/Ar	10% C_3H_8,30% CO_2 in Ar balance	Catalytic studies

2.3 Apparatus

Table 2. 3 General equipment used for the material preparation and catalytic studies

Apparatus	Model or specifications	Manufacturer
Hotplate & Magnetic stirrer	MGH-320	SIBATA
Oven	OF-02 GW	ISUZU
Furnace	DFT -50300	DH Science
Balance	DRAGON 204/5	Mettler Toledo
Gas chromatography	Micro-GC- Varian (CP-490)	Agilent
	DS-6200	DS science
FT-IR spectroscopy	FT-IR 7600	Lambda

2.4 Catalyst synthesis

The physicochemical properties of a catalyst have a significant role in determining reaction performance as well as reactor choice, and therefore the hidden aspects of its origin should be carefully treated to obtain an excellent activity [1-3]. However, moderately minor consideration is given to recognize the characteristic of catalyst preparation scientifically [3]. Miniature modification in the preparation conditions often has a remarkable influence on the ultimate catalyst characteristics [2]. Therefore, considerable attention was appropriately paid to the steps for catalyst preparation.

2.4.1 Sol-gel method

Sol-gel approach is one important technique that has many advantages, such as low cost, low-temperature processing, high purity products [4-6]. This method was specifically chosen since it produces a uniform substitution of metal into the crystal lattice [7]. All catalyst was prepared by a citrate sol-gel method [8,9]. Briefly, nitrate salts of precursors were mixed in distilled water (DW). The aqueous mixture of metal nitrates was then mixed with an aqueous citric acid solution. The citric acid: metal molar ratio was maintained at 1:1. The solution was then heated to ~80°C

and simultaneously stirred. This process ensured metal complexation. The solution could stir on a hot-plate until a transparent gel was obtained at 120°C. The beaker containing the gel was heated until combustion reaction occurred at 450°C. This resulted in the formation of the organic polymeric network which acted as a preliminary framework for the oxide material. The precursor mass that remained was oxidized by calcination at 900°C resulting in the formation of catalyst powders. $FeCe_2O_4$ and $SrNiO_3$ catalysts are prepared using the sol-gel method and presented in following chapters.

2.5 Materials characterization

The synthesized nanomaterials were analyzed using several characterizations techniques to identify the crystal phase, morphology, microstructure, size, composition, and surface area. The detailed experimental conditions are given below.

2.5.1 X-ray diffraction (XRD)

X-ray diffractometer (XRD) is an essential analytical technique to determine the phase purity, the phase of the crystal, structure, and crystal size. The synthesized samples were performed by using (D/MAX 2200H, Bede 200, Rigaku Instruments C) X-ray diffractometer (XRD) operated at the power of 40 kV and current of 40 mA with Cu-kα radiation in the range 2θ angle of 10-80° with a step of 0.02°. Additionally, the average crystallite size can be computed under this technique. The commercial devices adopt this technique for qualitative purposes by using X-ray detectors where the wavelength (λ). Once the wavelength and the angle of incidence (θ) are known, the inter-planar distance (*d*) of the mean size of the crystalline can be determined by using the Scherrer equation [10]:

$$t = \frac{k\lambda}{\beta \cos\theta}$$
.... (2.1)

where t = thickness of the crystal (Å)

k = Scherrer constant, taken as 0.94

λ = wavelength of incident radiation (Å)

β = full width at half maximum of the broadened peak (degree)

θ = angle of incidence (degree)

2.5.2 Brunauer, Emmett and Teller (BET) surface area analysis

Nitrogen (N_2) adsorption-desorption isotherm measurement was carried out to determine the surface area, pore-volume and pore-size distribution of the as-prepared samples. The Brunauer-Emmett-Teller (BET) analysis was performed with Quantachrome Autosorb-1, Quantachrome Instruments v2.11 and nitrogen (N_2) gas was used as an adsorptive for the determination of the above parameters. The specific surface area of the samples was calculated by using the multiple-point BET model. The pore size distributions were obtained from the adsorption/ desorption branch of the isotherm by the Barrett-Joyner-Halenda (BJH) method. The total pore volume was calculated from the volume of nitrogen adsorbed at a relative pressure of P/Po =0.95.

2.5.3 Raman spectroscopy

The Raman spectrum is a non-destructive tool towards and sensitive technique the structural defects and disorders, crystallization in nanostructures. Further, it is also used to study the bonding nature of various carbon materials such as graphite and carbon nanotube. Raman spectra of the prepared $FeCe_2O_4$ and $SrNiO_3$ was studied using a Model: LabRam HR800 micro Raman spectroscopy (manufacturer: Horiba Jobin-Yvon, France). The Raman spectrum was operated at an excitation wavelength of 514 nm at the different laser power using Ar_+ ion laser.

The spectral region of 100–3500 cm^{-1} was used to collect the data was using an acquisition time of 10-s data point.

2.5.4 Field-emission scanning electron microscopy

Scanning electron microscopy (SEM) analysis can provide some information about catalyst surfaces morphology (size and shape) through contrast with the three-dimensional image. Moreover, SEM images may also enhance knowledge about the catalyst surface topography (surface features) and crystallography (atomic arrangement). Here we used, FE-SEM (Model: FE-SEM, JSM- 6700F, JEOL Ltd) with a 10 kV of acceleration voltage and 10 µA of filament current. Prior to measurement, the as-prepared samples were fixed onto a double-face conducted tape mounted on a metal stud and coated with platinum with a sputter coater (Quorum Rotary-Pumped sputter coater -Q150R).

2.5.5 Energy dispersive spectroscopy analysis (EDS)

The elemental composition of the prepared samples was measured using Energy Dispersive Spectroscopy (EDS). The EDS analysis was done with the Field Emission Scanning Electron Microscopy (FE-SEM) instrument (TESCAN instruments, MIRA3) with a separate EDS detector (INCA) connected to that instrument.

2.5.6 X-ray photoelectron spectroscopy (XPS)

The chemical composition and the state of elements present in the outermost part of samples were obtained by X-ray photoelectron spectroscopy (XPS) techniques using ESCA- 2000, VG Microtech Ltd and Theta Probe AR-XPS system (Thermo Fisher Scientific, U.K). Here a monochromatic X-ray beam source at 1486.6 eV (Aluminum anode) and 14 kV was used to scan the sample surface. A high flux X-ray source with Aluminum anode was used for X-ray generation, and a quartz crystal monochromatic was used to focus and scan the X-ray beam on the sample.

2.5.7 Temperature–programmed desorption

Temperature–programmed desorption (TPD) determines the number of desorbed species from a solid surface under heating at a constant rate. Together with various desorption peaks temperatures can be used as the best approach to estimate the number, type, and strength of active sites located on the surface of a catalyst [11]. The process takes place as follows: adsorptive gas is initially introduced to the sample which is subsequently heated at a certain rate, whereupon at a certain temperature the activation energy would overcome the bond between adsorbate and adsorbent causing a release for desorbed gas from the catalyst surface to the mainstream. The quantity of this desorbed gas is measured by connected TCD and often represented in a plot against temperature as shown in **Chapter 4**.

2.5.8 Temperature Programmed Reduction

Temperature programmed reduction (TPR) of the catalysts was performed in fixed bed reactor. Briefly, about 100 mg of catalyst was loaded in a 6 mm ID U-shaped quartz tube. Catalysts were packed and held in the tube by quartz wool plugs. A thermocouple was inserted as close as possible to the catalyst bed and ran axially through the quartz reactor to measure and control the bed temperature. Before starting the experiment, all the catalysts were pretreated at 250°C with an Ar flowing at 50 ml min^{-1} for 45 min. This was done to ensure that any surface hydrated species was vaporized prior to the reaction. After this step, the catalyst was exposed to Ar, and the temperature was lowered to ambient and maintained at this temperature for 30 min. Then, a mixture of 10% H_2/Ar was passed over the catalyst with a flow rate of 50 ml min^{-1}. The temperature was ramped from ambient to 900°C with a rate of 5°C min^{-1}. After the run, amount of H_2 consumed (TCD signal) was plotted as a function of temperature.

2.5.9 Temperature-programmed oxidation

Temperature-programmed reduction-oxidation (TPO) runs to investigate the nature of surface carbon species on the used catalyst after DRP at high temperature. Indeed, a combination of these analyses is generally a more efficient approach to investigate the catalyst stability under similar conditions for dry reforming reaction, as the latter is a variable mixture of reducing and oxidizing conditions. Furthermore, TPO analysis was also used for investigating the carbonaceous species present in spent catalysts after the reaction, which provides insights about the reaction process.

2.6 Activity Investigation

The experimental rig of the reactor configuration that was generally used in this study is exhibited in **Figure 2.1.1** The set-up was modified under the application of a fluidized-bed operation whereas the flow was changed from downward to upward. Upon locating the catalyst sample in the furnace center, N_2 gas was utilized to flush the system prior to the catalyst activation process by heating at 700°C for 2.5 h. Subsequently, the catalyst cooled down to reaction temperature under the flow of the sweep gas, Ar before introducing the mixture of reactant gases. As can be seen in Figure 3.10, the experimental set-up consists of three divisions: flow controller unit, reactor rig and product analysis unit.
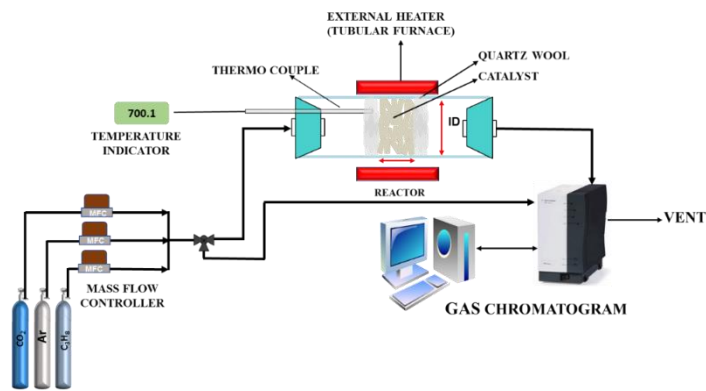

Figure 2.1.1 Outline of the experimental setup

2.6.1 Flow controller units

This division is the first part of the set-up where the gas flow rates can be controlled through the mass flow controllers and blended in a cylinder mixer. All the mass flow controllers are manufactured by ATOVAC instruments (model AFC500). Their gas flows are adjusted through a manual control panel which is supplied by ATOVAC instruments (model GMC1200). The maximum flow capacity for all mass flow controllers were 50, 100 and 200 ml min^{-1}. Each controller is calibrated for all gases that are expected to be used with a bubble flow meter and checked regularly. Prior to each reaction run, gas flow rates are set according to the desired feed ratio, R. However, a bypass line is connected to the analysis unit, gas chromatograph (GC), in order to verify the feed ratio.

Figure 2.1.2 (a) Mass flow controller and (b) Pressure & Flow controller

2.6.2 Reactor rig

In this division, the rig is designed to suit the reactor operations used in this study: fixed-bed. The electrical tube furnace is supplied by DH Science, South Korea (Model: DTF-50300) with dimensions of 50 mm ID and 30 cm length. The furnace is attached to a temperature control unit (240 volts, 10 AMPS, 3600 Watts, Model NX-4) provided by Hanyoung nux. While reactor temperature was controlled by a built-in controlling unit, the reaction temperature is measured through a 1 mm OD stainless steel thermocouple sited axially inside the reactor. The fixed bed

reactor is in the form of a quartz tube with 16 mm ID, and 600 mm length placed horizontally in the furnace reactor. The catalyst is placed in the center of the reactor and supported with a 2 cm thickness of quartz wool for both sides in the case of the fixed-bed to keep the catalyst within the reactor. Both ends of reactor tube were sealed by silicone cork fitting. The pressure drop across the reactor was measured through pressure gauges. The flow meter used to measure the inlet and outlet of the reactor to monitor the continuous flow and adjust sample feed volume of GC injection.

2.6.3 Product analysis

The dry product gas was then analyzed by a Varian Micro gas chromatograph (model: CP-490) fitted with a thermal conductivity detector (TCD) operated isothermally at 180°C. The separation of CO_2 and C_3H_8 components was achieved by Prop-Q column, and the separation of H_2, CO, and CH_4 components was achieved by Mole sieve- 5A. The column temperature was set at 110°C and Ar gas was used to carry gases at 25 ml min^{-1} throughout the GC. The result of the analysis was determined by a Galaxy compassCDS integrator where each gas was represented by a characteristic peak (i.e., retention time). Accordingly, gas concentrations were estimated based on GC calibration from the corresponding peak area for each gas. Actually, peak areas from GC analysis are known to vary with time, and according to environmental conditions, thus prior to each run a standard gas (1% CH_4/Ar balance) was daily tested. Subsequently, GC analysis consistency was always maintained through normalizing the measurements by standard gas reading to exclude the influence of random fluctuations on peak areas [12].

2.6.4 Infrared gas analyzer

The products (CO, CO_2,) formed during temperature programmed oxidation was measured by an infrared analyzer (Lambda Instrument, Australia Model FTIR 7600). Infrared radiation (IR)

is absorbed by gases such as CO, CO_2 at a characteristic wavelength. The working principle of the IR analyzer as shown in **Figure 2.1.3** When a component that does absorb IR radiation is present in the sample gas the radiation intensity reaching the detector will be reduced at the specific part of the spectrum. Two methods are in use for detecting the level of absorption a gas detector explicitly filled with the gas of interest will, from the broadband radiation leaving the measuring cell, detect only the component of interest with individual gaseous molecules. It's variations caused by the varying concentration of the component in the sample gas passing through the measuring cell. Radiation absorption affects the gas pressure in the detector cell; these pressure variations are used to generate a detector signal as a measure of the concentration of the gas of interest. A solid-state IR detector is used together with a narrow-band interference filter that allows from the broadband spectrum of IR radiation only the radiation range of the component of interest (e.g., CO_2) to pass through. As the IR radiation passes through the measuring cell, a variation in CO_2 concentration will cause a proportional variation in the IR absorption and thus in the detector.
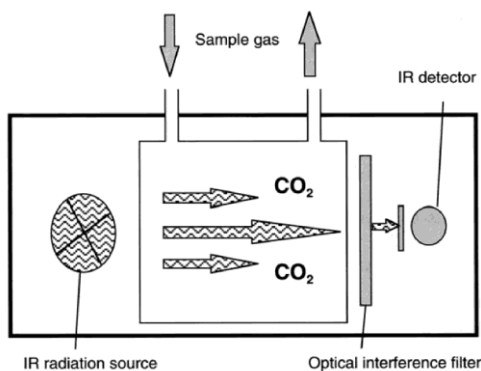

Figure 2.1.3 Working principle of the IR-analyzer.

2.7 Reference

1. Schwarz, J.A.; Contescu, C.; Contescu, A. Methods for preparation of catalytic materials. *Chemical Reviews* **1995**, *95*, 477-510.
2. Regalbuto, J. *Catalyst preparation: Science and engineering*. CRC press: 2016.

3. de Jong, K.P. *Synthesis of solid catalysts*. John Wiley & Sons: 2009.
4. Pechini, M.P. Method of preparing lead and alkaline earth titanates and niobates and coating method using the same to form a capacitor. 1967.
5. Tietz, F.; Schmidt, A.; Zahid, M. Investigation of the quasi-ternary system $LaMnO_3$–$LaCoO_3$–"$LaCuO_3$"—I: The series $La(Mn_{0.5}Co_{0.5})_{1-x}Cu_xO_{3-\delta}$. *Journal of Solid State Chemistry* **2004**, *177*, 745-751.
6. Majid, A.; Tunney, J.; Argue, S.; Wang, D.; Post, M.; Margeson, J. Preparation of SrFeO~ 2.85 perovskite using a citric acid assisted Pechini-type method. *Journal of alloys and compounds* **2005**, *398*, 48-54.
7. Haynes, D. The catalytic partial oxidation of n-tetradecane on Rh and Sr substituted pyrochlores. **2007**.
8. Zayat, M.; Levy, D. Blue $CoAl_2O_4$ particles prepared by the sol−gel and citrate−gel methods. *Chemistry of Materials* **2000**, *12*, 2763-2769.
9. Hwang, B.J.; Santhanam, R.; Liu, D.G. Characterization of nanoparticles of $LiMn_2O_4$ synthesized by citric acid sol-gel method. *Journal of Power Sources* **2001**, *97-98*, 443-446.
10. Bergeret, G.; Gallezot, P. Particle size and dispersion measurements. *Handbook of heterogeneous catalysis* **2008**.
11. Bhatia, S.; Beltramini, J.; Do, D. Temperature programmed analysis and its applications in catalytic systems. *Catalysis Today* **1990**, *7*, 309-438.
12. Adesina, A.A. Application of periodic operation to the Fischer-Tropsch synthesis of hydrocarbons. **1987**.

CHAPTER -3

Iron-ceria spinel (FeCe₂O₄) catalyst for dry reforming of propane to inhibit carbon formation

3.1 Introduction

The production of synthesis gas (syngas; a mixture of H_2 and CO) is an important industrial process in the conversion of natural gas to liquid fuels, petrochemical products and essential building blocks for chemicals [1,2]. In this regard, dry reforming has received much attention as a technology to produce syngas for the production of sulfur-free liquid fuels and oxygenated chemicals at a low H_2/CO ratio by syngas [3,4]. Dry reforming of methane with CO_2 is a well-known process that has been extensively studied owing to its industrial importance to produce syngas [5-7]. Recently, considerable attention has been paid to the dry reforming of light hydrocarbons such as ethane and propane as an alternative hydrocarbon for the production of syngas [8-14]. More precisely, propane has many advantages as a hydrogen source over natural gas; it can be stored as a compressible liquid and is easily transportable [15]. Propane was expected to produce more surface carbon species compared to natural gas due to a higher carbon atom content, consequently, creating an ideal environment for the challenge that needed to be overcome. Moreover, utilizing higher hydrocarbon substrate is preferred as it requires less energy for the bond breakup. Furthermore, higher hydrocarbons are known to have a lower flammability limit which is 5.3–15% for methane and 2.2–9.6% for propane. It exists in gaseous form at standard temperature and pressure. The overall reaction for the dry reforming of propane (DRP) is as follows:

$$C_3H_8 + 3CO_2 = 6CO + 4H_2 \quad \Delta H_{298k}^0 = 644.8 \; kJ.mol^{-1} \qquad \text{.......... (3.1)}$$
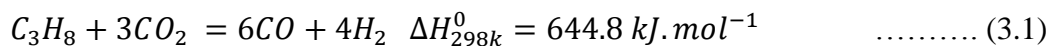
Up to now, many previous studies on the catalytic DRP using noble metals such as Pt, Ru, Rh, and Re have been reported [11, 16-19]. Even though the noble metals have high catalytic activity and selectivity for the dry reforming process, the high cost and limited availability restrict their applications in industry. Several transition-metal-based catalysts, typically nickel can be a cost-effective alternative (compare to noble metals), and many researchers have found that Ni-based catalysts also have good activity for dry reforming reactions [15,20]. However, Ni-based catalysts undergo rapid deactivation due to sintering as well as coke formation. Apart from the metal oxides, bimetallic catalysts, such as Ni-MgO, Ni-CeO$_2$, and Co-Ni, have been studied for dry reforming reactions; however, even though these catalysts were reported as being highly reactive in dry reforming, they led to the formation of a significant amount of coke and the sintering of catalysts [21]. One method to improve the coke-resistance is to design a catalyst with a site at which the phase (Fe, Ni) could be activated within a well-defined structure. In this regard, perovskite and spinel compound were reported to be an exciting catalytic material [22-25]. These structures increase the metal reduction temperature such that it is closer to the reaction temperature. An example is a noble spinel compound, which showed high reactivity and stability towards the dry reforming of methane [26]. A highly dispersed active phase could be obtained in this way with decreased coke formation. This method could also enhance the metal-support interaction, the formation of the solid solution, and thermal stability. Spinel compounds represented by the general empirical formula AB_2O_4 where A and B represent divalent and trivalent metal cations, respectively, have been extensively studied as a heterogeneous catalyst [27]. Guo et al. reported a comparison of the $MgAl_2O_4$ spinel oxide catalyst with $MgO\text{-}\gamma\text{-}Al_2O_3$ and $\gamma\text{-}Al_2O_3$. The authors observed high activity and coking resistance to enhanced control over sintering [28]. Kim et al. have reported that a bimetallic NiFe catalyst increases the catalytic stability and Fe actively reduces

56

the carbon deposition via Fe redox to FeO [29]. During the last decade, researchers have used lanthanide oxides such as La_2O_3 and CeO_2 as highly oxidative agents that are able to store and release oxygen [30] readily. CeO_2 has the ability to release lattice oxygen and be quickly re-oxidized, thereby enhancing the catalytic performance [13, 29, 31]. In this work, the use of iron as an A-site cation was investigated, because iron has redox properties and Fe can oxidize the carbon to CO during dry reforming to prevent deactivation [32]. Cerium was selected as a paired B-site cation since cerium oxides showed prominent oxidation activity and as a basic rare-earth metal it is capable of preventing coke formation. An iron ceriate spinel compound, prepared by the sol-gel method using citric acid as a chelating agent, was used in the DRP [33-35].

In this work, we have used propane as the primary reactant. Various other support materials have been investigated such as SiO_2, TiO_2, ZrO_2 and MgO [11, 36]. In many cases, Al_2O_3 has been used as catalyst support [37]. According to reports in the literature, the mechanism of dry reforming is strongly dependent on the support materials. Suitable supports have to be resistant to high temperature and should be able to maintain metal dispersion during operation [12, 38-40]. In the experiments described in this paper, mesoporous alumina foam was used as a catalyst support. The alumina foam has 60 pores per inch (PPI), and it can easily be used as a commercial system due to the low drop in pressure of packed bed reactors [41, 42]. The present study aims to discuss the results obtained for the dry reforming and the inhibition of coke formation by the combination of iron with cerium in the definite structure, in order to stabilize the structure and to limit the sintering of the active metal species. In addition, we also studied the stability of the catalyst in terms of DRP to syngas.

3.2 Materials and Methods

3.2.1 Catalyst preparation

The $FeCe_2O_4$ spinel, $NiO-CeO_2$ and CeO_2 catalysts on commercial alumina foam (Al-F) support were synthesized by the sol-gel method. The commercial Al-F supports were purchased from ShengQuan Ltd., China. The default size of commercial Al-F foam was 70 mm x 70 mm x 14 mm (length x width x height) and then cut into cylindrical shape pellets (14 mm in length and 10 mm OD) by a puncher. Each pellet weighs ~0.8g. The Al-F support was pretreated for 2 h at 150°C to remove moisture. Iron nitrate ($Fe(NO_3)_3 \cdot 9H_2O$), cerium nitrate ($Ce(NO_3)_3 \cdot 6H_2O$), nickel nitrate ($Ni(NO_3)_2 \cdot 6H_2O$ and citric acid were used as catalyst precursors. The chemicals were purchased from Daejung Chemicals Ltd., South Korea. The Fe-Ce spinel catalysts were formed by preparing 0.5 M aqueous solution of iron and cerium nitrates (each 20 mL). An appropriate volume (20 mL) of citric acid solution (1.0 M) was poured into metal nitrate solution. The initial citric/nitrate stoichiometric molar ratio was equal to 1. The mixed solutions were heated at 80°C and stirred continuously until a viscous gel was obtained. The pretreated Al-F pellets were poured into the gel solution to allow the solutions to be entirely absorbed by Al-F. The resulting foam was further dried at 110°C for 12 h. During the drying at 110°C, the gel started boiling with bubbling and foaming and with the rapid evolution of a massive quantity of gases, producing a foamy and voluminous powder. The Al-F after drying contained carbonaceous residues. These residues were eliminated by further heating the Al-F at 700°C for 2 h in air. Finally, the ~20 wt. % of Fe-Ce spinel catalyst on Al-F ($FeCe_2O_4$/Al-F) was obtained. The same procedure was used to prepare Ni-Ce($NiO-CeO_2$/Al-F) and CeO_2/Al-F catalysts. The total loaded weights of metal oxide in all catalysts on the surface of the Al-F were the same which was measured by the weight of the Al-F before and after synthesis.

제주대학교 중앙도서관
JEJU NATIONAL UNIVERSITY LIBRARY

3.2.2 Catalyst characterization

The powder X-ray diffraction(XRD) patterns of the prepared catalysts were obtained with a Rigaku powder diffractometer (Japan) using nickel-filtered CuKα radiation (λ = 0.154 nm) operated at 40mA and 40 kV. The X-ray diffractograms were analyzed using X'Pert ScorePlus software. The measurement was carried out in the 2θ angle range from 20° to 90° with a step of 0.04°. The crystallite size was calculated using Debye-Scherrer's equation (2) as follows:

$$D = \frac{K\lambda}{(\beta \cos \theta)}$$ ……… (3.2)

where D is the average crystallite size, K is a constant, λ is the wavelength of the X-ray radiation, β is the full width at half maximum of intensity peak, and θ is the diffraction angle. The Brunauer-Emmett-Teller(BET) surface area of the prepared samples was determined with a Quantachrome Auto absorber by N_2 adsorption at -196°C after outgassing the sample at 300°C for 3h. The Raman spectra of the samples were analyzed using a LabRam HR Evolution Raman spectrometer (Horiba, Japan). The instrument was operated at an Ar laser power of 10 mW, and an excitation wavelength was 514 nm. The surface morphology of the catalyst was evaluated by field emission-electron scanning microscopy(FE-SEM) (JSM-6700F: JEOL Ltd., Japan), operated at an accelerating voltage of 20kV and 10µA. The chemical characteristics of the catalyst surface were examined using X-ray photoelectron spectroscopy(XPS) (Thermo Fisher Scientific, U.K) with monochromatic Al Kα radiation (1488.6 eV) operated at 15 kV and a 150-W X-ray excitation source.

The temperature programmed reduction and temperature programmed oxidation(TPR/TPO) measurements were studied in a conventional flow system monitored by the gas chromatograph (GC) equipped with a thermal conductivity detector (TCD). In the TPR experiments, all the catalysts were examined in the temperature range of 25-900°C, using 100 mg

catalyst samples. Each sample was pretreated at 400°C for 1 h under Ar flow before TPR. After cooling down to room temperature under Ar flow, TPR experiments were conducted under a flow of a 5% H_2/Ar at a total flow rate of 50 mLmin^{-1}, with a linear temperature increase of 5°Cmin^{-1}. In the TPO experiments, all the catalysts that were studied in the temperature range of 25-900°C, in a stream consisting of the mixture 5% O_2/Ar (a gas flow rate of 50 mLmin^{-1}, at a heating rate of 5°Cmin^{-1}) to determine the nature of carbon and to estimate the coke after DRP.The TPO was carried out with 100 mg of used catalyst sample at 500°C with 10% O_2 flowing through the catalyst bed to oxidize the carbon deposited on the catalyst surface. The CO_2 formed from the oxidation of carbon was measured with the GC equipped with a TCD detector until there was no CO_2 from the outlet gas. The amount of carbon was quantified by integration of the concentration of CO2 desorbed (mol/l) at during TPO. The area(mol) was measured by the following equation.

$$Area(mol) = Q_{total}\int_0^t [CO_2]dt$$

………. (3.3)

Where Q_{total} is total flow rate, $[CO_2]$ is a concentration of CO_2 in mole.

3.2.3 Catalytic test

In this work, the activity and selectivity of all the catalysts for DRP were evaluated in a reactor designed as a standard fixed-bed type. The setup consists of feed gas (C_3H_8, CO_2, and N_2), a quartz reactor within a temperature-controlled tubular furnace and analysis equipment (GC). The reactor for DRP contained 1.0 g of catalyst sandwiched between glass wool to prevent the catalyst from moving in the fixed-bed reactor and a thermocouple fixed within this bed was connected to the furnace temperature controller to maintain isothermal operation. The overall reaction for the dry reforming of propane can be expressed in Eq. 3.1. Wang et al. detailed that the thermodynamic study of propane dry reforming with various ratio of CO_2/C_3H_8 (CPR) at a temperature range of

700- 1100 K and under atmospheric pressure. The optimum condition for synthesis gas generation has been found at 975 K (CPR=3) for an H_2/CO ratio of 1. As per that review, the equilibrium conversion of CO_2 could be achieved 71% at 975 K [43]. Based on the thermodynamic characteristic of the dry reforming reaction was feasible at any temperature higher than 750 K. In this study, the catalytic activities were examined in a temperature range of 650°C to 750°C under atmospheric pressure and with a feed gas containing C_3H_8: CO_2: N_2 in the ratio 1:3:6 (10%:30%:60%), respectively. The total flow rate was fixed at 200 mL• min-1and was passed through the reactor with a gas hourly space velocity (GHSV) of 9550 h^{-1}. The reaction products during DRP were analyzed by a TCD-equipped (Varian micro GC CP-4900) GC fitted with a PPQ column and a 5A molecular sieve column. The desired gas flow rates were maintained by using a set of mass flow controllers (MKS 1179A, USA). Prior to the reaction, moisture and gases captured on the surface of the catalyst were removed by pretreating all the catalysts with N_2 (flow of 100 mLmin^{-1}) at 700°C for 2 h before commencing the catalytic reaction. The stability test was carried out for each catalyst at 700°C for 60h with the same feed gas composition. The conversion efficiencies of propane and CO2 were monitored every 12 h interval of time with continuous operation. The conversion (XA) of C_3H_8(or CO_2) was defined as (Eq. 3.4):

$$X_A(\%) = \frac{C_{in} - C_{out}}{C_{in} + \varepsilon_A C_{out}} \times 100 \qquad \ldots\ldots\ldots (3.4)$$

where C_{in} and C_{out} are the inlet and outlet concentration of the reactant (C_3H_8 or CO_2), respectively. Further, ε_A is defined as the fractional change in volumetric flow rate between no conversion and complete conversion of the reactant (C_3H_8 or CO_2) [9, 44].

3.3 Results and Discussion

3.3.1 Characterization of the catalyst before reaction

3.3.1.1 XRD

The powder XRD patterns of the fresh catalysts calcined at 700°C is shown in **Figure 3.1.1**. The main XRD peaks for all the catalysts were observed at 2θ=25.40, 34.96, 37.64, 43.12, 52.36, 57.40, 66.36, 68.08 and 76.72, which correspond to α-Al_2O_3 [ICDD 02-1227]. In our catalyst, the peaks confirming the formation of spinel structured $FeCe_2O_4$ [ICDD 36-1253] were observed at 23.16°, 33.07°, 40.04°, 49.04°, 63.68° and 53.84° and correspond to $FeCe_2O_4$ in the $FeCe_2O_4$/Al-F sample. The peak positions for spinel are in good agreement with standard patterns. Along with the spinel phase, separate Fe_2O_3 and $FeCeO_3$ phases were not present. It could be the existence of trace amount in the catalyst, and it could not be measurable by XRD due to the limitation of XRD instrument. In this figure, the separate CeO_2 phase indicates the trace amount of Ce precursor that was not used to form $FeCe_2O_4$. Some peaks observed in the CeO_2/Al-F and NiO-CeO_2/Al-F samples (2θ=28.24, 47.52, 56.28, 61.12 and 79.08) correspond to CeO_2 [ICDD 65-2975] [45]. The above results also suggest the formation of a cubic phase with a fluorite structure for CeO_2. For the catalyst NiO-CeO_2/Al-F, low-intensity peaks were observed at 37.48°, 62.50°, and 75.40°, respectively, and are attributable to NiO [ICDD 71-1179] [46]. The XRD pattern of the catalyst NiO-CeO_2/Al-F clearly shows the presence of CeO_2, and it demonstrates that the NiO peaks overlap with those of the α-Al_2O_3 peaks. The XRD pattern shows that all the metal oxides are well distributed on the surface of the alumina foam. The average crystallite sizes for the prepared catalysts are listed in **Table 3.1**. As seen in **Table 3.1**, the crystallite size decreases in the order of CeO_2/Al-F<$FeCe_2O_4$/Al-F<NiO-CeO_2/Al-F<bare Al-F. The CeO_2 crystal sizes of the catalysts are 15.7 nm, 12.3 nm, and 8.4 nm for the CeO_2/Al-F, $FeCe_2O_4$/Al-F, and NiO-CeO_2/Al-F catalysts, respectively. The decrease in the crystal size is associated with broadening of the peak. The

measured BET surface areas and pore volumes for all the synthesized samples are summarized in Table 1. As seen, the bare Al-F showed the surface area (8.2 m^2g^{-1}) and pore volume (0.02 cm^3g^{-1}). The decreased surface area and pore volume of the $FeCe_2O_4$/Al-F and $NiO-CeO_2$/Al-F catalysts can be attributed to the metal oxide particles blocking the pores of Al-F.
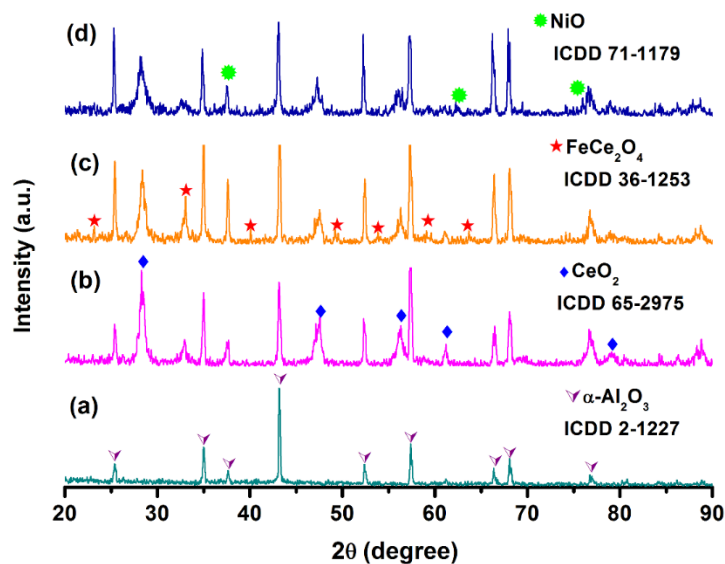
**Figure 3.1.1** X-ray diffraction patterns of freshly calcined catalysts. (a) Alumina foam (Al-F), (b) CeO_2/Al-F, (c) $FeCe_2O_4$/Al-F, and (d) $NiO-CeO_2$/Al-F.

Table 3. 1 Textural properties and mean crystallite sizes of prepared catalyst

Catalyst	SBET (m^2 g^{-1})	Vp (cm^3 g^{-1})	Crystal size (nm)	Crystal size of CeO_2 (nm)
Al-F	8.13	0.02	48.1	-
CeO_2/Al-F	9.24	0.03	15.7	15.7
$FeCe_2O_4$/Al-F	4.38	0.02	29.7	12.3
$NiO-CeO_2$/Al-F	4.61	0.01	37.1	8.4

SBET = Surface area; Vp = pore volume

3.3.1.2 Raman spectra study

The crystalline and bonding nature of the synthesized compounds were investigated by recording the Raman spectra of the catalyst samples at an excitation of 514 nm excitation, as depicted in **Figure 3.1.2**. The primary Raman active mode was observed for all the metal loaded

samples in the range of 440 cm^{-1} to 463 cm^{-1}, which corresponds to the typical F_{2g} modes of the cubic fluorite-type of ceria [47].
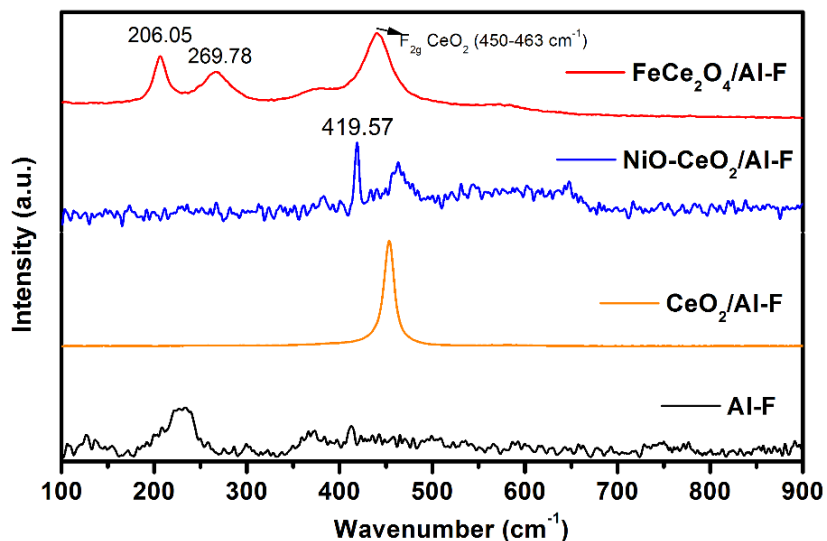

Fig. 3.1.2. Typical Raman spectra of freshly calcined catalysts

Especially, the F_{2g} band of Fe-Ce sample noticeably shifted to a lower wavenumber with broadening compared to pure CeO_2, a phenomenon that is more pronounced in the case of the $FeCe_2O_4$/Al-F sample. The noticed peak shift and its broadening depend on various parameters, phonon confinement, including crystal defects, and inhomogeneous strain related to the reduced ceria. The significant peaks that were observed in the spectrum of the $FeCe_2O_4$/Al-F catalyst at 206.05 cm^{-1} and 269.78 cm^{-1}, which correspond to Fe^{2+}. A small oxygen vacancy band, which was observed at around 572.06 cm^{-1}, corresponds to the incorporation of the trivalent metal ions into the Ce_2O_4 lattice and the presence of Ce^{3+}. The peak at 419.57 cm^{-1} is attributed to NiO.

The reducibility of metal ions was analyzed by obtaining the H_2-TPR profiles of all the catalysts, as shown in **Figure 3.1.3** In the case of $FeCe_2O_4$, the synthesized catalyst exhibited peaks that evolved around 236.6°C and 623.7°C. The former peak at 236.6°C could be attributed to the reduction of Fe_2O_3 to Fe_3O_4, whereas the latter peak at 623.7°C could be attributed to the reduction

제주대학교 중앙도서관
JEJU NATIONAL UNIVERSITY LIBRARY

of the mixed spinel-structure. It could be mixed oxide species Fe(II) ceriate and the complete reduction of FeO to Fe [48, 49].
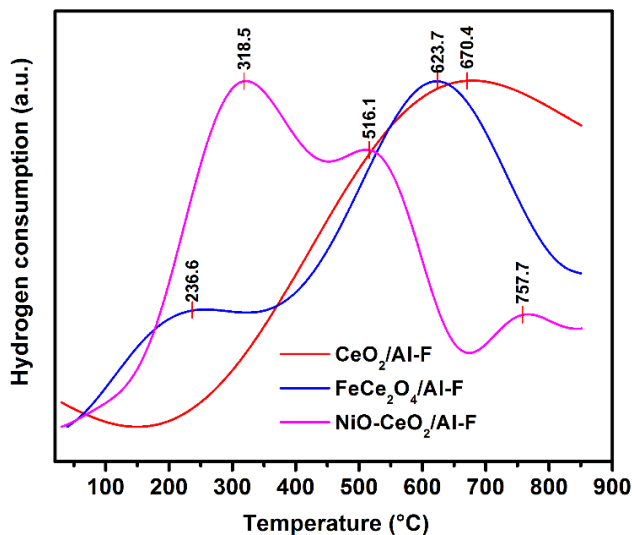
**Fig. 3.1.3** H_2-TPR profiles of all the fresh samples, CeO_2/Al-F, $FeCe_2O_4$/Al-F, and NiO-CeO_2/Al-F.

The CeO_2/Al-F profile shows only one broad peak around 670°C, which could correspond to CeO_2 reduction. The NiO-CeO_2/Al-F profile shows three peaks at 318.5°C, 516.1°C and 757.7°C, respectively, where the first two peaks are attributed to NiO species with moderate interaction with the support and the last one could correspond to the presence of $NiAl_2O_4$ [50]. This result suggests that the Ce could promote the mobility and activity of the surface lattice oxygen species and the formation of oxygen vacancy [51].

The O 1s XPS spectra of prepared catalysts are presented in the supplementary information **Figure. 3.1.4**. As shown in **Figure. 3.1.4**., the O 1s spectra were deconvoluted in three peaks in the binding energy (BE) range of 534-527 eV. The BE peak at ~528 eV could be assigned to the lattice oxygen (O_L) species. The higher BE peak at 530 eV and 532 eV are generally assigned to chemisorbed oxygen and weakly bonded oxygen species (O_S) [52-54]. From the observed results,

the CeO_2/Al-F shows the higher area of O_L than the NiO-CeO_2/Al-F and $FeCe_2O_4$/Al-F. The $FeCe_2O_4$/Al-F shows the relatively higher O_S than the other catalyst.
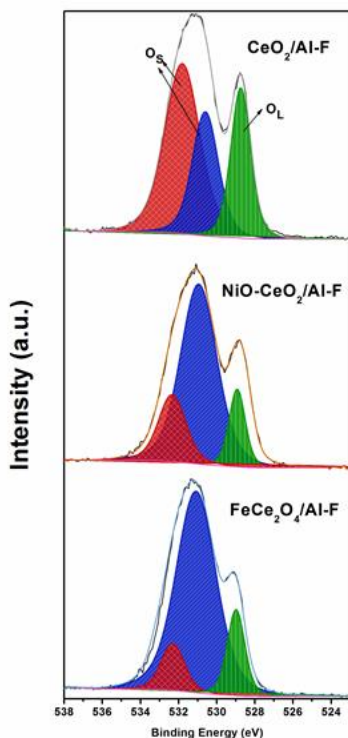
Figure 3.1.4 The O 1s XPS spectra of synthesized catalysts.

Moreover, the area of O_S (calculated by peak area) increases with the loading of secondary metals which suggests the chemical interaction of Fe and Ni species into the Ce species. The much surface oxygen might be beneficial to activate the C_3H_8 molecules that facilitated the catalytic oxidation reaction [55, 56].

3.3.2 Catalytic activity

All four samples were investigated as catalysts for DRP, and the results are shown in **Figure 3.1.5**. The catalytic activities, which are expressed in term of C_3H_8 and CO_2 conversions, were compared for the various catalysts as a function of reaction temperature (RT) ranging from

650°C to 750°C.The product gases from the outlet of the reactor were measured at the one-hour interval for each reaction temperature.
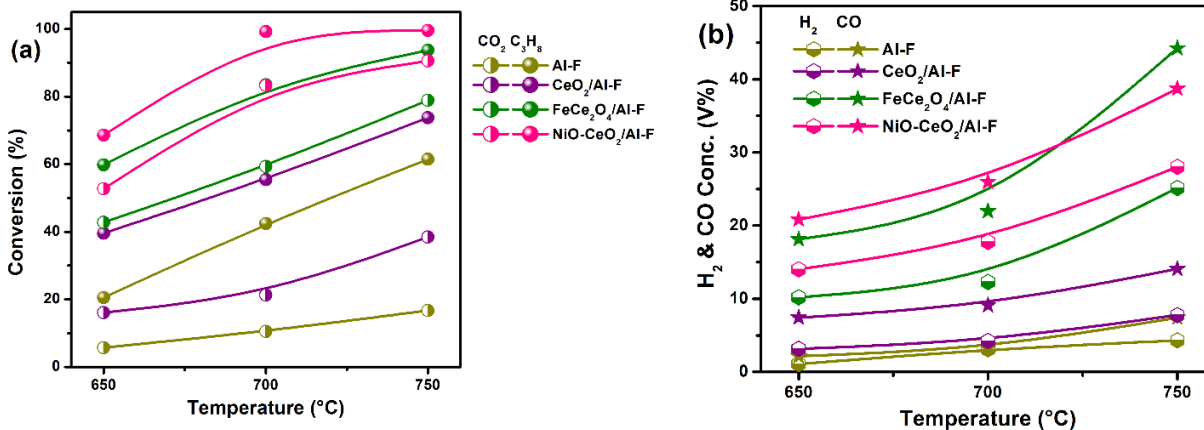
**Figure. 3.1.5**. Propane dry reforming activity for various catalysts as a function of temperature. (a) C_3H_8 and CO_2 conversions and (b) H_2 and CO concentrations. Feed composition: C_3H_8: CO_2: N_2 =10:30:60 (vol%).

As in **Figure 3.1.5a**, the conversion increased from ~59.8% to ~93.7% with increasing the temperature from 650°C to 750°C for the FeCe$_2$O$_4$/Al-F catalyst. The NiO-CeO$_2$/Al-F catalyst showed the maximum C$_3$H$_8$ conversion of ~99.5 % at 750°C. The FeCe$_2$O$_4$/Al-F, CeO$_2$/Al-F and bare Al-F exhibited C$_3$H$_8$ conversions of 93.7%, 73.7 %, and 61.4 %, respectively. The CO$_2$ conversion also followed the same pattern as the C$_3$H$_8$ conversion. The difference between the NiO-CeO$_2$/Al-F and FeCe$_2$O$_4$/Al-F were ~5.8 % for the C$_3$H$_8$ conversion and 11.6 % for the CO$_2$ conversion at 750°C. The NiO-CeO$_2$/Al-F catalyst showed higher performance than the others, which agrees well with previous reports [57, 58]. The C$_3$H$_8$ and CO$_2$ conversions of the FeCe$_2$O$_4$/Al-F catalyst at 750°C were 20.0 % and 40.4 % higher than the CeO$_2$/Al-F catalyst, which means that the FeCe$_2$O$_4$ enhanced the DRP and simultaneously CO$_2$ reduction. The FeCe$_2$O$_4$/Al-F catalyst could suppress propane cracking (**Eq. 3.5 and 3.6**) and Boudouard reaction (**Eq. 3.8**), due to the immense availability of lattice oxygens (O$_L$) and surface oxygen (O$_S$) supplied by the

$FeCe_2O_4$ spinel phase, and enhance the catalytic activity. In addition, the Fe in the $FeCe_2O_4$ reduces the CO_2 to produce CO and oxidizes the surface carbon.

$$C_3H_8 \rightarrow CH_4 + C_2H_4 \quad \Delta H^0_{298k} = 89 \; kJ.mol^{-1} \qquad \text{………. (3.5)}$$

$$C_3H_8 \rightarrow C_2H_6 + H_2 \quad \Delta H° = \; +124 \; KJmol^{-1} \qquad \text{………. (3.6)}$$

$$C_2H_4 \rightarrow 2H_2 + 2C \quad \Delta H^0_{298k} = -52 \; kJ.mol^{-1} \qquad \text{………. (3.7)}$$

$$2CO \rightarrow C + CO_2 \quad \Delta H^0_{298k} = -172 \; kJ.mol^{-1} \qquad \text{………. (3.8)}$$

$$CO_2 + H_2 \rightarrow CO + H_2O \quad \Delta H^0_{298k} = -90 \; kJ.mol^{-1} \qquad \text{………. (3.9)}$$
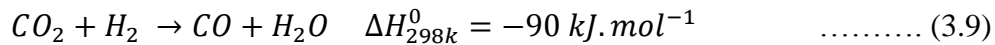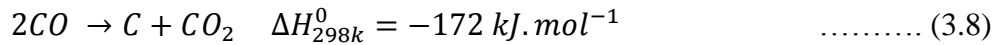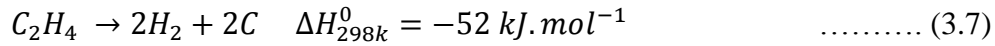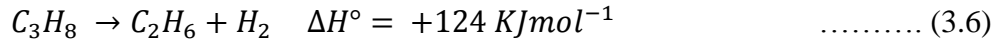
The similar trends were also observed at lower temperatures. Meanwhile, the C_3H_8 conversion was higher than the CO_2 conversion, which might be due to the high mobility of active oxygen in the surface of the catalyst [32]. Wang et al. reported that the CO_2 conversion increases with increasing temperature at CPR=3 in thermodynamic condition [43], and the similar trend was observed in this experiment. Notably, in this experiment parameters were CPR=3 (stoichiometric), the temperature at 973 K and 1 atm. The $FeCe_2O_4$/Al-F catalyst result showed that the CO_2 conversion was 59% at 973 K and which was 12% lesser than the thermodynamic equilibrium. It suggested that this catalyst promotes the reaction towards the equilibrium and enhance the CO_2 conversion and hydrogen production which leads to minimal carbon formation. **Figure 3.1.5b** shows the H_2 and CO concentrations obtained with various catalysts as a function of temperature. Apparently, the CO concentration was higher than the H_2 concentration for all the catalysts, which can be easily understood by **Eq. 3.1**. The CeO_2/Al-F catalyst showed 7.7 vol% H_2 and 14.1 vol% CO at 750°C, and the concentrations of H_2 and CO obtained with the $FeCe_2O_4$/Al-F catalyst increased to ~25.1 vol% and ~44.2 vol%, respectively. The concentrations of CO and H_2 were consistent with the propane and CO_2 conversions (**Figure 3.1.5a**). The ratio of H_2/CO revealed the reaction nature of the system.
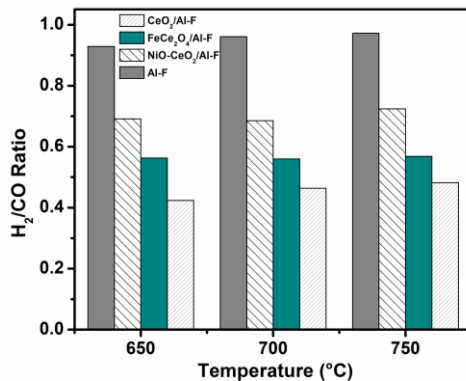
Figure. 3.1.6. H_2/CO ratios for all the catalysts at different temperatures. Feed composition: C_3H_8: CO_2: N_2=10:30:60 (vol%).

As seen in **Figure 3.1.6**, the H_2/CO ratio of the Al-F catalyst was close to unity (0.97), which might be due to the inadequate catalytic activity. The absence of active metal causes propane cracking and carbon formation at high temperatures. The H_2/CO ratio of the CeO_2/Al-F catalyst was 0.48, which is lower than the stoichiometric value of (4/6) (**Eq. 3.1**), indicating that side reactions such as (**Eq. 3.7**) occurred. The H_2/CO ratio of the NiO-CeO_2/Al-F was 0.72, which is close to the stoichiometric value (4/6). It means that the Ni metal reduced the C_3H_8 efficiently and then suppressed the side reactions including RWGS (**Eq. 3.9**). The $FeCe_2O_4$/Al-F exhibited the H_2/CO ratio of 0.57, which is also close to the stoichiometric value.
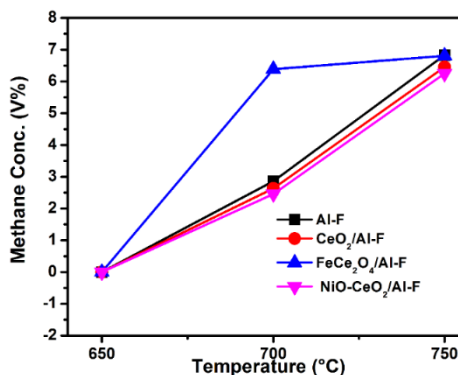

Figure 3.1.7 Methane concentration of various catalysts as a function of temperature at 650°C to 750°C. Feed composition: C_3H_8: CO_2: N_2=10:30:60 (vol%)

The main byproduct of the DRP was CH_4 (**Figure 3.1.7**). CH_4 is produced by propane cracking (**Eq. 3.5**) during the DRP. The significant amount of CH_4 has formed overall the catalyst at 750°C, and it decreased to zero at 650°C, which is compatible with the pattern of the C_3H_8 conversion. The $FeCe_2O_4$/Al-F catalyst produced ca. 6.8 vol% CH_4 and the carbon balance of this catalyst was ~100%. It suggests that the Fe metals reduced the C_3H_8 efficiently and suppressed side reaction including Boudouard (**Eq. 3.8**). The $FeCe_2O_4$ catalyst showed the significant catalytic activity in terms of the oxidation of propane and enabled Ce to retain its lattice position to generate lattice oxygen to hinder carbon formation during the DRP [59, 60]. The Fe increased the CO_2 conversion also to suppress the carbon formation [61].
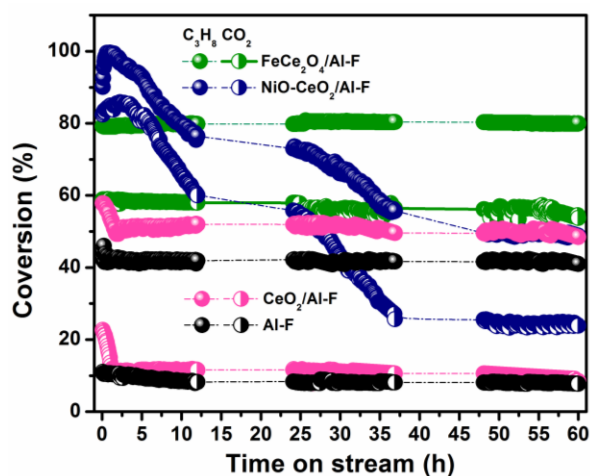
Figure 3.1.8. Stability of various catalysts in term of C_3H_8 and CO_2 conversion at 700°C for 12 h. Feed composition: C_3H_8: CO_2: N_2=10:30:60 (vol%).

In order to examine the catalytic stability of the prepared catalysts, the DRP was carried out at 700°C for time on stream (60 h), and results are illustrated in **Figure 3.1.8**. The conversions of all the catalysts seem to be quite stable with time, except for the Ni-loaded catalyst. Initially, the conversion of all the catalysts was higher for both reactant gases until 2 h, after which the conversion decreased slightly before reaching saturation state except for the NiO-CeO$_2$/Al-F

70

catalyst. With the NiO-CeO$_2$/Al-F catalyst, the conversion gradually decreased until 48 h and reached saturation state (C$_3$H$_8$ conversion: 49 %; CO$_2$ conversion: 24 %). The conversion of C$_3$H$_8$ were 42.8%, 52.3% and 83.4% for the Al-F, CeO$_2$/Al-F and FeCe$_2$O$_4$/Al-F catalysts, and those of CO2 were 10.5, 11.5 and 57.8% for the Al-F, CeO$_2$/Al-F, and FeCe$_2$O$_4$/Al-F, respectively. Noticeably, the spinel FeCe$_2$O$_4$/Al-F performed more optimally in terms of C$_3$H$_8$ conversion (83.4%) among these catalysts during 60-h DRP and was more stable than others. The conversions of C$_3$H$_8$ and CO$_2$ were maintained for 60 h. This might be indicative that Fe is the active phase while Ce acts as a promoter in Fe-rich material by improving its stability. However, the NiO-CeO$_2$/Al-F underwent severe deactivation in 48 h (48% activity loss compared to the initial conversion). The activity of the NiO-CeO$_2$/Al-F catalyst was observed to gradually decrease with time on stream, most probably because the formation of a significant amount of carbon on the surface of the catalyst covered the active sites. The carbon deposition could be ensured by the XRD and the TPO profiles of the spent catalyst sample. The continuous decrease in the C$_3$H$_8$ conversion indicates that the activity of the NiO-CeO$_2$ catalyst decreases with the contact time with C$_3$H$_8$, due to the gradual reduction in the amount of lattice oxygen available for the catalytic oxidation reaction. The formation of coke over the catalyst was the leading cause for its deactivation (**Eqs. 3.5, 3.6 and 3.8**). This observation indicates that the FeCe$_2$O$_4$/Al-F could be a potential catalyst for the dry reforming. The H$_2$/CO ratios of all the catalysts are illustrated in **Figure 3.1.9**. The Al-F catalyst showed the lower H$_2$/CO ratio of 0.24. The other three catalysts showed stable H$_2$/CO ratio with time.
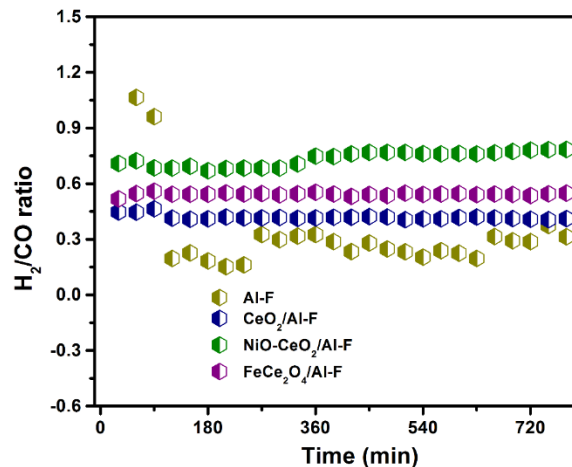
Figure 3.1.9 H_2/CO ratios of various catalysts at 700°C for 12 h. Feed composition: C_3H_8: CO_2: N_2=10:30:60 (vol%)

3.3.3 Characterization of the catalyst after reforming
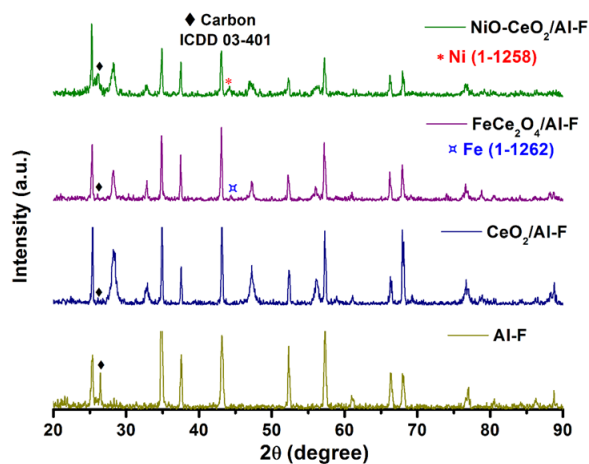
Figure 3.1.10 XRD patterns of the various spent catalysts after DRP.

The structural change of all the catalysts during the DRP was further evaluated by carrying out a test for a period of 24 h, after which the catalyst itself was characterized by XRD, Raman, XPS, FE-SEM, and TPO analyses. The XRD patterns of the spent catalysts after the DRP are shown in **Figure 3.1.10.** The spent Al-F, and NiO-CeO$_2$/Al-F samples displayed a high-intensity carbon peak at 2θ=26°, which shows the existence of carbon during the DRP [58]. It also reveals

the nature of carbon as the amorphous form. Meanwhile, the carbon peak was weak on the surface

of the CeO_2/Al-F and $FeCe_2O_4$/Al-F catalysts. This confirmed the retardant effect of carbon

deposition on the surface of those catalysts during the DRP. Moreover, the Ni (ICDD 1-1258) at

2θ= 44.2 and Fe (ICDD 1-1262) at 2θ=44.6° metal peaks were detected in the NiO-CeO_2/Al-F and

$FeCe_2O_4$/Al-F catalyst due to *in-situ* reduction during the DRP [62]. It can be further confirmed

by the XPS below. As seen in **Figure 3.1.10**, the intense primary peak of CeO_2 was observed at

28.2° in all the catalysts after the DRP. This was due to the fundamental behavior of lanthanide

group ions to interact with CO_2 in the gas phase to form carbonate phase on the surface during the

reaction, which is the main cause for minimizing the formation of carbon [63, 64].
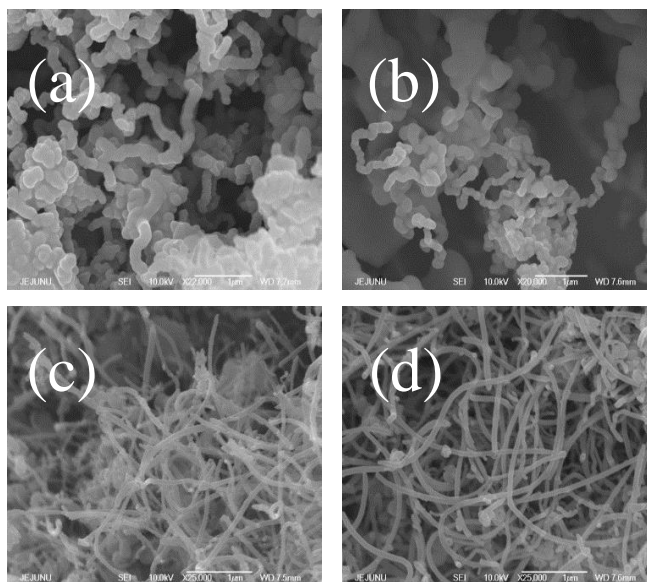
Figure 3.1.11 SEM images of (a) Al-F, (b) CeO_2/Al-F, (c) $FeCe_2O_4$/Al-F and (d) NiO-CeO_2/Al-F after DRP.

Further attempts to confirm the morphology of carbon led us to carry out FE-SEM and

Raman studies, the results of which are presented in **Figure 3.1.11**, and **Figure 3.1.12**. As seen in

the SEM images in **Figure 3.1.11**, various forms of carbon were formed in the catalysts after the

DRP. Carbon whiskers with a small diameter of less than 100 nm were observed to exist on all the catalytic surfaces, whereas thicker filamentous carbon was detected on the bare Al-F and CeO_2/Al-F catalysts. The amount of carbon found in the CeO_2/Al-F catalyst was less, compared with the Al-F, even though the appearance of the carbon on the surfaces of both of these catalysts was similar. The smooth strands of filamentous structured carbon, which had the appearance of a lengthy wired structure that covered most of the surface, were observed on the NiO-CeO_2/Al-F catalyst. Furthermore, fine tiny whiskers of carbon were observed on the surface of the $FeCe_2O_4$/Al-F catalyst. Therefore, the FE-SEM results confirm the formation of carbon during the DRP.
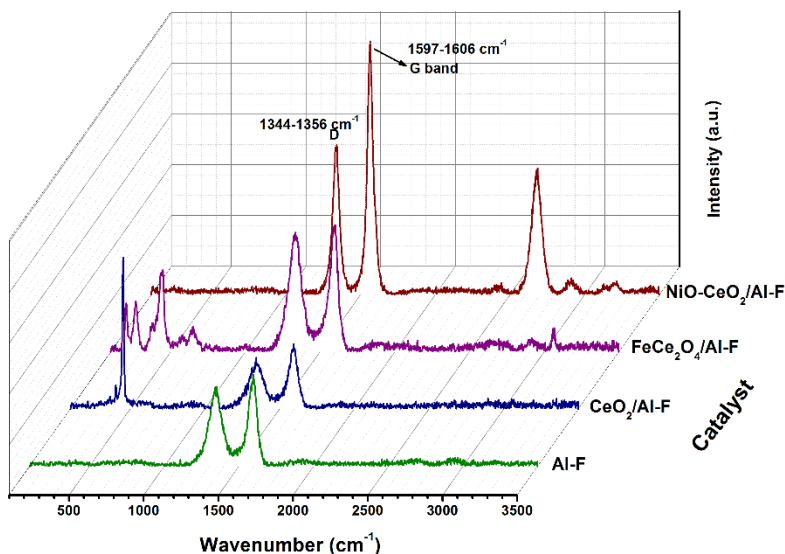
Figure 3.1.12 Raman spectra of all the catalysts after DRP.

Figure 3.1.12 shows the Raman spectroscopy studies of the used catalysts after DRP. These studies were conducted in an attempt to understand the nature of the carbon species deposited on the surface of the catalyst during DRP. The spectra revealed two major bands at 1344 cm^{-1} (D band) and 1600 cm^{-1} (G band), respectively, in all the spent catalysts. The first peak at ca.

1344 cm^{-1} is attributed to disordered sp^2 hybridized carbon atoms and the second peak at 1600 cm^{-1} corresponds to the E$_{2g}$ vibration mode of graphite in the two-dimensional hexagonal lattice of the graphite layer [65]. Particularly, the Raman spectrum of the spent NiO-CeO$_2$/Al-F catalyst shows that an additional peak is observed at 2565 cm^{-1} (2D band), which is attributed to the formation of single-wall carbon nanotubes on the surface of the catalyst during DRP. Furthermore, the results contribute to the understanding of the graphitization of carbon and the degree of disorder according to the relative intensity ratio, I$_D$/I$_G$, of the studied catalysts. Especially, the FeCe$_2$O$_4$/Al-F and CeO$_2$/Al-F catalysts exhibit firm metallic peaks on their respective spectra. This might be the result of a minimal amount of carbon deposition on the catalyst surface, which means that the surface of these catalysts remains active. A lower value of the intensity ratio (I$_D$/I$_G$=0) was determined for highly oriented pyrolytic graphite; thus, a higher value of this ratio suggests higher disorder within the crystalline structure, as reported in our previous work [66]. In our case, the value of the corresponding I$_D$/I$_G$ ratio of the FeCe$_2$O$_4$/Al-F catalyst is 0.93, which is higher than the ratio of all the other catalysts and indicates that more significant amount of amorphous carbon was formed on the surface of this catalyst. In contrast, the ratio of the NiO-CeO$_2$/Al-F catalyst was much lower (I$_D$/I$_G$ = 0.59) than that of the other catalysts. The latter value suggests the existence of crystalline carbon on the surface.

The typical TPO profiles of the used catalysts after the reaction at 700°C for 24 h are shown in **Figure 3.1.13.** These profiles show the existence of various types of carbonaceous species on the catalyst formed during the DRP. The deposited carbon was removed as CO$_2$, and no CO was observed during the subsequent O$_2$ oxidation. The peaks observed at 100°C to 300°C revealed that

the active carbon species reacted with oxygen at low temperatures can be assigned to amorphous carbon [67].
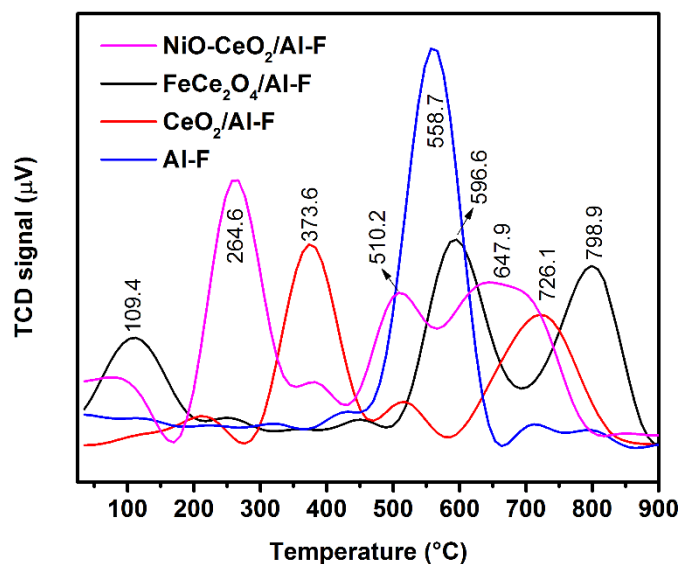
Figure 3.1.13 TPO profile of CO_2 for different catalysts after DRP for 24 h.

The second peak at 400°C to 700°C that was observed for the bare Al-F, $FeCe_2O_4$/Al-F, NiO-CeO$_2$/Al-F and CeO$_2$/Al-F catalysts can be ascribed to the presence of amorphous graphitic carbon. The graphite carbon was detected by XRD at 2θ=26° as shown in **Figure 3.1.10.** Another peak at ca. 780°C was attributed to the crystalline graphite [68, 69]. The TPO profile of the Fe spinel catalyst showed that the two forms of carbon were present in the catalyst, namely easily oxidized carbon and crystalline graphite carbon. The carbon contents of the spent catalysts after 24-h DRP were determined, as presented in **Table 3.2.** The catalysts have carbon contents from 16.5 to 90.1 wt.%. The CeO_2 and $FeCe_2O_4$ loaded catalysts exhibited a lower amount of carbon (ca. 16.5 and 17.0 wt.%, respectively). This carbon content is much less than that of the NiO-CeO$_2$ catalyst (90.1 wt.%). The $FeCe_2O_4$ loaded catalyst showed the long-time durability and low amount carbon formation in the catalyst even if carbon existence had no significant influence on the catalytic properties of the catalyst [70].

Table 3. 2 Amount of carbon deposits on spent samples

	Samples	Carbon Wt. %
1.	Al-F	23.0
1.	CeO_2/Al-F	16.5
2.	$FeCe_2O_4$/Al-F	17.0
3.	NiO-CeO_2/Al-F	90.1

3.3.4 XPS characterization before and after DRP
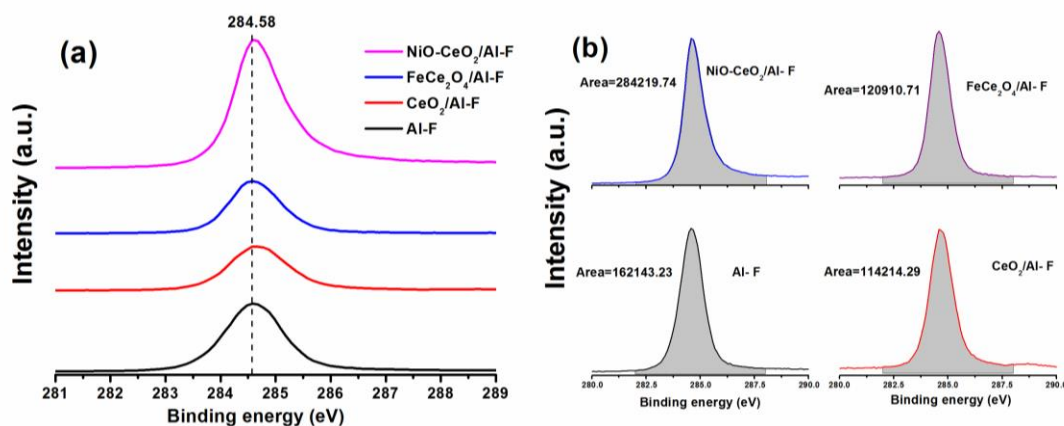
Figure 3.1.14. Survey spectrum from quantitative XPS of the C 1s peaks (a) and (b) for all catalysts after DRP.

The amounts and shapes of the carbon particles deposited on each catalyst were determined by using C 1s – XPS analysis, as shown in **Figure 3.1.14.** In this regard, the peak at 284.58 eV is assigned to the carbon deposited on the surface of the catalysts after DRP. The peak appeared at almost the same location for all the catalysts and might correspond to the three main types of carbon species, i.e., C-C, C-H as well as a few carbon nanotubes [71, 72]. As shown in Figure 11b, the area of the peak, which corresponds to the amount of carbon deposited, was most significant for the spent NiO-CeO_2/Al-F sample and the smallest for the CeO_2/Al-F sample, indicating the level of catalytic degradation caused by coke formation. The difference between the peak areas of the $FeCe_2O_4$/Al-F and CeO_2/Al-F shows that the area difference between these catalysts was small.

It shows that the carbon was not deposited over the Fe sites, suggesting that Fe plays a role in oxidizing C to CO_2, thereby promoting the production of hydrogen with less catalytic deterioration. It is consistent with the TPO results.
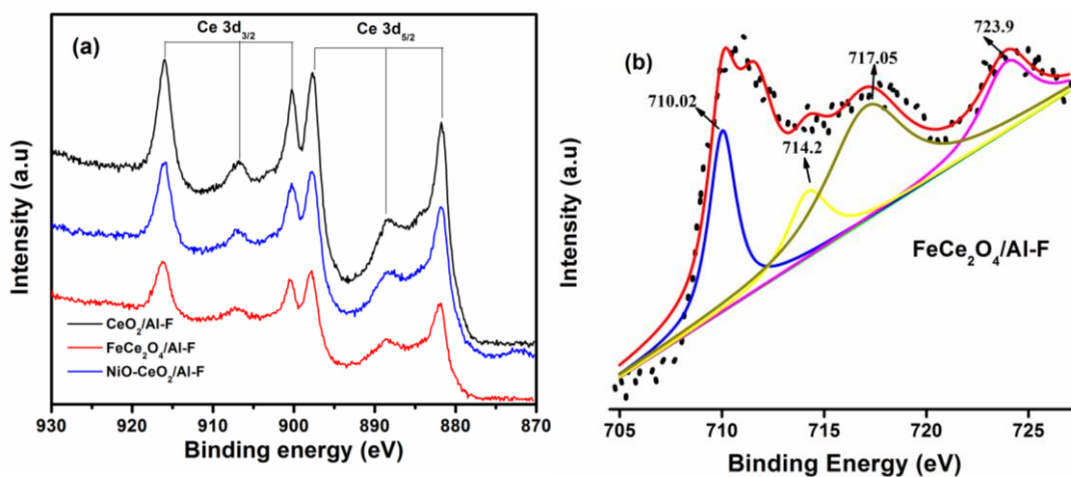
Figure 3.1.15 Survey spectrum from quantitative XPS of the Ce 3d peaks for the CeO_2/Al-F, NiO-CeO_2/Al-F and $FeCe_2O_4$/Al-F catalysts (a) and Fe 2p peaks for the $FeCe_2O_4$/Al-F fresh catalyst (b).

XPS studied the chemical environment and oxidation states of the elements present in the prepared catalysts before and after the reaction. The photoelectron peaks of Fe_{2p} and Ce_{3d} pertaining to $FeCe_2O_4$/Al-F, CeO_2/Al-F, and NiO-CeO_2/Al-F fresh sample are presented in **Figure 3.1.15a** and **3.1.15b**. In **Figure 3.1.15a**, the CeO_2 spectrum displays six peaks in the region of 881.7, 888.6, 897.6, 900.2, 906.7, and 916.8 eV. Among them, the six peaks were divided into two spin-orbit doublets attributable to Ce $3d_{3/2}$ and Ce $3d_{5/2}$, respectively. This distinctly shows the presence of the Ce^{4+} and Ce^{3+} states in all the catalysts. It is evident that the observed binding energy of Ce^{4+} and Ce^{3+} are in good agreement with the values in previous reports, [73, 74] even though the peak intensities were lower for the Ni and Fe loaded catalysts, respectively. Especially, the peaks of the $FeCe_2O_4$/Al-F catalyst had the low-intensity among the catalysts and might be the formation of $FeCe_2O_4$ compounds and Ce as a phase of Ce^{3+} at 904.4 eV. A closer examination of

the XPS results of the Fe 2p orbital of the $FeCe_2O_4$/Al-F catalyst (**Figure 3.1.15b**) shows that Fe^{2+} has a peak at 710 eV and a satellite peak located at around 716 eV. In view of these references, the de-convoluted peaks are assigned and presented. The Fe $2p_{3/2}$ peak of the $FeCe_2O_4$/Al-F catalyst was located at 710.0 eV with its satellites located at 714.2 eV and 717 eV, which is similar to the binding energy of Fe^{2+} ions in $FeCl_2$, [75-77] implying that the Fe phase in the $FeCe_2O_4$/Al-F catalyst primarily exists in the +2-valence state on the catalyst surface and is consistent with the XRD analysis (**Figure 3.1.1**).
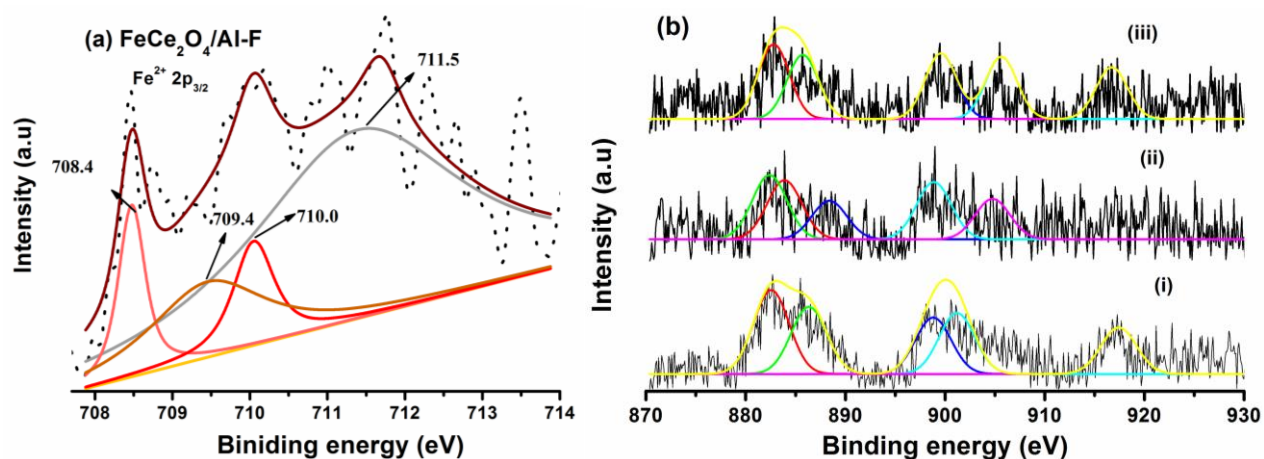
Figure 3.1.16 Survey spectrum from quantitative XPS of the Fe 2p peaks for the $FeCe_2O_4$/Al-F catalyst (a) and Ce 3d peaks for the CeO_2/Al-F (i), $FeCe_2O_4$/Al-F (ii) and NiO-CeO_2/Al-F (iii) catalysts (b) after DRP.

Figure 3.1.16a shows the XPS analysis of the elemental state of Fe 2p after DRP at 700°C for 24 h. The major peaks were observed at 708.4, 709.4, 710.7 eV and at 711.5 eV, which correspond to the Fe^{2+} ionic state. New peaks observed at lower binding energies of 708.4 eV and 709.4 eV correspond to the reduced state, i.e., Fe^o, and the peak at 710 eV corresponds to Fe^{2+}. The peak intensity decreased after DRP reaction; it means that the carbon was deposited on the surface [77]. **Figure 3.1.16b** shows the XPS results for Ce 3d to indicate the chemical state of Ce after DRP. For the CeO_2/Al-F catalyst (i) the quantitative evaluation revealed major peaks at 882.5

eV, 886.5 eV, 898.7 eV, 901.7 eV, and 917.4 eV, which correspond to Ce^{4+} ions. This result shows that there is no significant change in the Ce^{4+} band for the CeO_2/Al-F catalyst. This could indicate the existence of Ce^{4+} ions on the surface of the catalyst and less sintering, which is consistent with the seemingly small peak area of C 1s on the XPS spectra. Similarly, the NiO-CeO_2/Al-F catalyst (iii) also displays the same peaks as the Ce 3d XPS spectra. In addition, the intensity of the Ce^{4+} peak at 887.1 eV was observed to decrease for this catalyst. This might be due to the reduction Ce^{4+} to Ce^{3+} and the deposition of a large amount of carbon, which is consistent with the TPO results (**Table 3.2**) and the C 1s XPS spectra (**Figure 3.1.14b**). Especially, the Ce 3d XPS spectrum of the $FeCe_2O_4$/Al-F catalyst (ii) after DRP showed the appearance of a Ce^{3+} peak at 884.1 eV on the surface. This result reveals the limited sintering of Ce and Fe particles as well as good coking resistance. However, Fe^{2+} is also retained on the surface and leads to timeous inhibition of coke formation, which is consistent with the C 1s XPS and TPO profile, respectively.

3.4 Conclusions

In this work, we successfully prepared the $FeCe_2O_4$ spinel catalyst by the sol-gel method. The XRD patterns of the fresh catalyst confirmed the formation of $FeCe_2O_4$ on the Al-F support. The XPS analysis supported the phase and elemental nature of $FeCe_2O_4$. The hydrogen yield of the DRP process approached that of a stoichiometric reaction, and the catalyst exhibited excellent stability with time. The NiO-CeO_2/Al-F showed high initial C_3H_8 conversion, however, due to the rapid carbon formation on the catalyst surface, the catalytic activity kept decreasing with time. Compared to the Ni-based catalyst, the Fe spinel catalyst exhibited low initial catalytic activity. However, the Fe spinel catalyst showed superior catalytic performance in terms of stable activity, suppression of coke formation and sintering of metal particles. The XRD, FE-SEM, Raman, XPS, and TPO results indicated that the iron spinel catalyst is an efficient catalyst for DRP because of

its inherent ability to minimize carbon deposition. The findings of this study suggest that novel Fe spinel catalysts can be adequate replacements for spinel catalysts based on noble metals and that the development of these catalysts merits additionally investigate ponders in the dry reforming.

3.5 References

1. Aasberg-Petersen, K.; Dybkjær, I.; Ovesen, C.V.; Schjødt, N.C.; Sehested, J.; Thomsen, S.G. Natural gas to synthesis gas – catalysts and catalytic processes. *Journal of Natural Gas Science and Engineering* **2011**, *3*, 423-459.
2. Fang, K.; Li, D.; Lin, M.; Xiang, M.; Wei, W.; Sun, Y. A short review of heterogeneous catalytic process for mixed alcohols synthesis via syngas. *Catalysis Today* **2009**, *147*, 133-138.
3. Luk, H.T.; Mondelli, C.; Ferre, D.C.; Stewart, J.A.; Perez-Ramirez, J. Status and prospects in higher alcohols synthesis from syngas. *Chem Soc Rev* **2017**, *46*, 1358-1426.
4. Cheng, K.; Gu, B.; Liu, X.; Kang, J.; Zhang, Q.; Wang, Y. Direct and highly selective conversion of synthesis gas into lower olefins: Design of a bifunctional catalyst combining methanol synthesis and carbon-carbon coupling. *Angewandte Chemie International Edition* **2016**, *55*, 4725-4728.
5. Muraleedharan Nair, M.; Kaliaguine, S. Structured catalysts for dry reforming of methane. *New J. Chem.* **2016**, *40*, 4049-4060.
6. Pakhare, D.; Spivey, J. A review of dry (CO_2) reforming of methane over noble metal catalysts. *Chem Soc Rev* **2014**, *43*, 7813-7837.
7. Ayodele, B.V.; Khan, M.R.; Cheng, C.K. Catalytic performance of ceria-supported cobalt catalyst for Co-rich hydrogen production from dry reforming of methane. *International Journal of Hydrogen Energy* **2016**, *41*, 198-207.
8. Althenayan, F.M.; Yei Foo, S.; Kennedy, E.M.; Dlugogorski, B.Z.; Adesina, A.A. Bimetallic Co-Ni/Al_2O_3 catalyst for propane dry reforming: Estimation of reaction metrics from longevity runs. *Chemical Engineering Science* **2010**, *65*, 66-73.
9. Karuppiah, J.; Mok, Y.S. Plasma-reduced Ni/γ–Al_2O_3 and CeO_2–Ni/γ–Al_2O_3 catalysts for improving dry reforming of propane. *International Journal of Hydrogen Energy* **2014**, *39*, 16329-16338.
10. Kim, K.M.; Kwak, B.S.; Park, N.-K.; Lee, T.J.; Lee, S.T.; Kang, M. Effective hydrogen production from propane steam reforming over bimetallic Co-doped NiFe/Al_2O_3 catalyst. *Journal of Industrial and Engineering Chemistry* **2017**, *46*, 324-336.
11. Sutton, D.; Moisan, J.F.; Ross, J.R.H. Kinetic study of CO_2 reforming of propane over Ru/Al_2O_3. *Catalysis Letters* **2001**, *75*, 175-181.
12. Zhang, L.; Wang, X.; Tan, B.; Ozkan, U.S. Effect of preparation method on structural characteristics and propane steam reforming performance of Ni-Al_2O_3 catalysts. *Journal of Molecular Catalysis A: Chemical* **2009**, *297*, 26-34.
13. Natesakhawat, S.; Oktar, O.; Ozkan, U.S. Effect of lanthanide promotion on catalytic performance of sol-gel Ni/Al_2O_3 catalysts in steam reforming of propane. *Journal of Molecular Catalysis A: Chemical* **2005**, *241*, 133-146.
14. Huang, T.-J.; Wu, C.-Y.; Wang, C.-H. Fuel processing in direct propane solid oxide fuel cell and carbon dioxide reforming of propane over Ni–YSZ. *Fuel Processing Technology* **2011**, *92*, 1611-1616.
15. Råberg, L.B.; Jensen, M.B.; Olsbye, U.; Daniel, C.; Haag, S.; Mirodatos, C.; Sjåstad, A.O. Propane dry reforming to synthesis gas over Ni-based catalysts: Influence of support and operating parameters on catalyst activity and stability. *Journal of Catalysis* **2007**, *249*, 250-260.
16. Solymosi, F.; Tolmacsov, P.; Kedves, K. CO_2 reforming of propane over supported Rh. *Journal of Catalysis* **2003**, *216*, 377-385.

17. Solymosi, F.; Tolmacsov, P.; Zakar, T.S. Dry reforming of propane over supported Re catalyst. *Journal of Catalysis* **2005**, *233*, 51-59.
18. Shah, Y.T.; Gardner, T.H. Dry reforming of hydrocarbon feedstocks. *Catalysis Reviews* **2014**, *56*, 476-536.
19. Chueh, W.C.; Shao, Z.; Haile, S.M. Tunability of propane conversion over alumina-supported Pt and Rh catalysts. *Topics in Catalysis* **2007**, *46*, 402-413.
20. Chen, C.; Wang, X.; Zhang, L.; Zou, X.; Ding, W.; Lu, X. Synthesis of mesoporous Ni–La_2O_3/SiO_2 by poly(ethylene glycol)-assisted sol-gel route as highly efficient catalysts for dry reforming of methane with a H_2/CO ratio of unity. *Catalysis Communications* **2017**, *94*, 38-41.
21. Izquierdo, U.; Barrio, V.L.; Requies, J.; Cambra, J.F.; Güemez, M.B.; Arias, P.L. Tri-reforming: A new biogas process for synthesis gas and hydrogen production. *International Journal of Hydrogen Energy* **2013**, *38*, 7623-7631.
22. Alves, H.J.; Bley Junior, C.; Niklevicz, R.R.; Frigo, E.P.; Frigo, M.S.; Coimbra-Araújo, C.H. Overview of hydrogen production technologies from biogas and the applications in fuel cells. *International Journal of Hydrogen Energy* **2013**, *38*, 5215-5225.
23. Gallego, G.S.; Batiot-Dupeyrat, C.; Barrault, J.; Florez, E.; Mondragón, F. Dry reforming of methane over $LaNi_{1-y}B_yO_{3\pm\delta}$ (B = Mg, Co) perovskites used as catalyst precursor. *Applied Catalysis A: General* **2008**, *334*, 251-258.
24. Polo-Garzon, F.; Pakhare, D.; Spivey, J.J.; Bruce, D.A. Dry reforming of methane on Rh-doped pyrochlore catalysts: A steady-state isotopic transient kinetic study. *ACS Catalysis* **2016**, *6*, 3826-3833.
25. Chawl, S.K.; George, M.; Patel, F.; Patel, S. Production of synthesis gas by carbon dioxide reforming of methane over nickel based and perovskite catalysts. *Procedia Engineering* **2013**, *51*, 461-466.
26. Nair, M.M.; Kaliaguine, S.; Kleitz, F. Nanocast $LaNiO_3$ perovskites as precursors for the preparation of coke-resistant dry reforming catalysts. *ACS Catalysis* **2014**, *4*, 3837-3846.
27. Rydén, M.; Lyngfelt, A.; Mattisson, T.; Chen, D.; Holmen, A.; Bjørgum, E. Novel oxygen-carrier materials for chemical-looping combustion and chemical-looping reforming; $La_xSr_{1-x}Fe_yCo_{1-y}O_{3-\delta}$ perovskites and mixed-metal oxides of NiO, Fe_2O_3 and Mn_3O_4. *International Journal of Greenhouse Gas Control* **2008**, *2*, 21-36.
28. Guo, J.; Lou, H.; Zhao, H.; Chai, D.; Zheng, X. Dry reforming of methane over nickel catalysts supported on magnesium aluminate spinels. *Applied Catalysis A: General* **2004**, *273*, 75-82.
29. Khoo, H.H.; Tan, R.B.H. Environmental impact evaluation of conventional fossil fuel production (oil and natural gas) and enhanced resource recovery with potential CO_2 sequestration. *Energy & Fuels* **2006**, *20*, 1914-1924.
30. Sutthiumporn, K.; Kawi, S. Promotional effect of alkaline earth over Ni-La_2O_3 catalyst for CO_2 reforming of CH_4: Role of surface oxygen species on H_2 production and carbon suppression. *International Journal of Hydrogen Energy* **2011**, *36*, 14435-14446.
31. Dharanipragada, N.V.R.A.; Meledina, M.; Galvita, V.V.; Poelman, H.; Turner, S.; Van Tendeloo, G.; Detavernier, C.; Marin, G.B. Deactivation study of Fe_2O_3–CeO_2 during redox cycles for CO-production from CO_2. *Industrial & Engineering Chemistry Research* **2016**, *55*, 5911-5922.
32. Theofanidis, S.A.; Batchu, R.; Galvita, V.V.; Poelman, H.; Marin, G.B. Carbon gasification from Fe–Ni catalysts after methane dry reforming. *Applied Catalysis B: Environmental* **2016**, *185*, 42-55.
33. Niu, Y.; Fu, G.Y.; Wu, W.T.; Gesmundo, F. The oxidation of two Fe-Ce alloys under low oxygen pressures at 600-800°C. In *High Temperature Materials and Processes*, 1999; Vol. 18, p 159.
34. Niu, Y.; Fu, G.Y.; Gesmundo, F. The corrosion of a Fe-15 wt.% Ce alloy in coal gasification type atmospheres at 600 to 800 °C. *Journal of Phase Equilibria* **2002**, *23*, 61.
35. De Vos, Y.; Jacobs, M.; Van Der Voort, P.; Van Driessche, I.; Snijkers, F.; Verberckmoes, A. Optimization of spray dried attrition-resistant iron based oxygen carriers for chemical looping reforming. *Chemical Engineering Journal* **2017**, *309*, 824-839.
36. Rezaei, M.; Alavi, S.M.; Sahebdelfar, S.; Bai, P.; Liu, X.; Yan, Z.F. CO_2 reforming of CH_4 over nanocrystalline zirconia-supported nickel catalysts. *Applied Catalysis B: Environmental* **2008**, *77*, 346-354.

37. Lovell, E.C.; Fuller, A.; Scott, J.; Amal, R. Enhancing Ni-SiO$_2$ catalysts for the carbon dioxide reforming of methane: Reduction-oxidation-reduction pre-treatment. *Applied Catalysis B: Environmental* **2016**, *199*, 155-165.

38. Damyanova, S.; Bueno, J.M.C. Effect of CeO$_2$ loading on the surface and catalytic behaviors of CeO$_2$-Al$_2$O$_3$-supported Pt catalysts. *Applied Catalysis A: General* **2003**, *253*, 135-150.

39. Jiménez-González, C.; Boukha, Z.; De Rivas, B.; Delgado, J.J.; Cauqui, M.Á.; González-Velasco, J.R.; Gutiérrez-Ortiz, J.I.; López-Fonseca, R. Structural characterisation of Ni/alumina reforming catalysts activated at high temperatures. *Applied Catalysis A: General* **2013**, *466*, 9-20.

40. Seo, J.G.; Youn, M.H.; Jung, J.C.; Song, I.K. Hydrogen production by steam reforming of liquefied natural gas (LNG) over mesoporous nickel-alumina aerogel catalyst. *International Journal of Hydrogen Energy* **2010**, *35*, 6738-6746.

41. Korup, O.; Goldsmith, C.F.; Weinberg, G.; Geske, M.; Kandemir, T.; Schlögl, R.; Horn, R. Catalytic partial oxidation of methane on platinum investigated by spatial reactor profiles, spatially resolved spectroscopy, and microkinetic modeling. *Journal of Catalysis* **2013**, *297*, 1-16.

42. Horn, R.; Williams, K.A.; Degenstein, N.J.; Bitsch-Larsen, A.; Dalle Nogare, D.; Tupy, S.A.; Schmidt, L.D. Methane catalytic partial oxidation on autothermal Rh and Pt foam catalysts: Oxidation and reforming zones, transport effects, and approach to thermodynamic equilibrium. *Journal of Catalysis* **2007**, *249*, 380-393.

43. Wang, X.; Wang, N.; Zhao, J.; Wang, L. Thermodynamic analysis of propane dry and steam reforming for synthesis gas or hydrogen production. *International Journal of Hydrogen Energy* **2010**, *35*, 12800-12807.

44. Linga Reddy, E.; Karuppiah, J.; Lee, H.C.; Kim, D.H. Steam reforming of methanol over copper loaded anodized aluminum oxide (AAO) prepared through electrodeposition. *Journal of Power Sources* **2014**, *268*, 88-95.

45. Vimal, G.; Mani, K.P.; Biju, P.R.; Joseph, C.; Unnikrishnan, N.V.; Ittyachen, M.A. Structural studies and luminescence properties of CeO$_2$:Eu^{3+} nanophosphors synthesized by oxalate precursor method. *Applied Nanoscience* **2015**, *5*, 837-846.

46. Qurashi, A.; Zhang, Z.; Asif, M.; Yamazaki, T. Template-less surfactant-free hydrothermal synthesis NiO nanoflowers and their photoelectrochemical hydrogen production. *International Journal of Hydrogen Energy* **2015**, *40*, 15801-15805.

47. Cui, J.; Hope, G.A. Raman and fluorescence spectroscopy of CeO$_2$, Er$_2$O$_3$, Nd$_2$O$_3$, Tm$_2$O$_3$, Yb$_2$O$_3$, La$_2$O$_3$, and Tb$_4$O$_7$. *Journal of Spectroscopy* **2015**, *2015*, 1-8.

48. Zieliński, J.; Zglinicka, I.; Znak, L.; Kaszkur, Z. Reduction of Fe$_2$O$_3$ with hydrogen. *Applied Catalysis A: General* **2010**, *381*, 191-196.

49. Ge, X.; Li, M.; Shen, J. The reduction of Mg–Fe–O and Mg–Fe–Al–O complex oxides studied by temperature-programmed reduction combined with in situ mössbauer spectroscopy. *Journal of Solid State Chemistry* **2001**, *161*, 38-44.

50. Sahli, N.; Petit, C.; Roger, A.C.; Kiennemann, A.; Libs, S.; Bettahar, M.M. Ni catalysts from NiAl$_2$O$_4$ spinel for CO$_2$ reforming of methane. *Catalysis Today* **2006**, *113*, 187-193.

51. Campbell, C.T.; Peden, C.H. Chemistry. Oxygen vacancies and catalysis on ceria surfaces. *Science* **2005**, *309*, 713-714.

52. Mountapmbeme Kouotou, P.; Vieker, H.; Tian, Z.Y.; Tchoua Ngamou, P.H.; El Kasmi, A.; Beyer, A.; Golzhauser, A.; Kohse-Hoinghaus, K. Structure-activity relation of spinel-type Co-Fe oxides for low-temperature CO oxidation. *Catalysis Science & Technology* **2014**, *4*, 3359-3367.

53. Yang, P.; Liu, Y. Au/Co$_3$O$_4$/CeO$_2$ heterostructures: Morphology controlling, junction formation and enhanced catalysis performance. *Journal of Industrial and Engineering Chemistry* **2017**, *53*, 317-324.

54. Chen, D.; He, D.; Lu, J.; Zhong, L.; Liu, F.; Liu, J.; Yu, J.; Wan, G.; He, S.; Luo, Y. Investigation of the role of surface lattice oxygen and bulk lattice oxygen migration of cerium-based oxygen carriers: XPS and designed H$_2$-TPR characterization. *Applied Catalysis B: Environmental* **2017**, *218*, 249-259.

55. Ma, L.; Wang, D.; Li, J.; Bai, B.; Fu, L.; Li, Y. Ag/CeO$_2$ nanospheres: Efficient catalysts for formaldehyde oxidation. *Applied Catalysis B: Environmental* **2014**, *148-149*, 36-43.

56. Deng, W.; Dai, Q.; Lao, Y.; Shi, B.; Wang, X. Low temperature catalytic combustion of 1,2-dichlorobenzene over CeO_2–TiO_2 mixed oxide catalysts. *Applied Catalysis B: Environmental* **2016**, *181*, 848-861.

57. Laosiripojana, N.; Sangtongkitcharoen, W.; Assabumrungrat, S. Catalytic steam reforming of ethane and propane over CeO_2-doped Ni/Al_2O_3 at SOFC temperature: Improvement of resistance toward carbon formation by the redox property of doping CeO_2. *Fuel* **2006**, *85*, 323-332.

58. Wang, N.; Chu, W.; Zhang, T.; Zhao, X.S. Synthesis, characterization and catalytic performances of Ce-SBA-15 supported nickel catalysts for methane dry reforming to hydrogen and syngas. *International Journal of Hydrogen Energy* **2012**, *37*, 19-30.

59. Provendier, H.; Petif, C.; Estournes, C.; Kiennemann, A. Dry reforming of methane. Interest of La-Ni-Fe solid solutions compared to $LaNiO_3$ and $LaFeO_3$. **1998**, *119*, 741-746.

60. Sutthiumporn, K.; Maneerung, T.; Kathiraser, Y.; Kawi, S. CO_2 dry-reforming of methane over $La_{0.8}Sr_{0.2}Ni_{0.8}M_{0.2}O_3$ perovskite (M = Bi, Co, Cr, Cu, Fe): Roles of lattice oxygen on C–H activation and carbon suppression. *International Journal of Hydrogen Energy* **2012**, *37*, 11195-11207.

61. Theofanidis, S.A.; Galvita, V.V.; Poelman, H.; Marin, G.B. Enhanced carbon-resistant dry reforming Fe-Ni catalyst: Role of Fe. *ACS Catalysis* **2015**, *5*, 3028-3039.

62. Galvita, V.V.; Poelman, H.; Detavernier, C.; Marin, G.B. Catalyst-assisted chemical looping for CO_2 conversion to CO. *Applied Catalysis B: Environmental* **2015**, *164*, 184-191.

63. Goldwasser, M.R.; Rivas, M.E.; Pietri, E.; Pérez-Zurita, M.J.; Cubeiro, M.L.; Gingembre, L.; Leclercq, L.; Leclercq, G. Perovskites as catalysts precursors: CO_2 reforming of CH_4 on $Ln_{1−x}Ca_xRu_{0.8}Ni_{0.2}O_3$ (Ln = La, Sm, Nd). *Applied Catalysis A: General* **2003**, *255*, 45-57.

64. Pakhare, D.; Schwartz, V.; Abdelsayed, V.; Haynes, D.; Shekhawat, D.; Poston, J.; Spivey, J. Kinetic and mechanistic study of dry (CO_2) reforming of methane over Rh-substituted $La_2Zr_2O_7$ pyrochlores. *Journal of Catalysis* **2014**, *316*, 78-92.

65. Ferencz, Z.; Erdőhelyi, A.; Baán, K.; Oszkó, A.; Óvári, L.; Kónya, Z.; Papp, C.; Steinrück, H.P.; Kiss, J. Effects of support and Rh additive on Co-based catalysts in the ethanol steam reforming reaction. *ACS Catalysis* **2014**, *4*, 1205-1218.

66. Karuppiah, J.; Reddy, E.L.; Sudhakaran, M.; Lee, S. Production of synthesis gas from dry reforming of propane with carbon dioxide over ceria-promoted nickel foam catalysts.

67. Wolfbeisser, A.; Sophiphun, O.; Bernardi, J.; Wittayakun, J.; Föttinger, K.; Rupprechter, G. Methane dry reforming over ceria-zirconia supported Ni catalysts. *Catalysis Today* **2016**, *277*, 234-245.

68. Alipour, Z.; Rezaei, M.; Meshkani, F. Effects of support modifiers on the catalytic performance of Ni/Al_2O_3 catalyst in CO_2 reforming of methane. *Fuel* **2014**, *129*, 197-203.

69. García-Diéguez, M.; Herrera, C.; Larrubia, M.Á.; Alemany, L.J. CO_2-reforming of natural gas components over a highly stable and selective $NiMg/Al_2O_3$ nanocatalyst. *Catalysis Today* **2012**, *197*, 50-57.

70. Károlyi, J.; Németh, M.; Evangelisti, C.; Sáfrán, G.; Schay, Z.; Horváth, A.; Somodi, F. Carbon dioxide reforming of methane over $Ni–In/SiO_2$ catalyst without coke formation. *Journal of Industrial and Engineering Chemistry* **2017**.

71. Koo, K.Y.; Lee, S.H.; Jung, U.H.; Roh, H.S.; Yoon, W.L. Syngas production via combined steam and carbon dioxide reforming of methane over $Ni-Ce/MgAl_2O_4$ catalysts with enhanced coke resistance. *Fuel Processing Technology* **2014**, *119*, 151-157.

72. Montero, C.; Ochoa, A.; Castaño, P.; Bilbao, J.; Gayubo, A.G. Monitoring Ni^0 and coke evolution during the deactivation of a Ni/La_2O_3–$α$-Al_2O_3 catalyst in ethanol steam reforming in a fluidized bed. *Journal of Catalysis* **2015**, *331*, 181-192.

73. Pradhan, G.K.; Parida, K. Fabrication of iron-cerium mixed oxide: An efficient photocatalyst for dye degradation. *International Journal of Engineering, Science and Technology* **2010**, *2*.

74. Pechimuthu, N.A.; Pant, K.K.; Dhingra, S.C. Deactivation studies over $Ni−K/CeO_2−Al_2O_3$ catalyst for dry reforming of methane. *Industrial & Engineering Chemistry Research* **2007**, *46*, 1731-1736.

75. Yamashita, T.; Hayes, P. Analysis of xps spectra of Fe^{2+} and Fe^{3+} ions in oxide materials. *Applied Surface Science* **2008**, *254*, 2441-2449.

76. Kong, H.; Song, J.; Jang, J. One-step fabrication of magnetic γ-Fe$_2$O$_3$/polyrhodanine nanoparticles using in situ chemical oxidation polymerization and their antibacterial properties. *Chemical Communications* **2010**, *46*, 6735-6737.

77. Grosvenor, A.P.; Kobe, B.A.; Biesinger, M.C.; McIntyre, N.S. Investigation of multiplet splitting of Fe$_{2p}$ xps spectra and bonding in iron compounds. *Surface and Interface Analysis* **2004**, *36*, 1564-1574.

CHAPTER -4

Syngas production via propane dry reforming over SrNiO₃ perovskite catalyst

4.1 Introduction

The conventional production of synthesis gas (syngas) by methane steam reforming (**4.1**) regularly produces a product with higher H_2/CO values greater than 3[1,2]. Recently, the focus has been drawn to the conversion of light hydrocarbons with carbon dioxide into valuable products (syngas) by catalytic reactions, which known as dry reforming (**4.2**) [3]. The results in a product with a lower H_2/CO ratio ≤ 2. This ratio is more suitable as precursors for the synthesis of liquid fuels, and chemicals such as olefins, methanol synthesis and Fisher-Tropsch synthesis [4-7]. Propane is a significant element of natural gas and also produced in a variety of petroleum refining operations. Primarily, it readily activates at a lower reaction temperature than methane [8].

$$CH_4 + H_2O = CO + 3H_2 \ (\Delta H°_{298} = 222.4 \ kJmol^{-1}) \qquad \ldots\ldots\ldots (4.1)$$

$$C_3H_8 + 3CO_2 = 6CO + 4H_2 \ (\Delta H°_{298} = 644.1 \ kJmol^{-1}) \qquad \ldots\ldots\ldots (4.2)$$
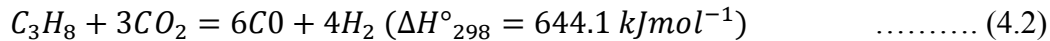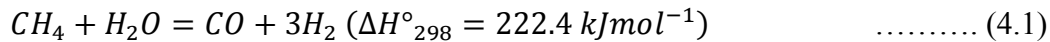
However, the steam and dry are an endothermic reaction require constant high energy to occur reaction. Numerous catalysts have been described for each of the processes mentioned above for various hydrocarbons [9-11]. Noble metal catalysts show superior performance regarding the activity and the durability than non-noble metal catalysts [16]. Moreover, the Ni-based catalyst is attractive and promising due to their high activity, low cost, and abundant availability [12]. It has been widely studied with different support materials such as Al_2O_3, SiO_2, CeO_2, SiC and among them, Al_2O_3 is the most widely used to produce dry reforming [13,14]. The main limitations of Ni/Al_2O_3 have reported to particle sintering and coke formation. Perovskites are ABO_3 type crystal structured materials with alkaline earth or rare earth metal at the A-site and a transition metal at

the B-site [15,16]. These possess some exciting chemical and physical properties, e.g., high thermal stability, the excellent reactivity of lattice oxygen, low cost and abundant resources [15]. A-site replacement with alkaline earth metal is expected to enhance the carbon susceptible and thermal stability, and the B-site alteration is expected to increase the activity of the catalyst [17,18]. In last decade, many researchers have been widely reported $LaNiO_3$, [19-21] $LaFeO_3$, [22] $SmCoO_3$ [23] and also partial substitution of B- site perovskite catalysts show the higher activity, stability, and resistance to coke formation even at elevated temperature. It increases the syngas production in dry reforming reaction [24-26]. However, La-based perovskite catalysts showed excellent activity due to the basicity of La elements but it is rare earth element, expensive and less availability. Hence, this study has focused on low-cost and high basicity material with key features such as high catalytic activity and coking resistance.

Hence, the objectives of this study are to synthesize, characterize, and investigate the catalytic activity of novel $SrNiO_3$ perovskite as a catalyst to produce syngas via dry reforming of propane in an experimental gas phase reactor setup. The conversion of reactants and production of syngas was carried out with emphasis on exploiting the effects of reaction temperature. In addition, the effects of H_2 reduction were also investigated by comparing the conversion of the reduced and unreduced $SrNiO_3$ perovskite catalyst prior to the propane dry reforming reaction.

4.1   Experimental section

4.2.1 Materials and methods

Strontium nitrate ($Sr(NO_3)_2$, Nickel nitrate hexahydrate ($Ni(NO_3)_2 \cdot 6H_2O$), citric acid anhydrous, hydrochloric acid (HCl), and anhydrous ethanol (C_2H_5OH) were purchased from Daejung Chemicals Ltd, South Korea. Gamma alumina (γ-Al_2O_3) pellets were purchased from Alfa Aesar Co., Inc, South Korea. Nickel foam (NiF) was purchased from MTI Crop., Ltd., South

Korea. All the chemicals used in this experiment were of research grade, and distilled water (DW) was used in whole experiments.

4.2.2 Synthesis of SrNiO₃ compound

SrNiO₃ based perovskite catalyst was prepared by the citric acid sol-gel method. In typical preparation method, the precursor of 0.02 M of $Sr(NO_3)_2$, and $Ni(NO_3)_2 \cdot 6H_2O$ in distilled water were prepared in two separate beakers. These two solutions were mixed until a transparent solution. Citric acid (0.06 m) in water was added by dropwise in the above nitrate solution to ensure miscibility. The solution was kept at 80°C hot plate and stirred gently with Teflon-coated magnetic stir bar until the solution becomes viscous liquid. The resulting solution was kept at 110°C for 12 h to dried off the excess of water. The dried powder was treated at 450°C for 5 h to allow combustion reaction the resulting product was foamy. The final powder was ground well then calcined at 900°C for 10 h, resulting in the synthesis of SrNiO₃ perovskite compound.

4.2.3 Preparation of catalyst

The 10 wt.% of catalyst was prepared with different support materials (Al_2O_3 and NiF) as follow procedure. In order to remove undesired materials on the surface of support materials, both supports were pretreated by removed of moisture and HCl treatment to remove oxide layers Al_2O_3 and NiF, respectively. The γ-Al_2O_3 pellets were washed several times with DW to swipe out of loss bound particles on the surface final rinse with ethanol and then kept at 150°C for 2h to remove moistures. The purchased NiF was soaked in 1.0 M HCl solution for 30 min to remove the oxide layer on the surface and then washed several times with DW to the removed excess of acid and finally rinsed with ethanol and kept 110°C for 1h. The 16.0 mm of OD discs of pretreated NiF was cut by hole puncher to make a disc shape. The pretreated γ-Al_2O_3 pellets were ground well and made a fine powder, the 1.8 gm of fine γ-Al_2O_3 powder was mixed with 0.2 gm of SrNiO₃ powder

to ensure the blending. A hydraulic press was used to prepare the pressured pellet, and the pellet was broken down into a small size by manually to around 2 mm of beads and sieved with 2 mm of mesh to remove the fine powder. The desired amount (0.2 gm) of $SrNiO_3$ was ground with polyvinylidene difluoride (PVDF; catalyst ratio: 95:5) using N-methyl pyrrolidone (NMP) as a solvent. The 1.8 gm of the disc of NiF (16 mm; ID) support was then coated with the prepared slurry, and the coated support was allowed to dry in an air oven at 85°C for 12 h.

4.2.4 Material characterization

X-ray diffractograms (XRD) were recorded an X-ray diffractometer (D/MAX 2200H, Bede 200, Rigaku Instruments C) with a horizontal goniometer performed by a fine focus copper X-ray tube (40 kV, 40 mA). BET specific surface area measurements were carried out on an Autosorb-1-MP instrument at liquid nitrogen temperature. Prior to the analysis, the sample was degassed at 150 °C for 3 h, and the BET multi-point method was applied to estimate the surface area. The surface morphology of the prepared materials was analyzed by Field-emission scanning electron microscopy (FE-SEM, JSM-6700F, JEOL). The Raman spectroscopy was evaluated on the samples using Raman HR Evolution Raman Spectrometer (LabRAM Horiba, France) used at Ar^+ ion laser operating at 10 mW and a wavelength of 514 nm. Temperature-programmed desorption/reduction (TPD/TPR) experiments were carried out on the gas-chromatography (DS science, DS-6500, Korea) equipped with TCD detector. The 100 mg of the catalyst samples were loaded in a U- Shaped quartz tube and placed on the glass wool. The temperature of the sample was measured using a thermocouple fixed with quartz tube near the sample. The sample was pretreated at 250 °C for 30 min in a flow of Ar (45 ml min^{-1}) and the reactor was cooled to attain room temperature, and the gas flow changed to 5%H_2/Ar (50 ml min^{-1}). The hydrogen consumption was measured with the ramping of sample temperature to 900 °C with a heating rate

of 5°C min^{-1}. The change in the thermal conductivity of the gas mixture, due to the hydrogen consumption, was measured as the signal. The following equation calculated the active site of the catalyst.

$$Area(mol) = \int_0^t [H_2]Q_{total}dt$$ .... (4.2)

where [H_2] is a concentration of H_2 in mol l^{-1} and Q_{total} is total flow rate 1 min^{-1}. Temperature-programmed oxidation (TPO) experiments of spent catalyst were carried out on the Fourier transform infrared spectroscopy (FTIR) (FTIR-7600 spectrometer, Lambda) in order to understand the nature of carbon species. The 100 mg of spent catalyst was placed in a U-shaped quartz tube and flush with 50 ml/min of N_2 at 250°C for 30 min prior to remove surface oxygen and to attain inert atmosphere and reactor cool down to room temperature with continues flow of N_2 gas. The 10%O_2/N_2 (50 ml/min) of oxidant gas feed was changed over, and outlet of gas (CO_2) was monitor through online FTIR at a ramped temperature from 300K to 1200K at the rate of 5 K/min.

4.2.5 Catalytic activity and selectivity

The catalytic activity of prepared catalysts was measured in fixed-bed quartz reactor (16 mm ID and 600 mm length). A 2.0 g of the catalyst was placed in the reactor between a sandwich of quartz wool. A tubular furnace has maintained the reaction temperature of the catalyst with an external temperature controller equipped with a K-type thermocouple. The temperature of the catalyst was measured by a K-type thermocouple which fixed on it. The ratio of feed gases of carbon dioxide (CO_2) and propane (C_3H_8) (CPR) was 3, the total composition of feed gases are C_3H_8: CO_2: Ar in percentage (10:30:60) and controlled by a mass flow controller (MFC). The total flow rate of the reactant gas is 200 ml/min for all catalytic studies. The concentration of C_3H_8 and CO_2 were measured by online gas chromatography (GC- Micro-GCCP-4900, 10m PPQ column)

and the concentration of H_2 and CO were measured by GC (DS-Science- 20m- HayeSep-Q column) equipped with a thermal conductive detector (TCD). The catalytic activity of all catalysts was examined at every 50°C interval of the temperature range of 550°C to 700°C The conversion of reactants (X_A) and selectivity (S) of various products were calculated by the following equations [3,27].

$$X_A \,(\%) = \frac{C_{A_0} - C_A}{C_{A_0} + \varepsilon_A C_A} \times 100 \qquad\qquad \text{.......... (4.4)}$$

$$S_{H_2} = \frac{[H_2]_{out} \cdot F_{out}\left(\frac{ml}{min}\right)}{4 \cdot ([C_3H_8]_{in} \cdot F_{in} - [C_3H_8]_{out} \cdot F_{out})\left(\frac{ml}{min}\right)} \qquad\qquad \text{.......... (4.5)}$$

$$S_{CO} = \frac{[CO]_{out} \cdot F_{out}\left(\frac{ml}{min}\right)}{3 \cdot ([C_3H_8]_{in} \cdot F_{in} - [C_3H_8]_{out} \cdot F_{out}) + ([CO_2]_{in} \cdot F_{in} - [CO_2]_{out} \cdot F_{out})\left(\frac{ml}{min}\right)} \qquad \text{.......... (4.6)}$$

$$\frac{H_2}{CO} = \frac{F_{H_2}}{F_{CO}} \qquad\qquad \text{.......... (4.7)}$$

where, X_A is the conversion of C_3H_8 and CO_2, C_{A0}, and C_A are inlet and outlet concentration of reactants C_3H_8 and CO_2, respectively, F_{in} and F_{out} are inlet and outlet flow rates (ml/min). $[C_3H_8]_{in}$, $[CO_2]_{in}$, $[C_3H_8]_{out}$, $[CO_2]_{out}$, $[H_2]_{out}$, and $[CO]_{out}$ were inlet and outlet concentration of C_3H_8, CO_2, H_2, and CO, respectively. The F_{H2} and F_{CO} molar flow rate of H_2 and CO in the outlet.

4.2   Result and discussion

4.3.1 Materials characterization

XRD patterns of the calcined perovskite and reduced perovskite are shown in **Figure 4.1.1**. The sample was calcined at 900°C and reduced by hydrogen at 700°C. The fresh catalyst shows the real pattern of $SrNiO_3$ perovskite state and the somewhat slight secondary peak of NiO also found.
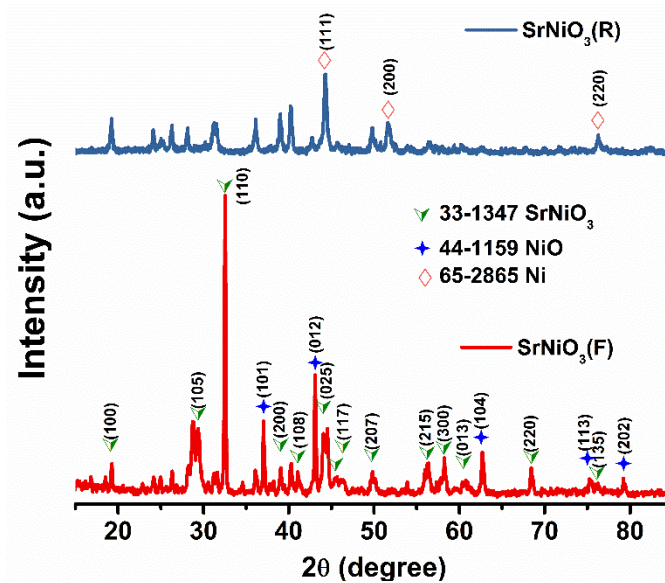
Figure 4.1.1. X-ray diffraction patterns of $SrNiO_3$ unreduced (F) and reduced (R) perovskite catalysts

As seen from **Figure 4.1.1**, The highest sharp peaks at 2θ with a value of 32.52°. It indicates the formation of $SrNiO_3$ crystalline phase. The other peaks at 2θ values of 19.24°, 29.36°, 39.04°, 41.08°, 44.04°, 49.84°, 56.24°, 58.24°, 68.4°, and 76.24° also correspond to $SrNiO_3$ species. Beside $SrNiO_3$ phase, some peaks were evolved at 37.04°, 43.08°, and 62.76°, which belongs to the NiO crystalline phase. All Ni precursors were not used to form $SrNiO_3$. The desired $SrNiO_3$ catalyst was synthesis successfully, and the diffractogram pattern confirms the formation of the hexagonal perovskite structure, matched with standard pattern (JCPDS card no: 33-1347) [28]. The N_2 physisorption isotherm of the $SrNiO_3$ perovskite was shown in **Figure 4.1.2**. This type of isotherms is characteristic of mesoporous solids having a pore diameter between 2 and 50 nm [29]. The BET surface area is 3.3 m^2g^{-1}, which is agreed with perovskite materials as reported in the literature. The pore radius and pore volumes are 1.9 nm and 2.2 x 10^{-3} cm^3g^{-1}, respectively, which

is also an agreement with previous studies of perovskite structure synthesized by the sol-gel method.
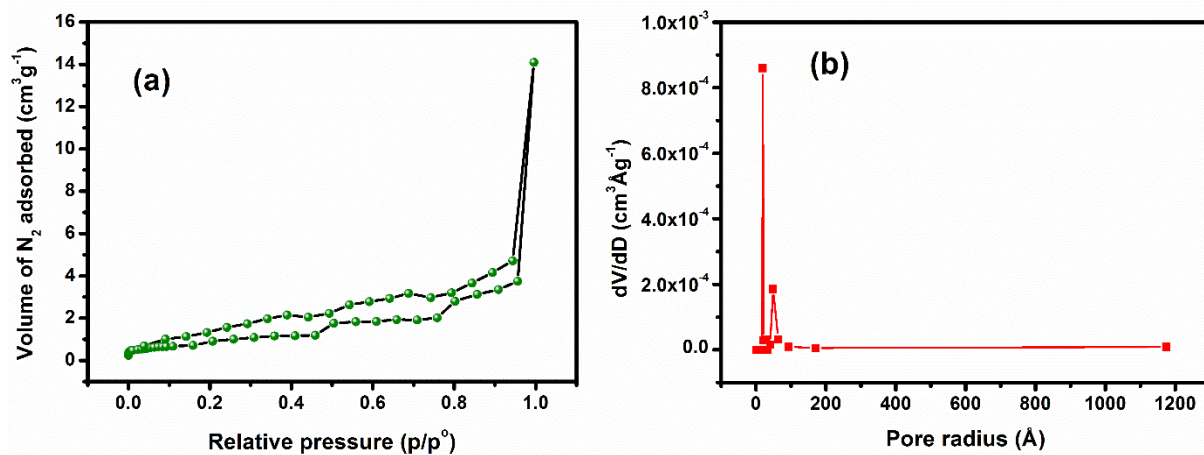
**Figure 4.1.2.** N_2-adsorption and desorption isotherm of $SrNiO_3$ perovskite catalyst (a) and pore size distribution (b)
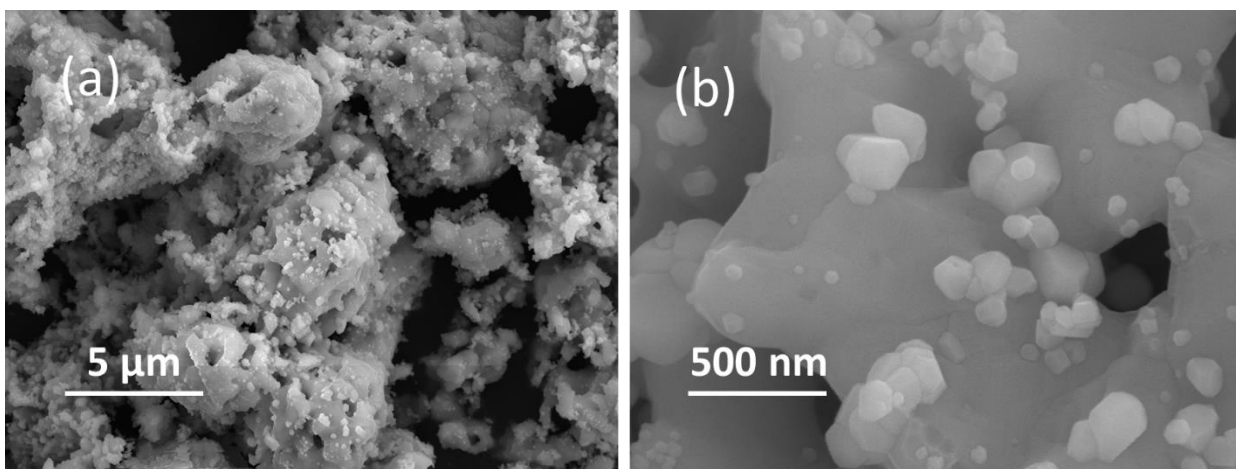
Figure 4.1.3. FE-SEM images of $SrNiO_3$ perovskite catalyst at low (a) and high magnifications (b)

The surface morphology of the $SrNiO_3$ perovskite catalyst was shown in **Figure 4.1.3**. As from the **Figure 4.1.3**, the high-resolution SEM image reveals the porous structure of the material. There is no bulk agglomerated shaped particle were observed in low resolution and high-resolution images. **Figure 4.1.4** shows the EDS coupled with SEM measurement was measured at different

points of the samples using a focused beam at 1µm to determine the mean element proportions of the sample. The EDS pattern of the typical crystalline $SrNiO_3$ sample where the peaks were attributed to Sr, Ni, and O. It could be explained the homogenous mixing of the components in the solid state.
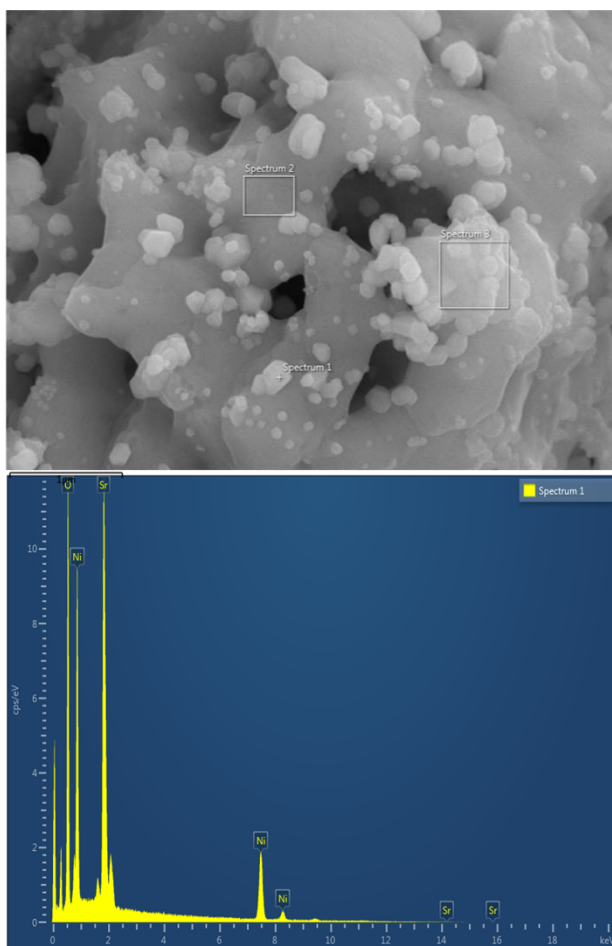
Figure 4.1.4. SEM and EDS pattern of $SrNiO_3$ calcined at 900°C

Temperature programmed reduction (H_2-TPR) analysis was determined by the reduction behavior of the fresh catalyst and reduced catalyst. **Figure 4.1.5** shows the H_2-TPR profile of the fresh catalyst and reduce $SrNiO_3$ perovskite catalyst. The two distinct peaks were observed at lower and higher temperatures 600 K and 987 K of the $SrNiO_3$ fresh catalyst. The reduced $SrNiO_3$

exhibited one broad peak at higher temperature 1096 K. Also, the fresh calcined $SrNiO_3$ catalyst reduction process occurred by the following step.
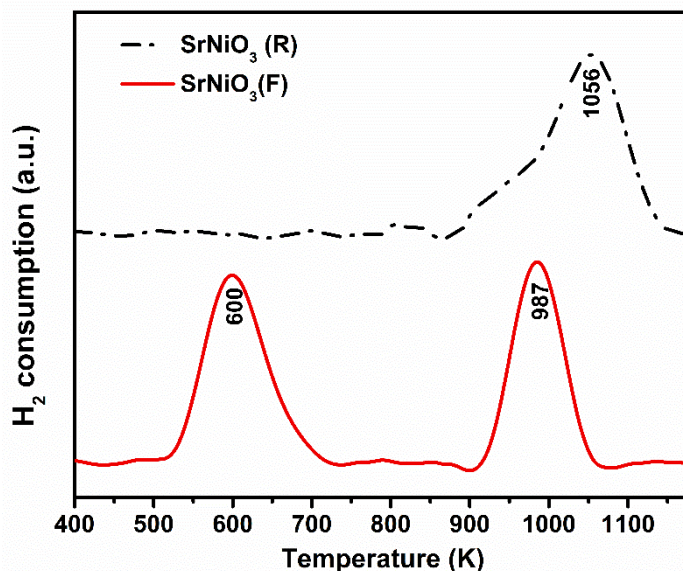

Figure 4.1.5. H_2-TPR of unreduced (F) and reduced (R) $SrNiO_3$ perovskite catalysts

The first step at lower temperature 600 K is indicative of the formation of an oxygen-deficient perovskite structure, while the second peak at 987 K corresponds to the complete reduction of the perovskite to form Ni^0 [26].

$$SrNiO_3 + H_2 \rightarrow SrO + Ni^0 + 2H_2O$$ ………. (4.8)
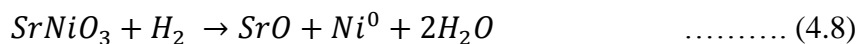
The reduced $SrNiO_3$ perovskite shows the single reduction peak at high temperature, which means the complete formation of $SrNiO_3$ phase after reduction. Perovskite compounds reduction took place at high temperature, which agreed with the previous report [30].

The **Figure 4.1.6** shows the chemisorption characters of $SrNiO_3$ perovskite by H_2 temperature programmed desorption method. As seen in **Figure 4.1.6**, the two distinct peaks were

제주대학교 중앙도서관
JEJU NATIONAL UNIVERSITY LIBRARY

observed at 373°C, and 426°C, the first peaks attributed to the H_2 molecules desorbed from the metal particles, and they represent the outer positioned of Ni atoms in the perovskite lattice [31,32].
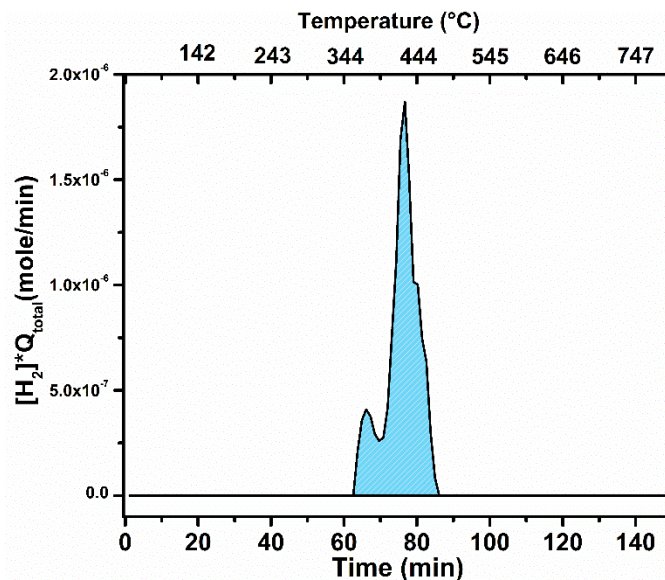

Figure 4.1.6. H_2-TPD of the SrNiO$_3$ perovskite catalyst

The second sharp peak attributed to the H_2 located in the subsurface layers to spillover H_2 in the perovskite lattice [33]. It reveals the high energy requires to unbound the H_2 molecules and strong enough of chemisorption. From the results, the amount of H_2-chemisorbed molecules was estimated under the curve. The total active site of the SrNiO$_3$ catalyst is 3.79 X 10^{20} g^{-1}.

4.3.2 Catalytic activity

The activity of perovskite catalysts has been studied in two forms without reduction and reduced with H_2 prior to reaction. The reduced catalysts have shown the significant activity than a fresh catalyst. The reduction process is occurred to reduce the transition metal phase of the catalyst to metallic phase, which is located at the active site of the catalyst [34]. It has also been reported that reduction would enhance the metal dispersion, thereby providing an adequate platform for methane dry reforming reaction to occur. Reduction step, in the long run, has been reported to

improve the reactant conversion as well as syngas formation [35]. In this experiment, catalytic activity was carried out to determine reactants conversion for the reduced and unreduced catalyst with different supports.
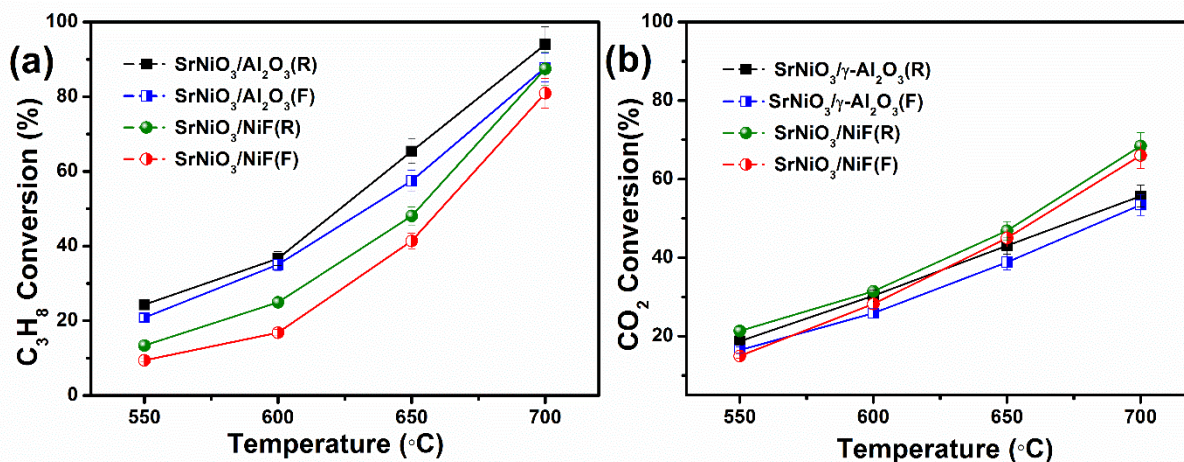

Figure 4.1.7. Catalytic activity of DRP as a function of temperature over $SrNiO_3/\gamma\text{-}Al_2O_3$(F and R) and $SrNiO_3$/NiF (F and R) catalysts at 550°C to 700°C under atmospheric pressure in CPR =3 (a) C_3H_8 conversion (b) CO_2 conversion.

As seen in **Figure 4.1.7**, the catalytic activity of $SrNiO_3/\gamma\text{-}Al_2O_3$(F and R) and $SrNiO_3$/NiF (F and R) catalysts showed that the increasing trend with increases reaction temperature range from 550°C to 700°C. In term of C_3H_8 conversion, the $SrNiO_3/\gamma\text{-}Al_2O_3$(R) shows the higher conversion among all other catalysts. It shows the maximum conversion of 94 % at 700°C even it shows 24% conversion of C_3H_8 at 550°C and higher than the $SrNiO_3/\gamma\text{-}Al_2O_3$(F) catalyst. In the same trend was observed Ni supported catalysts. The C_3H_8 conversion of $SrNiO_3$/NiF (F and R) catalyst is 81% and 87% at 700°C, respectively. The unreduced catalyst shows lower C_3H_8 conversion with both support than the reduced catalyst. These indicate that in-situ catalyst reduction occurred by H_2 arising from the C_3H_8 cracking to produce H_2 and carbon formed [36]. Interestingly, regarding CO_2 conversion the $SrNiO_3$/NiF (F and R) catalysts showed the significant

제주대학교 중앙도서관
JEJU NATIONAL UNIVERSITY LIBRARY

conversion of CO_2 than the SrNiO$_3$/γ-Al$_2$O$_3$(F and R) catalyst. Among the all catalyst SrNiO$_3$/NiF(R) shows the 69% of CO_2 conversion, which is 13% higher than the SrNiO$_3$/γ-Al$_2$O$_3$(R). It suggests that the SrNiO$_3$/NiF(R) leads to the dry reforming reaction even at increasing temperature trend while the SrNiO$_3$/γ-Al$_2$O$_3$(F and R) has no significant ability to convert CO_2 to CO since it leads the C_3H_8 cracking reaction and produces more carbon on the surface.
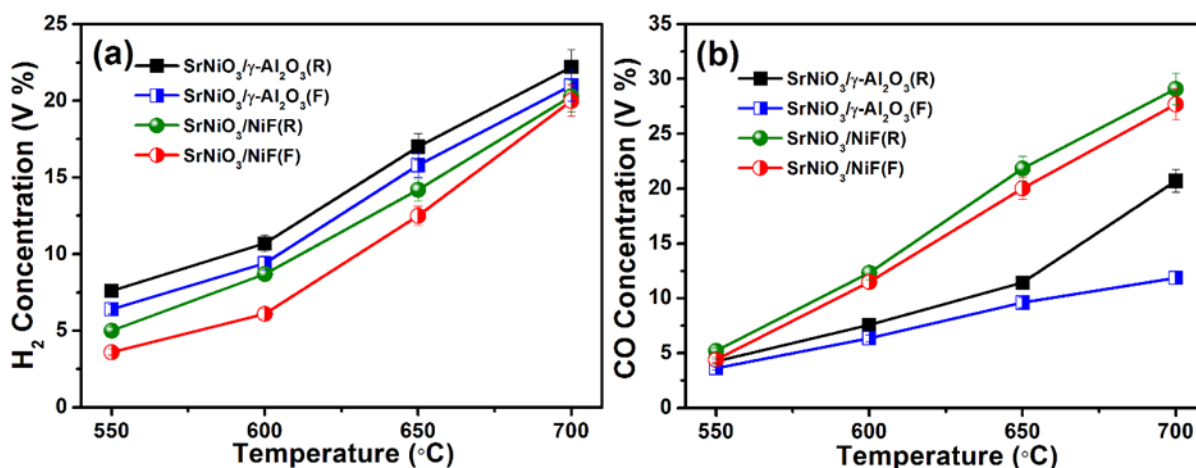

Figure 4.1.8 The product of DRP as a function of temperature over SrNiO$_3$/γ-Al$_2$O$_3$(F and R) and SrNiO$_3$/NiF (F and R) catalysts at 550°C to 700°C under atmospheric pressure in CPR =3 (a) H$_2$ concentration (vol %) and (b) CO concentration (vol %)

The production of H$_2$ and CO all catalyst shown in **Figure 4.1.8**. As shown in **Figure 4.1.8**, the H$_2$ production increases with increasing temperature for all catalyst. The SrNiO$_3$/γ-Al$_2$O$_3$(F and R) catalysts showed that the higher H$_2$ production compares with SrNiO$_3$/NiF (F and R) catalyst. The highest H$_2$ production was observed by SrNiO$_3$/γ-Al$_2$O$_3$(R) is 23 % at 700°C since it shows the highest production but CO production was only 24%. It suggests that Al$_2$O$_3$ supported catalyst primarily enhance the C_3H_8 cracking reaction instead of DRP, which leads to the formation of coke and severe catalytic deactivation. Notably, the SrNiO$_3$/NiF (F and R) catalyst have shown the 21%, 20% and 27%, 29% of H$_2$ and CO production, respectively. The CO_2 conversion always shows lower than the C_3H_8 conversion, and the H$_2$/CO ratio is significantly 0.6 for the SrNiO$_3$/NiF

(F and R). This observation could be explained by a low amount of coke formation on the surface of the catalyst, and DRP reaction took place in thermodynamic equilibrium.
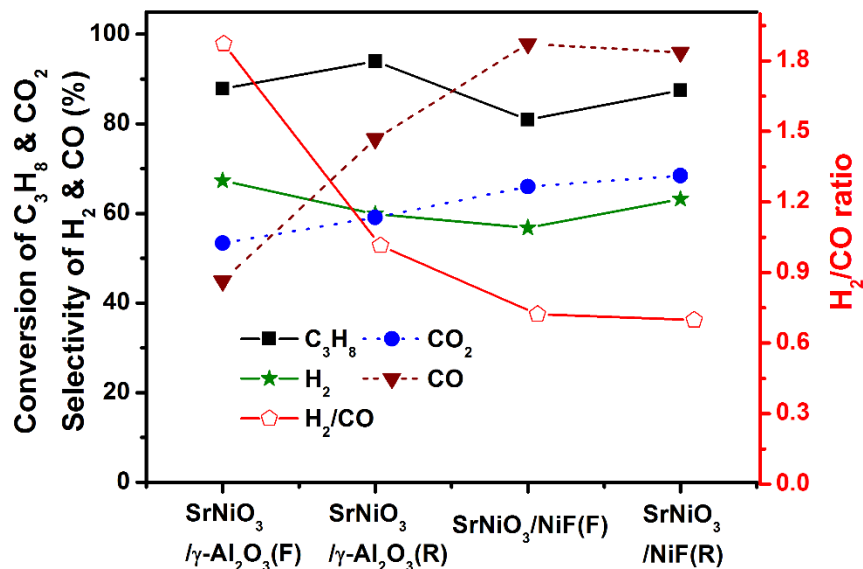

Figure 4.1.9. Catalytic performance of DRP over SrNiO$_3$/γ-Al$_2$O$_3$(F and R) and SrNiO$_3$/NiF (F and R) catalysts at 700°C, CPR=3 and total flow rate=200 ml/min.

As seen in **Figure 4.1.9**, we could compare the SrNiO$_3$ activity in two different supports materials at the isothermal condition. From the results, the NiF foam-supported catalyst shows superior catalytic activity. It could be active in two form, and the results were almost same. These suggest that the NiF could be facilitated the significant interaction of the catalytic surface and efficiently enhance the syngas production, which closes to the thermodynamic equilibrium. As a result of **Figure 4.1.9**. The SrNiO$_3$/NiF(R) revealed the significant conversion of C$_3$H$_8$ and CO$_2$ among all. In term of CO and H$_2$ selectivity were 96 % and 63.1 %, respectively. Moreover, the H$_2$/CO ratio of the catalyst revealed that reaction mechanism, the SrNiO$_3$/γ-Al$_2$O$_3$(F and R) catalysts shows higher values 1.8 and 1.0, respectively, which suggest that the CO selectivity is less than the H$_2$ selectivity. The CO$_2$ conversion was lower than C$_3$H$_8$ conversion due to the additional CO$_2$ produced by water gas shift reaction (WGSR) (**Eq. 4.9**). The WGSR is confirmed

by the value of H_2/CO ratio higher than 1 [37]. The CO selectivity severely affected due to the predominantly produced CO molecules could react with H_2O to produce CO_2 and H_2. Notably, the $SrNiO_3/NiF$ (F and R) catalysts have shown the significant conversion of C_3H_8, CO_2 and higher selectivity of CO than the selectivity of H_2. The H_2/CO ratio is 0.6, which closes to the stoichiometric reaction value of DRP(**Eq. 4.1**). These indicate that the NiF supported catalysts performed excellently in term of activity, which aid the DRP reaction and also significantly support the side reaction reverse water gas shift reaction (**Eq. 4.10**).

$$CO + H_2O \rightarrow CO_2 + H_2 \qquad\qquad \text{………. (4.9)}$$

$$CO_2 + H_2 \rightarrow H_2O + CO \qquad\qquad \text{………. (4.10)}$$
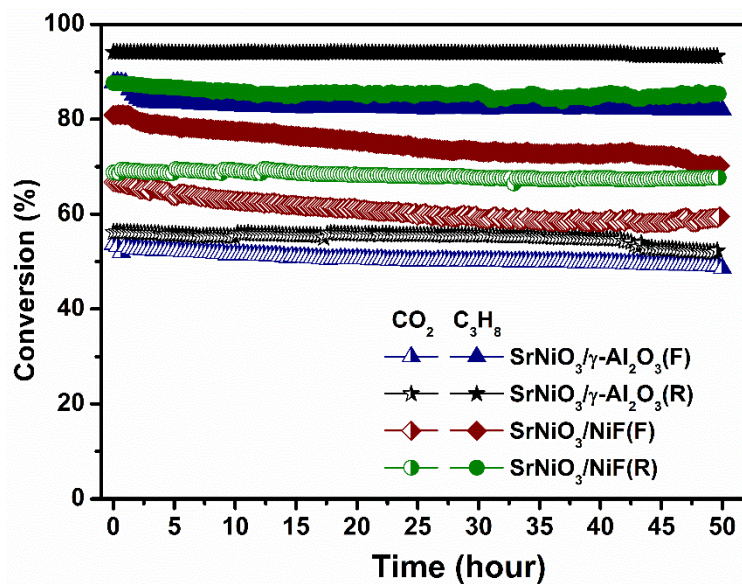
Figure 4.1.10. Stability of DRP over $SrNiO_3/\gamma$-Al_2O_3(F and R) and $SrNiO_3/NiF$ (F and R) catalysts at 700°C, CPR=3 and total flow rate=200 ml/min for 50 h.

The catalyst stability of the $SrNiO_3$ perovskite catalysts was examined over the period of 50h at 700°C shown in **Figure 4.1.10**. It indicates that the $SrNiO_3/NiF$(R) showed the significantly stable catalytic activity during the DRP, among other catalysts. For instance, the $SrNiO_3/NiF$(R)

showed the no significant conversion loss of C_3H_8 and CO_2 was 85% and 66% from the begin 87% and 69%, respectively, after 50 h of the DRP. The significant activity and long-term stability of SrNiO$_3$/NiF(R) are exhibited for its high thermal stability, high dispersion, microstructured of support and surface basicity. In notably, the unreduced SrNiO$_3$ perovskite catalyst showed gradually decrease the catalytic activity even in two support material for the period. The conversion of C_3H_8 and CO_2 over the SrNiO$_3$/γ-Al$_2$O$_3$(F) was 87% and 53% until 2 h of the reaction, which gradually decreased to 82% and 48%, respectively, after 50 h due to the amphoteric property of γ-Al$_2$O$_3$.

Table 4. 1 C_3H_8 and CO conversion, CO, and H_2 selectivity and the H_2/CO ratio

Catalyst	$X_{C_3H_8}$ (%)	X_{CO_2} (%)	S_{CO} (%)	S_{H_2} (%)	H_2/CO
SrNiO$_3$/γ-Al$_2$O$_3$(F)	82.0	48.0	20.2	61.0	2.9
SrNiO$_3$/γ-Al$_2$O$_3$(R)	92.0	52.1	46.2	63.2	1.4
SrNiO$_3$/NiF(F)	70.2	59.5	94.1	64.3	0.6
SrNiO$_3$/NiF(R)	85.3	67.0	94.7	66.7	0.6

W=1.0 g, P = 1 atm, T = 700°C,TOS = 50 h

The catalytic stability results were shown in **Table 4.1**, the conversion of C_3H_8 and CO_2 and the H_2/CO ration in the steady state at 700°C after 50 h. The C_3H_8 and CO_2 conversion over SrNiO$_3$/NiF(R) were superior to other catalysts. Besides, the H_2/CO ratio was 0.6 for SrNiO$_3$/NiF(R) and (F), which close to the thermodynamic value of DRP. Moreover, the results claimed that the higher selectivity towards resists the carbon formation than SrNiO$_3$/γ-Al$_2$O$_3$(F) and (R). According to the results, The SrNiO$_3$ perovskite catalyst is a basic oxide. Due to its strong basicity, low surface area, and supported by NiF, CO_2 might interact actively with sites favoring the formation of carbonates to coverts CO, which minimize the carbon formation during DRP.

Several authors found that [2,38-40], the highly basic catalysts like lanthanum oxide, $SmCoO_3$, which is almost the presence of carbonate phase on the catalyst surface after reforming reaction. These prevent the sintering of particles and extraction of particles from the surface of carbon filaments during the reaction.

4.3.3 Catalytic characterization of spent catalyst

The post characterization of catalyst was examined by several techniques such as FE-SEM, Raman, and TPO to understand the catalyst after DRP at elevated temperature. **Figure 4.1.11** shows the FE-SEM of all examined catalysts after DRP over time on stream (TOS) 50 h at 1μm magnification. As seen in **Figure 4.1.11**, the morphology of carbon formation on the catalyst was observed in whisker/filament form. It is agreed with many previous reports because most of Ni present catalysts is the response to the carbon growth like tubular at high temperature [41,42]. As shown in **Figure 4.1.11**, the $SrNiO_3$/NiF (R) catalyst shows significantly low carbon on the surface among others, and the form of carbon also is a filament in nature. It agrees with catalytic activity too.
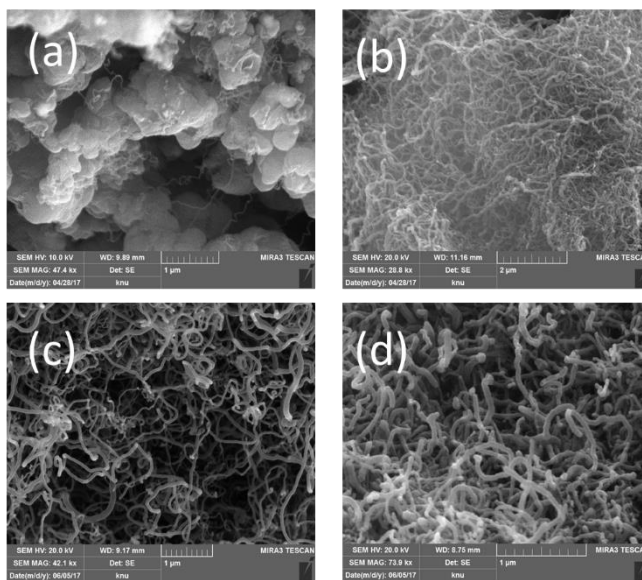

Figure 4.1.11. FE-SEM images of spent catalysts after DRP over 50 h (a) $SrNiO_3$/NiF(R), (b) $SrNiO_3$/NiF(F), (c) $SrNiO_3$/γ-Al_2O_3(R), and $SrNiO_3$/γ-Al_2O_3(F)
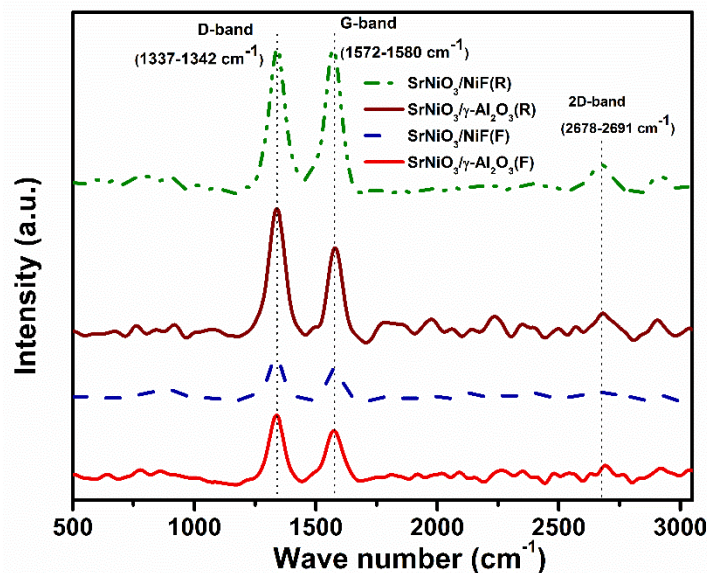
Figure 4.1.12. Raman spectra of spent catalysts after DRP over 50 h

Figure 4.1.12 exhibits the carbon species for all catalysts after DRP by Raman spectra. From the results of Raman spectra, The carbon species is majorly in the form of graphitic. The three active peaks were observed in all catalysts. The first peak at 1337-1342 cm^{-1} belongs to the D-band of Raman active mode of C—C bond stretching. The second peak at 1572-1580 cm^{-1} corresponds to the G-band, which attributed to graphitized carbon foram and also the third peak at 2678-2691 cm^{-1} is attributed to the 2D-band of carbon nanotubes or filaments. The intensity of ID and IG could explain the graphitic disorder [43,44], in this case of $SrNiO_3/\gamma-Al_2O_3$(F and R) catalyst, the ID is always higher than the IG, which indicates deposited carbon could be in the form of graphite. The $SrNiO_3$/NiF (F and R) catalyst shows different trend ID, and IG was almost same, which suggests the existence of crystalline graphite [45]. To understand carbon species formation during DRP has examined TPO studies of spent catalysts and its results were shown in **Figure 4.1.13**. As seen in **Figure 4.1.13**, the three primary type of carbon occurred on the surface of the catalyst after DRP.
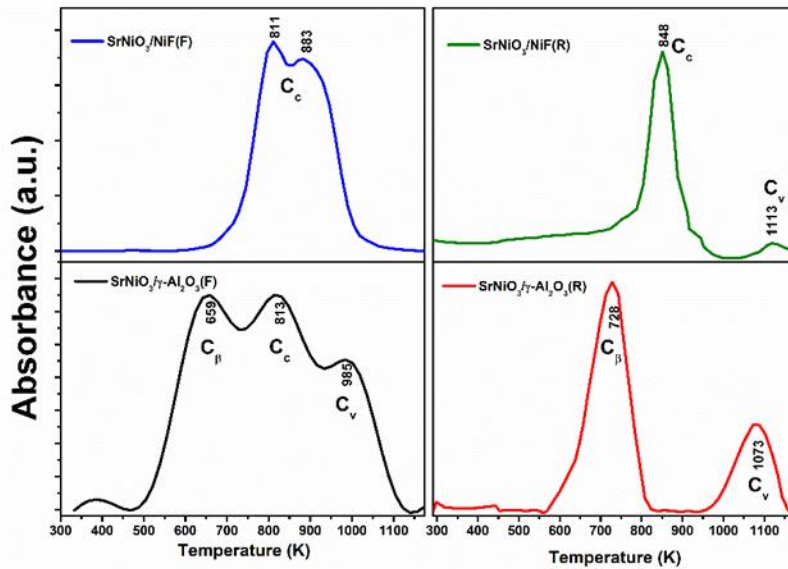
Figure 4.1.13. TPO profiles of used catalysts after DRP over 50 h

These types were distinguished by oxidation temperature of solid carbon with O_2. These are polymeric amorphous films or filaments (C_β) at 523-773 K, the vermicular carbon filaments/fibers/tubes (C_v) at 573-1273 K and the crystalline graphite (C_C) at 773- 823 K [46-48]. The results of TPO profile, the reduced catalysts show the three kinds of C_β, C_C, and C_v on the surface, interestingly the both of reduced catalyst have vermicular carbon filaments. The un-reduce catalyst shows the polymeric amorphous films or filaments and crystalline graphite majorly [49]. These suggest that all catalyst produce carbon during DRP, even though the fresh catalyst shows higher amount carbon compare with reduced catalyst and the Al_2O_3 supported catalysts produced more carbon instead of NiF, which suggest that the NiF allows increasing the molecule interaction due to their porous properties.

4.4 Conclusions

SrNiO$_3$ perovskite catalyst successfully synthesized by the sol-gel citrate method and used as a catalyst with Al_2O_3 and NiF supports for the first time in propane dry reforming and found to

104

have propane and CO_2 activity for syngas production efficiently. The effect of reduced $SrNiO_3$ perovskite catalyst on DRP has been investigated. For comparison study, the reduced and unreduced $SrNiO_3$ catalyst shows significant improvement in conversion of C_3H_8 and CO_2. The $SrNiO_3/NiF(R)$ showed excellent activity regarding syngas production, the syngas produced with a significant selectivity of H_2 and CO and H_2/CO ratio was maintained close to the thermodynamic value. These measurements of catalytic activity with two different support materials have significantly affected the production of syngas. The strong basicity of strontium metal with NiF could aid the CO production and reduce carbon formation. The finding of this study has presented $SrNiO_3$ perovskite as a suitable catalyst in the DRP experiment and also could be the replacement of rare earth perovskite in reforming reaction and cost effective with the less health-hazardous catalyst.

4.5 References

1. Xu, J.; Yeung, C.M.Y.; Ni, J.; Meunier, F.; Acerbi, N.; Fowles, M.; Tsang, S.C. Methane steam reforming for hydrogen production using low water-ratios without carbon formation over ceria coated ni catalysts. *Applied Catalysis A: General* **2008**, *345*, 119-127.
2. Sutthiumporn, K.; Maneerung, T.; Kathiraser, Y.; Kawi, S. CO_2 dry-reforming of methane over $La_{0.8}Sr_{0.2}Ni_{0.8}M_{0.2}O_3$ perovskite (M = Bi, Co, Cr, Cu, Fe): Roles of lattice oxygen on C–H activation and carbon suppression. *International Journal of Hydrogen Energy* **2012**, *37*, 11195-11207.
3. M.S.P, S.; Sultana, L.; Hossain, M.M.; Pawlat, J.; Diatczyk, J.; Brüser, V.; Reuter, S.; Mok, Y.S. Iron–ceria spinel ($FeCe_2O_4$) catalyst for dry reforming of propane to inhibit carbon formation. *Journal of Industrial and Engineering Chemistry* **2018**, *61*, 142-151.
4. Siahvashi, A.; Adesina, A.A. Synthesis gas production via propane dry (CO_2) reforming: Influence of potassium promotion on bimetallic Mo-Ni/Al_2O_3. *Catalysis Today* **2013**, *214*, 30-41.
5. Staniforth, J.; Evans, S.E.; Good, O.J.; Darton, R.J.; Ormerod, R.M. A novel perovskite-based catalyst with high selectivity and activity for partial oxidation of methane for fuel cell applications. *Dalton Trans* **2014**, *43*, 15022-15027.
6. Nojoumi, H.; Dincer, I.; Naterer, G.F. Greenhouse gas emissions assessment of hydrogen and kerosene-fueled aircraft propulsion. *International Journal of Hydrogen Energy* **2009**, *34*, 1363-1369.
7. Gnanamani, M.K.; Jacobs, G.; Shafer, W.D.; Davis, B.H. Fischer–tropsch synthesis: Activity of metallic phases of cobalt supported on silica. *Catalysis Today* **2013**, *215*, 13-17.
8. Pashchenko, D. Thermodynamic equilibrium analysis of combined dry and steam reforming of propane for thermochemical waste-heat recuperation. *International Journal of Hydrogen Energy* **2017**, *42*, 14926-14935.
9. Pakhare, D.; Spivey, J. A review of dry (CO_2) reforming of methane over noble metal catalysts. *Chem Soc Rev* **2014**, *43*, 7813-7837.

10. Karuppiah, J.; Mok, Y.S. Plasma-reduced Ni/γ–Al₂O₃ and CeO₂–Ni/γ–Al₂O₃ catalysts for improving dry reforming of propane. *International Journal of Hydrogen Energy* **2014**, *39*, 16329-16338.

11. Malaibari, Z.O.; Amin, A.; Croiset, E.; Epling, W. Performance characteristics of Mo–Ni/Al₂O₃ catalysts in LPG oxidative steam reforming for hydrogen production. *International Journal of Hydrogen Energy* **2014**, *39*, 10061-10073.

12. Barroso-Quiroga, M.M.; Castro-Luna, A.E. Catalytic activity and effect of modifiers on Ni-based catalysts for the dry reforming of methane. *International Journal of Hydrogen Energy* **2010**, *35*, 6052-6056.

13. Foo, S.Y.; Cheng, C.K.; Nguyen, T.-H.; Adesina, A.A. Kinetic study of methane CO₂ reforming on Co–Ni/Al₂O₃ and Ce–Co–Ni/Al₂O₃ catalysts. *Catalysis Today* **2011**, *164*, 221-226.

14. Corthals, S.; Van Nederkassel, J.; Geboers, J.; De Winne, H.; Van Noyen, J.; Moens, B.; Sels, B.; Jacobs, P. Influence of composition of MgAl₂O₄ supported NiCeO₂ZrO₂ catalysts on coke formation and catalyst stability for dry reforming of methane. *Catalysis Today* **2008**, *138*, 28-32.

15. Yamazoe, N.; Teraoka, Y. Oxidation catalysis of perovskites --- relationships to bulk structure and composition (valency, defect, etc.). *Catalysis Today* **1990**, *8*, 175-199.

16. Rynkowski, J.; Samulkiewicz, P.; Ladavos, A.K.; Pomonis, P.J. Catalytic performance of reduced La₂₋ₓSrₓNiO₄ perovskite-like oxides for CO₂ reforming of CH₄. *Applied Catalysis A: General* **2004**, *263*, 1-9.

17. Mawdsley, J.R.; Krause, T.R. Rare earth-first-row transition metal perovskites as catalysts for the autothermal reforming of hydrocarbon fuels to generate hydrogen. *Applied Catalysis A: General* **2008**, *334*, 311-320.

18. Dinka, P.; Mukasyan, A.S. Perovskite catalysts for the auto-reforming of sulfur-containing fuels. *Journal of Power Sources* **2007**, *167*, 472-481.

19. Gallego, G.S.; Mondragón, F.; Barrault, J.; Tatibouët, J.-M.; Batiot-Dupeyrat, C. CO₂ reforming of CH₄ over La–Ni based perovskite precursors. *Applied Catalysis A: General* **2006**, *311*, 164-171.

20. Chawl, S.K.; George, M.; Patel, F.; Patel, S. Production of synthesis gas by carbon dioxide reforming of methane over nickel based and perovskite catalysts. *Procedia Engineering* **2013**, *51*, 461-466.

21. Nair, M.M.; Kaliaguine, S.; Kleitz, F. Nanocast LaNiO₃ perovskites as precursors for the preparation of coke-resistant dry reforming catalysts. *ACS Catalysis* **2014**, *4*, 3837-3846.

22. Kondakindi, R.R.; Kundu, A.; Karan, K.; Peppley, B.A.; Qi, A.; Thurgood, C.; Schurer, P. Characterization and activity of perovskite catalysts for autothermal reforming of dodecane. *Applied Catalysis A: General* **2010**, *390*, 271-280.

23. Osazuwa, O.U.; Setiabudi, H.D.; Rasid, R.A.; Cheng, C.K. Syngas production via methane dry reforming: A novel application of SmCoO₃ perovskite catalyst. *Journal of Natural Gas Science and Engineering* **2017**, *37*, 435-448.

24. Goldwasser, M.R.; Rivas, M.E.; Pietri, E.; Pérez-Zurita, M.J.; Cubeiro, M.L.; Gingembre, L.; Leclercq, L.; Leclercq, G. Perovskites as catalysts precursors: CO₂ reforming of CH₄ on Ln₁₋ₓCaₓRu₀.₈Ni₀.₂O₃ (Ln = La, Sm, Nd). *Applied Catalysis A: General* **2003**, *255*, 45-57.

25. Pichas, C.; Pomonis, P.; Petrakis, D.; Ladavos, A. Kinetic study of the catalytic dry reforming of CH₄ with CO₂ over La₂₋ₓSrₓNiO₄ perovskite-type oxides. *Applied Catalysis A: General* **2010**, *386*, 116-123.

26. Valderrama, G.; Kiennemann, A.; Goldwasser, M.R. La-Sr-Ni-Co-O based perovskite-type solid solutions as catalyst precursors in the CO₂ reforming of methane. *Journal of Power Sources* **2010**, *195*, 1765-1771.

27. Mok, Y.S.; Jwa, E.; Hyun, Y.J. Regeneration of C₄H₁₀ dry reforming catalyst by nonthermal plasma. *Journal of Energy Chemistry* **2013**, *22*, 394-402.

28. Takeda, Y.; Hashino, T.; Miyamoto, H.; Kanamaru, F.; Kume, S.; Koizumi, M. Synthesis of SrNiO₃ and related compound, Sr₂Ni₂O₅. *Journal of Inorganic and Nuclear Chemistry* **1972**, *34*, 1599-1601.

29. Goldwasser, M.R.; Rivas, M.E.; Pietri, E.; Pérez-Zurita, M.J.; Cubeiro, M.L.; Grivobal-Constant, A.; Leclercq, G. Perovskites as catalysts precursors: Synthesis and characterization. *Journal of Molecular Catalysis A: Chemical* **2005**, *228*, 325-331.

30. Valderrama, G.; Goldwasser, M.R.; Navarro, C.U.d.; Tatibouët, J.M.; Barrault, J.; Batiot-Dupeyrat, C.; Martínez, F. Dry reforming of methane over Ni perovskite-type oxides. *Catalysis Today* **2005**, *107-108*, 785-791.

31. Chen, H.-Y.T.; Tosoni, S.; Pacchioni, G. Hydrogen adsorption, dissociation, and spillover on Ru10 clusters supported on anatase TiO_2 and tetragonal ZrO_2 (101) surfaces. *ACS Catalysis* **2015**, *5*, 5486-5495.

32. Boudjahem, A.-G.; Monteverdi, S.; Mercy, M.; Bettahar, M.M. Nanonickel particles supported on silica. Morphology effects on their surface and hydrogenating properties. *Catalysis Letters* **2004**, *97*, 177-183.

33. Lu, X.; Gu, F.; Liu, Q.; Gao, J.; Liu, Y.; Li, H.; Jia, L.; Xu, G.; Zhong, Z.; Su, F. Vox promoted ni catalysts supported on the modified bentonite for CO and CO_2 methanation. *Fuel Processing Technology* **2015**, *135*, 34-46.

34. Al-Doghachi, F.A.J.; Rashid, U.; Taufiq-Yap, Y.H. Investigation of Ce(III) promoter effects on the tri-metallic Pt, Pd, Ni/MgO catalyst in dry reforming of methane. *RSC Advances* **2016**, *6*, 10372-10384.

35. Batiot-Dupeyrat, C.; Gallego, G.A.S.; Mondragon, F.; Barrault, J.; Tatibouët, J.-M. CO_2 reforming of methane over $LaNiO_3$ as precursor material. *Catalysis Today* **2005**, *107-108*, 474-480.

36. Luo, J.Z.; Yu, Z.L.; Ng, C.F.; Au, C.T. CO_2/CH_4 reforming over Ni–La_2O_3/5a: An investigation on carbon deposition and reaction steps. *Journal of Catalysis* **2000**, *194*, 198-210.

37. Pereñíguez, R.; González-DelaCruz, V.M.; Holgado, J.P.; Caballero, A. Synthesis and characterization of a $LaNiO_3$ perovskite as precursor for methane reforming reactions catalysts. *Applied Catalysis B: Environmental* **2010**, *93*, 346-353.

38. Slagtern, A.; Schuurman, Y.; Leclercq, C.; Verykios, X.; Mirodatos, C. Specific features concerning the mechanism of methane reforming by carbon dioxide over Ni/La_2O_3 catalyst. *Journal of Catalysis* **1997**, *172*, 118-126.

39. Olafsen, A.; Slagtern, Å.; Dahl, I.M.; Olsbye, U.; Schuurman, Y.; Mirodatos, C. Mechanistic features for propane reforming by carbon dioxide over a Ni/Mg(Al)O hydrotalcite-derived catalyst. *Journal of Catalysis* **2005**, *229*, 163-175.

40. Pakhare, D.; Schwartz, V.; Abdelsayed, V.; Haynes, D.; Shekhawat, D.; Poston, J.; Spivey, J. Kinetic and mechanistic study of dry (CO_2) reforming of methane over Rh-substituted $La_2Zr_2O_7$ pyrochlores. *Journal of Catalysis* **2014**, *316*, 78-92.

41. Sutthiumporn, K.; Kawi, S. Promotional effect of alkaline earth over Ni-La_2O_3 catalyst for CO_2 reforming of CH_4: Role of surface oxygen species on H_2 production and carbon suppression. *International Journal of Hydrogen Energy* **2011**, *36*, 14435-14446.

42. de Sousa, F.F.; de Sousa, H.S.A.; Oliveira, A.C.; Junior, M.C.C.; Ayala, A.P.; Barros, E.B.; Viana, B.C.; Filho, J.M.; Oliveira, A.C. Nanostructured Ni-containing spinel oxides for the dry reforming of methane: Effect of the presence of cobalt and nickel on the deactivation behaviour of catalysts. *International Journal of Hydrogen Energy* **2012**, *37*, 3201-3212.

43. de Sousa, H.S.A.; da Silva, A.N.; Castro, A.J.R.; Campos, A.; Filho, J.M.; Oliveira, A.C. Mesoporous catalysts for dry reforming of methane: Correlation between structure and deactivation behaviour of Ni-containing catalysts. *International Journal of Hydrogen Energy* **2012**, *37*, 12281-12291.

44. Pinheiro, A.L.; Pinheiro, A.N.; Valentini, A.; Filho, J.M.; Sousa, F.F.d.; Sousa, J.R.d.; Rocha, M.d.G.C.; Bargiela, P.; Oliveira, A.C. Analysis of coke deposition and study of the structural features of MAl_2O_4 catalysts for the dry reforming of methane. *Catalysis Communications* **2009**, *11*, 11-14.

45. Pimenta, M.A.; Dresselhaus, G.; Dresselhaus, M.S.; Cancado, L.G.; Jorio, A.; Saito, R. Studying disorder in graphite-based systems by Raman spectroscopy. *Physical Chemistry Chemical Physics* **2007**, *9*, 1276-1290.

46. Xu, L.; Song, H.; Chou, L. Carbon dioxide reforming of methane over ordered mesoporous NiO–MgO–Al_2O_3 composite oxides. *Applied Catalysis B: Environmental* **2011**, *108-109*, 177-190.

47. Swaan, H.M.; Kroll, V.C.H.; Martin, G.A.; Mirodatos, C. Deactivation of supported nickel catalysts during the reforming of methane by carbon dioxide. *Catalysis Today* **1994**, *21*, 571-578.

48. Rezaei, M.; Alavi, S.M.; Sahebdelfar, S.; Yan, Z.-F. Effects of CO_2 content on the activity and stability of nickel catalyst supported on mesoporous nanocrystalline zirconia. *Journal of Natural Gas Chemistry* **2008**, *17*, 278-282.

49. Chesnokov, V.V.; Zaikovskii, V.I.; Buyanov, R.A.; Molchanov, V.V.; Plyasova, L.M. Morphology of carbon from methane on nickel-containing catalysts. *Catalysis Today* **1995**, *24*, 265-267.

CHAPTER -5

Summary and Recommendations

5.1 Summary

This chapter describes the general conclusions of overall thesis and recommendations of this work. This thesis mainly focuses on the improvement of syngas production by improving better catalyst of crystalline oxide. For this, we focused on the synthesis of ferrite spinel and nickel perovskite and investigated to improve the catalytic performances in possible ways. First, two chapters described the introduction of production of syngas from hydrocarbon (C_3H_8) with carbon dioxide and its typical available reactions and materials/techniques used in the research work.

❖ The novel spinel $FeCe_2O_4$ catalyst was prepared by sol-gel method and investigated its physicochemical and catalytic properties in **Chapter-3**. It shows the significant catalytic activity with extended durability and resistance of carbon formation than a conventional $Ni-CeO_2$ catalyst.

❖ Based on this, in order to further improve the syngas production with $SrNiO_3$ perovskite catalyst, we prepared by sol-gel technique and examine the catalytic behavior in **Chapter-4**. The strong basicity of strontium cation induces the conversion of CO_2 to CO by the reaction of cyclic deformation of $SrCO_3$ to SrO and the conversion of CO. It enhanced the syngas production and achieved to the closest thermodynamic value of H_2/CO ratio.

Overall, The spinel $FeCe_2O_4$ catalyst was successfully synthesized by sol-gel method. XRD, Raman further confirmed it. The chemical state of prepared catalyst examined by XPS, it reveals the Fe^{2+} oxidation state in spinel crystal entities. The crystal structure, particle size, specific surface area, redox property and lattice oxygen of the synthesized material influenced the catalytic properties of the catalyst support with mesoporous alumina foam. This posses the CO_2 reduction

to CO and oxidation of carbon to CO during reforming reaction. This could enhance the syngas production and inhibit the carbon formation. The post characterization of catalyst confirmed the crystal entities intact after at elevated temperature, which indicates the sustainability of catalyst on time stream. The novel $SrNiO_3$ perovskite catalyst with microporous nickel foam structured support shows the improved syngas production via dry reforming reaction. The pre-reduced process might prevent the *in-suit* reduction during the dry reforming reaction, which reduces the risk of deactivation by sintering and promotes the syngas production with high selectivity of H_2 and CO. Higher hydrocarbons are known to require lower activation energy. The feed gas composition was fixed with respective of the thermodynamic equation of propane dry reforming (CPR=3), which helps reaction behavior of the catalyst through the thermodynamic condition. The crystalline structure of spinel and perovskite has high lattice oxygen on its structure, which plays an essential role in the reforming reaction to improve the syngas production and reduce carbon formation and overcome the deactivation catalysts by sintering.

5.2 Recommendations

Based on the outcomes of this projects, the crystalline catalysts open the possibility of improving syngas production via thermodynamical way. As for following, the recommendation for the future work and the perspective directions for the development of a new crystalline catalyst for syngas production are discussed.

❖ Catalyst preparation stages should be investigated based on the surface chemistry.

❖ The new crystalline nanostructured catalyst should be synthesis directly on the surface of the support by various preparation techniques.

❖ To enhance the high-performance catalytic properties by tuning the shape, size and morphology of the catalytic material could be investigated. The suitable high porous

110

support should be found to improve the reforming reaction in order to reduce pressure and long durability at high temperature for industrial application.

❖ Based on the traces of deactivation through physical properties for spent catalysts at various time. The broad pore sizes support suggest that the enhanced performance against deactivation.

❖ To identify the combination of different transition crystalline catalysts should be examined the highest syngas production and carbon resistance along with the lowest price.

APPENDIX A: List of Publications

1. **Sudhakaran M.S.P.**, Sultana, L. Hossain, Md. Mokter. Pawlat, J. Diatczyk, J. Brüser, V, Reuter, S., Mok, Y. S., Iron–ceria spinel (FeCe$_2$O$_4$) catalyst for dry reforming of propane to inhibit carbon formation. Journal of Industrial and Engineering Chemistry 2017 (I.F: 4.421)

2. **Sudhakaran, M. S. P.**, Trinh, H. Q., Karuppiah, J., Hossain, M. Md Hossain, Mok, Y. S., Plasma Catalytic Removal of p-Xylene from Air Stream Using γ-Al$_2$O$_3$ Supported Manganese Catalyst. Topics in Catalysis 2017, 60 (12), 944-954 (I.F: 2.486)

3. **Sudhakaran M.S.P.**, J. Karuppiah, E. Linga Reddy, M. Sanjeeva Gandhi, Quang Hung Trinh, Y.S. Mok, "Catalytic Non-Thermal Plasma Reactor for the Decomposition of p-Xylene Over MnOx and CoOx Supported on Anodized Aluminum Oxide" J J Environ Sci. 2016, 2(2): 015.

4. **Sudhakaran M.S.P.**, Jo, Jin Oh, Trinh, Quang Hung, Mok, Y. S., "Characteristics of Packed-bed Plasma Reactor with Dielectric Barrier Discharge for Treating" Applied Chemistry of Engineering. 2015, 26 (4), 495-504.

5. Veerasubramani, G. K, **Sudhakaran, M. S. P.**; Alluri, N. R.; Krishnamoorthy, K.; Mok, Y. S., Kim, S. J., Effective use of an idle carbon-deposited catalyst for energy storage applications. J. Mater. Chem. A 2016, 4 (32), 12571-12582. (I.F: 8.262)

6. J. Karuppiah, E. Linga Reddy, **Sudhakaran M.S.P.**, S.B. Lee. Production of synthesis gas from dry reforming of propane with carbon dioxide over ceria-promoted nickel foam catalysts. Renewable Energy and Power Quality Journal, 1(14), p742-747 (2016)

7. Pazhamalai, P., Krishnamoorthy, K., **Sudhakaran, M. S. P.**, Kim, S. J., Fabrication of High-Performance Aqueous Li-Ion Hybrid Capacitor with LiMn$_2$O$_4$ and Graphene. ChemElectroChem 2017, 4 (2), 396-403 (I.F: 4.136)

8. Veerasubramani, G. K., Chandrasekhar, A., **Sudhakaran M. S. P**, Mok, Y. S., Kim, S. J., Liquid electrolyte mediated flexible pouch-type hybrid supercapacitor based on binderless core-shell nanostructures assembled with honeycomb-like porous carbon. Journal of Materials Chemistry A 2017, 5 (22), 11100-11113 (I.F: 8.262)

9. Chandrasekhar, A., Alluri, N. R., **Sudhakaran, M. S. P.**, Mok, Y. S., Kim, S.-J., "A smart mobile pouch as a biomechanical energy harvester towards self-powered smart wireless power transfer applications. Nanoscale" 2017, 9 (28), 9818-9824 (I.F: 7.367)

List of submitted papers

1. **Sudhakaran M.S.P**., Pawlat, J. Diatczyk, J. Brüser, V, Reuter, S., Mok, Y. S., "Syngas production via propane dry reforming over $SrNiO_3$ perovskite catalyst" – Nanomaterials

2. Md. Mokter Hossain, Quang Hung Trinh, **Sudhakaran M.S.P**, Lamia Sultana, Mok, Y.S., "Improvement of mechanical strength of hydrophobic coating on glass surfaces by an atmospheric pressure plasma jet" - Surface and Coatings Technology

3. Md. Mokter Hossain, Quang Hung Trinh, Duc Ba Nguyen, **Sudhakaran M.S.P**., Mok, Y. S., "Investigation of robust hydrophobic coating on glass surface by an atmospheric pressure plasma jet for plasma-polymerization of hexamethyldisiloxane conjugated with (3-aminopropyl) triethoxysilane" - Surface Engineering

APPENDIX B: List of Conferences

1. **Sudhakaran M.S.P**, Young Sun Mok, "Controlled growth of $NiMoO_4$ Nanosheet and Nanoflower exhibits on γ-Al_2O_3 as a catalyst for dry reforming of propane" (May 3-5, 2018) **KSIEC 2018**, Daegu, Republic of Korea **(ORAL -Excellent Presentation Award)**.

2. **Sudhakaran M.S.P**, Duc Ba Nguyen, Md. Mokter Hossain, Sultana Lamia, Young Sun Mok, "$SrNiO_3$ perovskite catalyst for dry reforming of propane with heterogeneous support to produce syngas and physical-chemistry study" (November 24, 2017) **BK21+ 2017**, Jeju, Republic of Korea **(POSTER).**

3. **Sudhakaran M.S.P**, Md. Mokter Hossain, Sultana Lamia, Young Sun Mok, "$SrNiO_3$ perovskite catalyst for dry reforming of propane with heterogeneous support to produce syngas" (July 19-21, 2017) **ANM 2017**, Portugal **(POSTER).**

4. **Sudhakaran M.S.P**, Md. Mokter Hossain, Sultana Lamia, Young Sun Mok, "$FeCe_2O_4$ catalyst for dry reforming of propane to inhibition of carbon formation" (May 10-12, 2017) **KSIEC 2017**, Gwangju, Republic of Korea **(POSTER).**

5. **Sudhakaran M.S.P**., J Karuppiah, Young Son Mok, "Decomposition of p-xylene from air stream by plasma catalytic oxidation at different temperatures over Mn supported on γ-Al_2O_3" (August 21-26, 2016) **IVC20 2016**, Busan, Republic of Korea **(POSTER).**

6. **Sudhakaran M.S.P**., J. Karuppiah, Y. S. Mok, "Removal of p-xylene from Air Stream by Plasma-Catalytic Oxidation using metals oxides (Ti, Zn & Mn) Catalysts Supported on Nickel foam" (November 4-6, 2015) **KSIEC 2015**, Jeju, Republic of Korea **(POSTER).**

7. **Sudhakaran M.S.P**., J. Karuppiah, Y. S. Mok, "Catalytic nonthermal plasma reactor for decomposition of p-xylene by MnO_x and CoO_x/AAO supported catalysts" (April 29 to May 1, 2015) **KSIEC 2015** Busan, Republic of Korea **(POSTER).**

8. **Sudhakaran M.S.P**., P. Kalyani, "Nanomaterials VIZ–A–VIZ energy' on national level UGC sponsored seminar Nanomaterials for energy harvesting, (December 2-4, 2009) **NaMEH 2009**, Thiagarajar College of Engineering, India **(POSTER).**

9. **Sudhakaran M.S.P**., P. Kalyani, "Recovery of Manganese oxide from spent cell application in electrochemical capacitor" (September 18, 2009) **NCRAC-2009**, Tiruchirappalli, India **(ORAL).**

10. Sultana Lamia, **Sudhakaran M.S.P**, Md Shahinur Rahman, Md Mokter Hossain, Y.S. Mok, "Syngas production via dry reforming of propane over Ni supported on γ-Al_2O_3 modified with CeO_2 catalysts" (May 10-12, 2017) **KSIEC 2017**, Gwangju, Republic of Korea **(POSTER).**

11. Ganesh Kumar V., **Sudhakaran M.S.P**., Y.S. Mok, S.J. Kim, "Efficient utilization of futile catalyst for energy storage applications" International Union of Materials research Societies – International Conference of Electronic Materials (July 4-8, 2016) **IUMRS-ICEM 2016**, Singapore **(ORAL).**

12. Karuppiah J., **Sudhakaran M.S.P**., Y.S. Mok, "Synthesis and characterization of nanostructured catalysts NiO, CoO_x, CeO_2 and CuO on NiF support for SCR of N_2O by C_3H_8" (November 4-6, 2015) **KSIEC 2015**, Jeju, Republic of Korea **(ORAL -Excellent Presentation Award).**

13. Mokter Md Hossain, Duc Ba Nguyen, **Sudhakaran M.S.P,** Young Sun Mok "Atmospheric pressure plasma polymerization to investigate robust hydrophobic coating on glass surface by using Tetramethylsilane conjugated with 3-Aminopropyl(diethoxy)methylsilane" (May 3-5, 2018) **KSIEC 2018**, Daegu, Republic of Korea **(ORAL -Excellent Presentation Award).**

14. Md. Mokter Hossain, Quang Hung Trinh, Duc Ba Nguyen, **Sudhakaran M.S.P**, Young Sun Mok, "Investigation of robust hydrophobic coating on glass surface by an atmospheric pressure plasma jet for plasma-polymerization of Hexamethydisiloxane conjugated with (3-Aminopropyl)triethoxysilane" (March 28-30, 2018) **SurfCoat Korea 2018**, Incheon, Republic of Korea **(POSTER)**.

15. Md Mokter Hossain, Quang Hung Trinh, Sudhakaran M.S.P., Lamia Sultana,Young Sun Mok, "Improving of Mechanical Strength of Hydrophobic Coating by Using Plasma Torch at Atmospheric Pressure" (November 8-10, 2017) **KSIEC 2017**, Busan, Republic of Korea **(ORAL -Excellent Presentation Award).**

16. Md. Mokter Hossain, Quang Hung Trinh, **Sudhakaran M.S.P**, Lamia Sultana, Young Sun Mok "Improving of mechanical strength of hydrophobic coating on glass surface by using plasma torch at atmospheric pressure" (September 11-15, 2017) **AEPSE 2017**, Jeju, Republic of Korea **(ORAL)**.

17. Hossain Md Mokter, Quang Hung Trinh, **Sudhakaran M.S.P**, Lamia Sultana, Y.S. Mok, "Improving of Mechanical Strength of Hydrophobic coating by using dielectric barrier discharge at atmospheric pressure" (May 10-12, 2017) **KSIEC 2017**, Gwangju, Republic of Korea **(POSTER).**

18. Ganeshkumar Verrasubramanian, Arunkumar Chandrasekhar, **Sudhakaran M.S.P**, Young Sun Mok, Sang-Jae Kim, 유연파우치형 슈퍼커패시터의 제작, **KMEMS 2017**, Mar 30 ~Apr 01, Jeju Island, Korea

19. Veerasubramani, G. K., Chandrasekhar, A., **Sudhakaran M. S. P**, Mok, Y. S., Kim, S. J., "Flexible Pouch-type Hybrid Supercapacitor" (February 20-24, 2017) **MCARE 2017**, Jeju, Republic of Korea **(POSTER).**

20. Arunkumar Chandrasekhar, Nagamalleswara Rao Alluri, **Sudhakaran M.S.P**, Young Sun Mok, Sang Jae Kim "Human Interactive Smart Mobile Pouch Triboelectric Nanogenerator and its Self-Powered Applications" (November 6-9, 2016) **ENGE 2016**, Jeju, Republic of Korea **(POSTER).**

21. Karuppiah J., Linga Reddy E., **Sudhakaran M.S.P**., S.B. Lee, "Production of synthesis gas from dry reforming of propane with carbon dioxide over ceria-promoted nickel foam catalysts" (May 4-6, 2016) **ICREPQ'16**, Spain **(POSTER).**

Declaration

I, **Sudhakaran M.S.P**, hereby declare that the thesis entitled "**Propane dry reforming over crystalline catalyst: Enhancement of synthesis gas production and its catalytic properties**", submitted to the Jeju National University, in partial fulfillment of the requirements for the award of the Degree of Doctor of Philosophy in **Faculty of Applied Energy systems, Major of Energy & Chemical Engineering** is a record of original and independent research work done and published by me during the period September 2014 to August 2018 under the supervision and guidance of **Prof. Young Sun Mok**, Department of Chemical and Biological Engineering, Jeju National University. This thesis solely based on our publication in reputed journals, and it has not been formed for the award of any other Degree / Diploma / Associateship / Fellowship to any candidate of any University.

Sudhakaran M.S.P